Fabrication of AgCl/$Bi_{24}O_{31}Cl_{10}$ for Vis-Light Activated Photocatalytic Degradation of Tetracycline and Other Related Phenolic Organics in Aqueous Systems

By

Dorcas Oluyemisi Adenuga

Fabrication of AgCl/$Bi_{24}O_{31}Cl_{10}$ for Vis-Light Activated Photocatalytic Degradation of Tetracycline and Other Related Phenolic Organics in Aqueous Systems

By

Dorcas Oluyemisi Adenuga

Submitted in partial fulfilment of the requirements for the degree

Doctor of Philosophy

Chemical Engineering

In the

Department of Chemical Engineering

Faculty of Engineering, Built Environment and Information Technology

University of Pretoria

2022

ABSTRACT

Title: Fabrication of AgCl/$Bi_{24}O_{31}Cl_{10}$ for Vis-Light Activated Photocatalytic Degradation of Tetracycline and Other Related Phenolic Organics in Aqueous Systems.

Author: Dorcas Oluyemisi Adenuga
Supervisor: Professor Evans M.N Chirwa
Co-Supervisor: Professor Shepherd M. Tichapondwa
Department: Chemical Engineering
University: University of Pretoria
Degree: Doctor of Philosophy (Chemical Engineering)

Photocatalysis has attracted attention as a viable technology for use in the environmental and energy generation fields. In the last couple of decades, researchers have continued to develop new photocatalysts in the area of photocatalysis for environmental remediation. In this study, a AgCl/$Bi_{24}O_{31}Cl_{10}$ composite heterostructure was synthesized. Varying ratios of AgCl nanoparticles were immobilized onto the $Bi_{24}O_{31}Cl_{10}$ rod-like structure. The physical and optical properties of the synthesized catalysts were characterized using a range of techniques. The photocatalytic activity of the catalysts was investigated by the degradation of 2,4-dichlorophenoxy acetic acid (2,4-D) and tetracycline (TC) under visible light irradiation. The performance of the composite photocatalysts was 18 and 3.4 times better in 2,4-D and TC photodegradation when compared to $Bi_{24}O_{31}Cl_{10}$ alone. The improved photocatalytic performance was attributed to the surface plasmon resonance (SPR) effects of the AgCl nanoparticles deposited on the surface of the Xwt%AgCl/BOC thereby improving the separation of the electron-hole pair. The effects of the initial contaminant concentration, pH, and

photocatalyst loading were investigated. Trapping experiments were also carried out to deduce the reactive species responsible for the degradation process and a preliminary mechanism of degradation was proposed. Mineralization of 2,4-D and TC at 65% and 63% efficiency was measured after 24 h and the potential for reusability of the as-synthesized photocatalyst was established.

It was also important to investigate the activity of the semi-conductor materials with real water samples. The photocatalytic activity of the photocatalyst was investigated in the secondary effluent of a wastewater treatment plant (WWTP) in Pretoria, South Africa for the degradation of phenol under visible light irradiation. The experimental design was done using the Taguchi method L16 orthogonal tray with three factors (pH, initial phenol concentration and photocatalyst dosage) and four levels. The results showed that pH was the highest-ranked significant factor influencing the degradation rate, closely followed by the initial concentration of the pollutant. The photocatalyst dosage had the least significant impact on degradation. The effects of individual anions components such as Cl^-, NO_3^-, NO_2^- and SO_4^{2-} and cations such as Ca^{2+}, Mg^{2+}, Zn^{2+} and K^+ were investigated. While Cl^- did not negatively influence the degradation rate, the results show that NO_3^- and SO_4^{2-} inhibit the degradation of phenol. More specifically, total inhibition of the degradation process was achieved when nitrite concentration of 20 ppm or more was added. This illustrates that nitrite concentrations $\geq$ 20 ppm should be removed from wastewater prior to photocatalytic degradation. The cations investigated promoted the degradation of phenol. Generally, there was enhanced degradation in the water matrix when compared to DI water and the results revealed improved degradation efficiency due to the cumulative impact of various components of the wastewater. This work reports a promising photocatalyst for the visible-light-driven removal of pollutants such as phenol, tetracycline and 2,4-dichlorophenoxy acetic acid from wastewater.

Keywords: bismuth, phenol, plasmonic, matrix effect, tetracycline, water treatment, 2,4-dichlorophenoxy acetic acid

DECLARATION

I, Dorcas Oluyemisi Adenuga, hereby declare that all the work provided in this dissertation is to the best of my knowledge original and that neither the whole work nor any part of it has been, or is to be submitted for another degree at this or any other University or tertiary education institution or examining body.

Signature: …… Date: …….

DEDICATION

To God Almighty.

ACKNOWLEDGEMENT

First and foremost, I'd like to thank God for the Grace and assistance he provided in order for me to accomplish this feat.

I am grateful to my supervisor, Professor Evans M.N. Chirwa for accepting me into his research group and allowing me to carry out research in the Water Utilization group at the University of Pretoria. I am appreciative of his mentoring and advice along this process. I respect him for recognizing potential and developing it.

My sincere appreciation to my co-supervisor, Professor Shepherd Tichapondwa for his dedication to the project, his support, vision and passion for research.

Mrs. Alette Devega and Mrs. Elmarie Otto – Thank you for the exceptional administrative and laboratory management that makes our lives easy.

I am thankful to the staff at the XRD and SEM/TEM units as well as all who helped with the various characterization techniques.

This work would not have been possible if not for the scholarship received from the National Research Foundation and the University of Pretoria. I will forever be thankful for the funding that allowed me the opportunity to further my education.

I thank my Parents, Kayode and Olusola, and my siblings, Adeniyi, Oluwatosin and Oluwaseyi for their constant and unwavering support through this journey. Thank you for always believing in me.

I am grateful for the privilege to work with my colleagues at the Water Utilization Division, South campus, University of Pretoria. We held hands and got through difficult times. From the bottom of my heart, I wish you all a successful career.

I am also thankful for the gift of family and friendships far and wide. Thank you for your motivation and support.

Table of Contents

LIST OF FIGURES

LIST OF TABLES

LIST OF SCHEMES

LIST OF NOMENCLATURE

AOPs	Advanced oxidation processes
BOC	$Bi_{24}O_{31}Cl_{10}$
CB	Conduction band
E_g	Band gap energy
FTIR	Fourier-transform infrared spectroscopy
HPLC	High-pressure liquid chromatography
LSPR	Localized surface plasmon resonance
NOM	Natural organic matter
PPM	Parts per million
ROS	Reactive oxygen species
SEM	Scanning electron microscopy
SPR	Surface plasmon resonance
TEM	Transmission electron microscopy
TC	Tetracycline
TOC	Total organic carbon
TGA	Thermogravimetric analysis
UV	Ultraviolet
UV-VIS	Ultraviolet-visible spectrometry
XRD	X-ray powder diffraction
2,4-D	2,4-dichlorophenoxy acetic acid
VB	Valence band
e	Electron
h^+	Hole
hv	Photon energy

RESEARCH OUTPUTS

From PhD work:

1. **Dorcas O. Adenuga**, Shepherd M. Tichapondwa, Evans M.N. Chirwa. Influence of wastewater matrix on visible light degradation of selected organic pollutant using AgCl/$Bi_{24}O_{31}Cl_{10}$ photocatalyst, 2022. *Environmental Science and Pollution Research*. DOI: 10.1007/s11356-022-23872-2

2. **Adenuga, D.**, Skosana, S., Tichapondwa, S. & Chirwa, E. 2021. Synthesis of a plasmonic AgCl and oxygen-rich $Bi_{24}O_{31}Cl_{10}$ composite heterogeneous catalyst for enhanced degradation of tetracycline and 2,4-dichlorophenoxy acetic acid. *RSC Advances*, 11, 36760-36768.

3. **Dorcas O. Adenuga**, Adedapo O. Adeola, Shepherd M. Tichapondwa, Evans M.N. Chirwa. Various applications of Silver-Bismuth-Based photocatalysts in environmental remediation, Target Journal: *Catalysts* [Manuscript in preparation].

Other related publications:

4. Adedapo O. Adeola, Bayode A. Abiodun, **Dorcas O. Adenuga**, Philiswa N. Nomngongo, Adsorptive and photocatalytic remediation of hazardous organic chemical pollutants in aqueous medium: A review, *Journal of Contaminant Hydrology*, Volume 248, 2022, 104019, ISSN 0169-7722, https://doi.org/10.1016/j.jconhyd.2022.104019.

5. **Dorcas O. Adenuga**, Shepherd M. Tichapondwa, Evans M.N. Chirwa, Facile synthesis of a Ag/AgCl/BiOCl composite photocatalyst for visible – light –

driven pollutant removal, *Journal of Photochemistry and Photobiology A: Chemistry*, Volume 401, 2020,112747,ISSN 1010-6030,https://doi.org/10.1016/j.jphotochem.2020.112747

6. **Adenuga, D.**, Tichapondwa, S., & Chirwa, E. (2019). Synthesis and Characterization of Potential Visible-light Photocatalyst and Its Photocatalytic Activity in the Decomposition of Phenol. *Chemical Engineering Transactions*, *74*, 1087-1092. https://doi.org/10.3303/CET1974182

7. **Adenuga, D. O.**, Tichapondwa, S. M., & Chirwa, E. M. N. (2019). Ternary Ag/AgCl/BiOCl Synthesis and the Effects of its Constituents on Phenol Degradation. *Chemical Engineering Transactions*, *76*, 127-132. https://doi.org/10.3303/CET1976022

Conference presentations

1. 26th International Congress of Chemical and Process Engineering CHISA, 21 to 25 August 2022, Prague, Czech Republic ("Experimental study on the photocatalytic performance of AgCl/$Bi_{24}O_{31}Cl_{10}$" – oral presentation).

2. The 14th International Conference on the challenges in Environmental Science and Engineering, 6th – 7th November, 2021 ("Synthesis of Plasmonic AgCl and Oxygen-rich $Bi_{24}O_{31}Cl_{10}$ Composite Heterogeneous catalysts for Enhanced degradation of Polluted Water" – oral presentation).

CHAPTER 1 – INTRODUCTION

1.1. Background

The flow of toxic organic pollutants present in wastewater effluents continues to pose detrimental impacts on human health and the aquatic environment (Mao et al., 2019). Many technologies have been explored to remove these pollutants from water sources to mitigate their effects (Gangu et al., 2019). Semi-conductor photocatalysis has been identified as one of the most futuristic means of remediating environmental and air pollution as well as for energy conversion (Ran et al., 2019). It has attracted attention as a viable technology for use in the environmental and energy generation fields (Li et al., 2019b). In the last couple of decades, researchers have continued to develop new photocatalysts in the area of photocatalysis and give more attention to more toxic compounds (Majumder et al., 2021). This is especially true in cases where non-biodegradable, recalcitrant organic compounds are present in wastewater (Fónagy et al., 2021).

The highly reactive free radicals generated when photocatalysts are irradiated with suitable light sources are capable of degrading and mineralizing recalcitrant compounds (Bi et al., 2016). However, commonly used photocatalysts such as TiO_2 and ZnO have a major drawback in that they are only active under ultraviolet light irradiation, which constitutes less than 5% of solar radiation (Yan et al., 2019). This limits the practical application of these materials, as external sources of energy are required. It is therefore important to develop photocatalysts that are capable of functioning under visible light irradiation and ultimately utilise direct sunlight for the degradation and mineralisation of organic contaminants in wastewater.

In recent years, bismuth oxyhalide photocatalysts BiOX (X=Cl, Br, and I) have been widely investigated due to their excellent electrical, catalytic and optical characteristics (Jin et al., 2015). Bismuth-based materials are characterized by a narrow bandgap that aids photocatalytic activity in visible light due to their hybridized O 2*p* and Bi $6s^2$ valence bands (Wang et al., 2014). They have been used in the photodegradation and decoloration of dyes, water splitting and the removal of contaminants in wastewater systems (Shabani et al., 2019). Literature shows that various $Bi_xO_yCl_z$ forms have been synthesized and studied. Examples include $Bi_{24}O_{31}Cl_{10}$ (Jin et al., 2015), $Bi_{12}O_{17}Cl_2$ (Xiao et al., 2013), Bi_3O_4Cl (Xu et al., 2020a) and $Bi_{12}O_{15}Cl_6$ (Wang et al., 2016). It is generally accepted that the superior photocatalytic activity of these compounds is a result of their lower bandgap and superior surface area (Jin et al., 2017, Yao et al., 2021). $Bi_{24}O_{31}Cl_{10}$ is said to have high electron mobility making it a good material for photoanode and photocatalysis applications (Wang et al., 2014).

Noble-metal-based nanoparticles such as Au, Pt and Ag are characterized by strong absorption in the UV-Vis region as a result of the oscillations of surface electrons (Feng et al., 2016). This phenomenon is referred to as surface plasmon resonance (SPR). Ag-based nanoparticles are selected as a result of their relatively cheaper cost which makes them a good candidate for the fabrication of nanocomposite photocatalysts (Ai et al., 2019). AgCl is reported to have a wide bandgap of 3.25-3.26 eV which is only excited by UV light irradiation (Gou et al., 2018, Raizada et al., 2020b). During irradiation, plasmonic Ag is formed on the surface of the AgCl, therefore improving the photocatalytic activity of the photocatalyst.

Band engineering strategies has therefore been used to create heterojunctions through coupling of semi-conductor materials such as AgCl and $Bi_{24}O_{31}C_{l0}$. The intrinsic advantages of these strategies include wider light-harvesting efficiencies

and hindered rate of charge combination thereby improving degradation and the visible-light activity of the composite photocatalyst (Tahir et al., 2020).

It is also important to study the effects of water matrix in photocatalytic activity. Surface water and wastewater also consist of natural organic matter (NOM) which can influence photocatalytic activity through; (1) the formation of singlet (^{1}NOM*) and triplet states (^{3}NOM*) during irradiation and (2) the action of NOM components acting as filtering agents of photochemical light due to their lack of being photoinductive (Yuan et al., 2019). Since important reactive oxygen species (ROS) are generated during photocatalytic degradation (Wang et al., 2015), they could be affected by components in a water matrix. This could stem from light attenuation, scavenging, formation of iron complexation, adsorption to a catalyst and less active radical formation and could be advantageous in the formation of ROS which acts as an additional catalyst source and aids the regeneration of photocatalyst (Lado Ribeiro et al., 2019).

1.2. Aim and objectives

The main aim of this study was to synthesize a visible-light-activated photocatalyst material that can be utilized in the degradation of organic pollutants in wastewater. The detailed specific objectives of the study were:

1. The synthesis and characterization of the silver bismuth – based visible-light-driven photocatalyst.
2. The determination of the optimum deposition of silver chloride nanoparticles on the surface of the bismuth-based semi-conductor material.
3. To investigate the effect of factors such as pH, initial pollutant concentration and photocatalyst dosage in the photocatalytic degradation

of tetracycline and 2,4-dichlorophenoxy acetic acid in visible light irradiation.

4. Investigate the main reactive species responsible for the degradation process and propose a degradation mechanism to explain the process.
5. To determine the effects of the real water matrix on the photocatalytic efficiency of the photocatalyst material on the degradation of phenol while taking factors such as pH, initial pollutant concentration and catalyst dosage into account.

1.3. Framework for the thesis

This thesis consists of seven chapters of which some of the work has already been published. The work presented in Chapters 3, 4 and 5 has been published in *RSC Advances* while Chapter 6 has been published in *Environmental Science and Pollution Research*.
The chapters are described as follows:

Chapter 1 Introduction

Provides a brief background to the research study, its objectives, and thesis framework. The aim and objectives of the study were defined.

Chapter 2 Literature review

The chapter gives a comprehensive review of the past literature on the subject study of photocatalysis. Specifically, the development of heterojunction photocatalyst materials, bismuth-based photocatalyst and organic pollutants such as tetracycline, 2,4-dichlorophenoxy acetic acid and phenol. It also briefly discusses conventional water treatment methods.

Chapter 3 Materials and methods

The materials and techniques utilized in the synthesis and characterization of the materials are the main topics of this chapter. The procedures employed in the synthesis, degradation, and analytical research are also covered in this chapter.

Chapter 4 Material characterization

The characterization of the photocatalyst material to ascertain its optical, photonic, and physicochemical properties is discussed in this chapter.

Chapter 5 Photocatalytic degradation studies of tetracycline and 2,4-dichlorophenoxy acetic acid

This chapter investigates the degradation efficiency of the synthesized materials under visible light irradiation. The optimum photocatalyst is derived for the photodegradation of tetracycline and 2,4-dichlorophenoxy acetic acid. Various factors affecting the degradation efficiency such as the initial pollutant concentration, photocatalyst dose and pH were investigated. The extent of mineralization was also investigated as well as the stability of the photocatalyst. The reactive species for each pollutant degradation was studied and a degradation mechanism was proposed.

Chapter 6 Influence of wastewater matrix on the visible light degradation of phenol

The efficacy of the synthesized material in the presence of actual water matrix was done and compared with the degradation in DI water. The individual effects

of anions and cations were investigated in this chapter for the visible light degradation of phenol.

Chapter 7 Conclusions and Recommendations

This chapter discusses the overall findings from the study, the difficulties encountered, and suggestions for potential future research.

1.4. Significance of the research

Water is an important resource required for human development. The human population which is expected to reach 9.2 billion in 2050 is the major driver of the increasing demand for water (Haddout et al., 2020). This means that wastewater streams need to be remediated and rendered usable for various applications ranging from potable water supply to industrial use. Previously, conventional wastewater treatment techniques have been utilized for the removal of organic pollutants from wastewater. However, due to the persistent nature of organic pollutants being released into the environment, other more efficient technologies need to be developed. Photocatalysis which is a type of advanced oxidation processes (AOP) has gained attention in the area of treating organic wastewater (Ma et al., 2021a). Two major factors in the successful application of photocatalysis are the photocatalyst material and the source of irradiation. In this study, experimental results showed the synthesis of a suitable material that can be irradiated under visible light for the removal of organic pollutants such as tetracycline, 2,4-dichlorophenoxy acetic acid and phenol from wastewater. The synthesized material showed good mineralization potential as well as prospects for future industrial application.

CHAPTER 2 – LITERATURE REVIEW

2.1. Water pollution

Water is regarded as the most crucial natural resource needed for human survival out of all natural resources, yet fresh water is only present in 2.5% of the world's water supply (Tang et al., 2022b). In the 21st century, the problem of water pollution is a major global challenge that needs to be addressed. The Sustainable Development Goals (SDGs) developed by the United Nations have listed 17 goals to be achieved by 2030 of which SDG 6 aims to "ensure availability and sustainable management of water and sanitation for all" (Kanchanamala Delanka-Pedige et al., 2021). Over the years, water pollution has gotten worse in various regions of the world including China, India, South America and parts of Africa (Evans et al., 2019). It has been estimated that about 1.8 billion people across the world may face water scarcity by 2025 (Hasan et al., 2019).

Water pollution is a result of natural and anthropogenic activities such as discharges from mining waste, metal processing wastes, pesticides, fungicides, sewage, organic and inorganic waste into wastewater bodies as illustrated in Figure 2.1. These types of pollution alter the chemical and physical properties of water (Agrawal et al., 2010). Over the years, it has been reported that agriculture is a leading source of pollution globally as it results in the discharge of large amounts of agrochemical nutrients, drug residues, organic matter, sediments and pathogens (Evans et al., 2019). An example is antibiotics which are commonly used in the swine industry for the treatment and prevention of bacterial infections through the killing or inhibition of the causative bacteria (Cheng et al., 2020). Other sources of the occurrence of antibiotics in surface water are wastewater treatment plants and the release of untreated sewage (Anh et al., 2021).

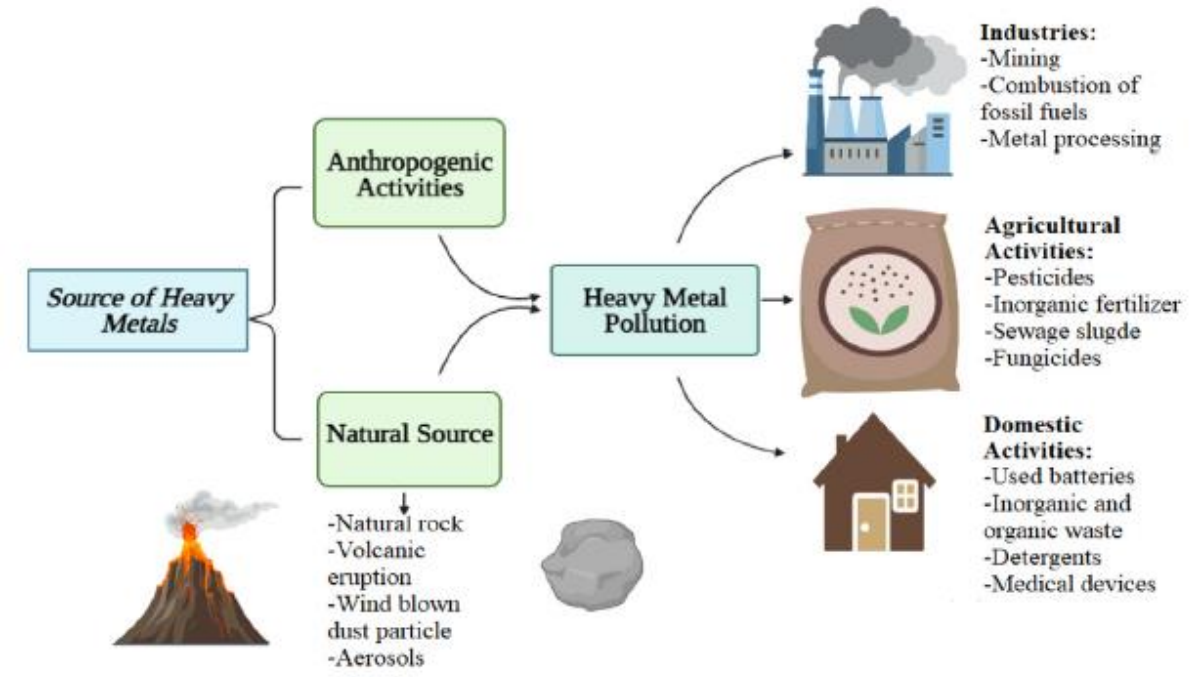

Figure 2.1: Sources of water pollution (Zamora-Ledezma et al., 2021)

Water pollution has various effects on the environment, human beings and the entire ecosystem. Persistent contaminants in water, such as chemicals and pharmaceuticals, pose a high risk to the environment even at low concentrations. (Raizada et al., 2020a). They act as endocrine disruptors in both aquatic and human organisms (Quesada et al., 2019). In aquatic systems, they lead to the eutrophication of water bodies and the death of aquatic plants and animals (Srivastava et al., 2021). Water pollution has also been connected to various water-borne diseases such as hepatitis, dysentery, cholera, typhoid and diarrhea (Wang and Yang, 2016).

2.2. Conventional wastewater treatment methods

Conventional wastewater treatments are a combination of chemical, physical and biological processes utilized for the removal of organic matter, solids and pollutants from wastewater effluent (Crini and Lichtfouse, 2018). These treatment technologies typically include: chemical precipitation, coagulation/flocculation, biodegradation, adsorption and filtration using activated carbon. These methods have various drawbacks such as expensive disposal procedures, limited operating conditions, poor efficiency and insufficient removal of contaminants (Chai et al., 2021). Chemical precipitation involves the use of chemical agents such as pH adjustment for the conversion of pollutants into less soluble compounds such as hydroxides, carbonates and sulphides that can be removed through physical processes like filtration and sedimentation (Chen et al., 2018). Coagulation/flocculation entails the addition of coagulants, which can neutralize the charges of particles, destabilizing them. The particles develop gradually and aggregate into larger flocs (Zhao et al., 2021). It is advantageous in its simple process of application and low capital cost but has drawbacks such as the generation of a large amount of sludge (Kurniawan et al., 2020).

Biodegradation is the use of suitable microorganisms such as fungi and bacteria for the degradation of micro pollutants in polluted water (Kanaujiya et al., 2019). This is carried out in aerobic and anaerobic conditions through activated sludge, aerobic lagoons, trickling filters, anaerobic filters and other treatment methods (Joshiba et al., 2019). Environmental factors such as pH and temperature have been reported to limit the enzymatic degradation of antibiotics such as tetracycline (Chen et al., 2022). In conventional water treatment plants, continuous inflow of TC affects the microbial community in the biological system thereby affecting the removal of phosphates and nitrates. This could happen

through the eventual development of antibiotic resistant bacteria in the treatment system (Liao et al., 2021).

Adsorption is a process that involves the use of a solid phase known as the adsorbent for the removal of dissolved contaminants in polluted water through the transfer of the contaminant to the surface of the adsorbent (Dotto and McKay, 2020). Yazidi et al. (2020) studied the adsorption of tetracycline and amoxicillin on activated carbon prepared from durian shell and the results showed a higher adsorption of amoxicillin in comparison to tetracycline. While it has various advantages, even commonly used adsorbents like powdered activated carbon are not only difficult to remove from the solution but also expensive (Chai et al., 2021).

Filtration involves the removal of particulate matter, pathogens and suspended solids in water to increase disinfection efficiency (Cescon and Jiang, 2020). Techniques such as slow sand filtration are advantageous in their cost-effectiveness and low energy consumption during operation (Verma et al., 2017). Other techniques such as ultrafiltration are easily maintained and have no chemical pollution but membrane fouling due to the accumulation of inorganic components and organic matter results in reduced efficiency (Guo et al., 2018). Filtration is used in conjunction with other technologies, such as adsorption, to remove organic contaminants like antibiotics from wastewater (Sharma et al., 2017). In other combinations, bioremediation is combined with filtration in a membrane bioreactor for the removal of pharmaceutical compounds from wastewater (Akhil et al., 2021).

In general, existing wastewater treatment plants are not designed to remove contaminants such as pharmaceuticals and herbicides as the main focus of such

plants was to remove readily biodegradable organic matter (de Oliveira et al., 2020).

2.3. Advanced oxidation processes (AOPs)

AOPs involve the generation of reactive oxygen species or free radicals for the degradation of pollutants into simpler or non-toxic compounds (Kanakaraju et al., 2018). The method is highly advantageous over other methods of organic pollutant removal (Ma et al., 2021a). Its advantages include little to no secondary pollution, a high rate of mineralization efficiency and a rapid oxidation reaction rate. Types of AOP's include ozonation, Fenton and photo-Fenton processes, photocatalysis and others (Akkari et al., 2018). AOPs can be characterized based on their different physical-chemical processes and mode of application, and are classified in Figure 2.2.

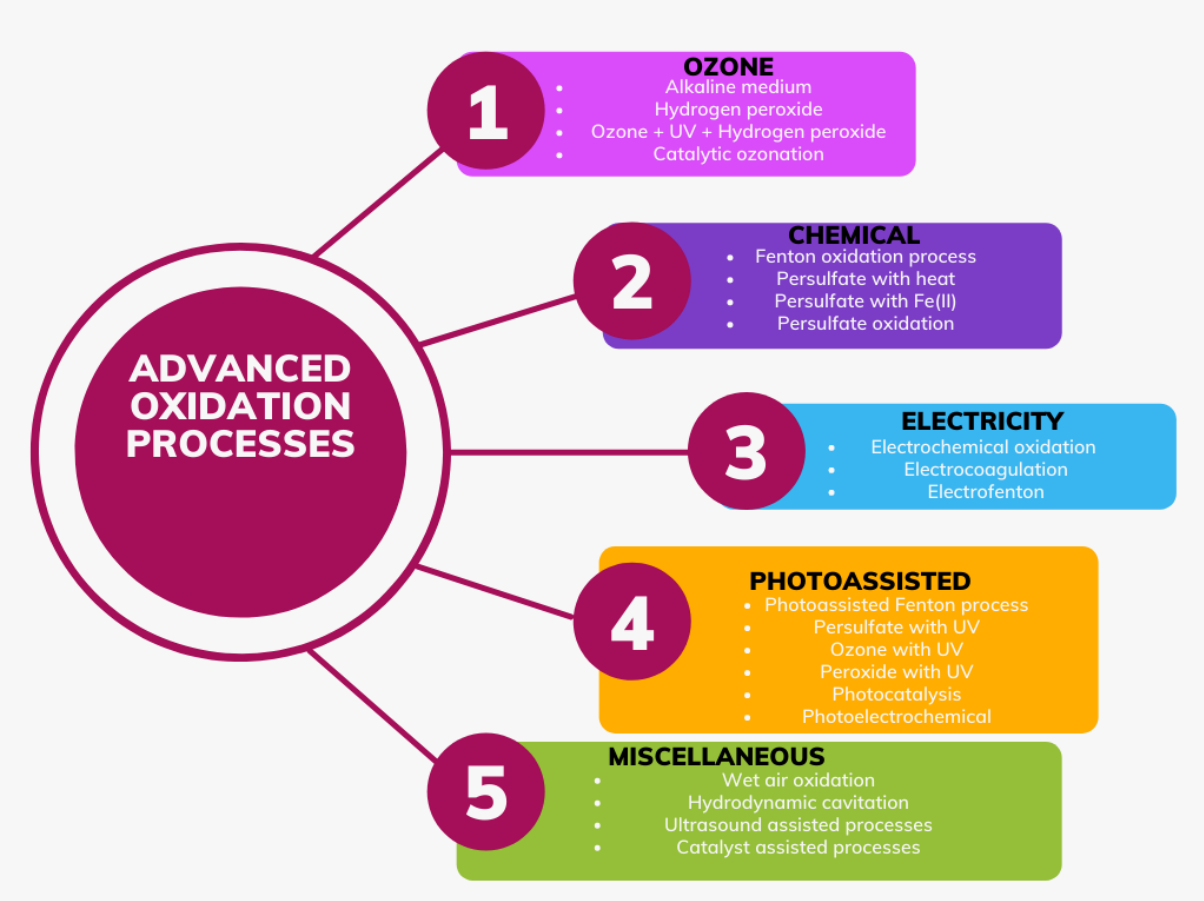

Figure 2.2: Advanced oxidation processes (Adapted from Gautam et al. (2019))

Ozone is a strong oxidizing agent used in water and wastewater treatment due to its effectiveness in disinfection, oxidation of pollutants, taste and odor improvement and reduction in turbidity (Mecha and Chollom, 2020). In catalytic ozonation, the catalysts promote the decomposition of ozone for the generation of reactive radicals which will be responsible for the degradation process (Wang and Chen, 2020). A limitation of ozonation is that the reactions of ozone with organic compounds result in the formation of carboxylic acids and aldehydes. This means that the complete mineralization of the organic pollutant is not achieved (Nawrocki and Kasprzyk-Hordern, 2010). In recent times, reagents such as ozone and hydrogen peroxide are combined with UV-vis irradiation due to its potential for treating organic substances in water (Heebner and Abbassi, 2022).

Fenton and Fenton-like processes involve the generation of hydroxyl radicals through the reaction that occurs between ferrous ions and hydrogen peroxide (Babu et al., 2019). It has advantages such as high degradation efficiency and ease of operation but is limited in application as a result of the high amount of iron-containing sludge that is formed (Wang and Zhuan, 2020). Persulfate oxidation has high stability, high activity and a range of applications (Chen et al., 2021a). Sulfate radicals have been reported to have a high redox potential in comparison to other reactive species (Wang and Wang, 2020). While persulfate is a powerful oxidant that reacts very slowly with common pollutants and as such requires activation to form radicals required for pollutant degradation (Ike et al., 2018). They are usually activated through various methods which include: catalysis, sonolysis, thermolysis and photolysis (Yang et al., 2021). Other physical AOP's include plasma, ultrasound, microwave and electron beams (Miklos et al., 2018). Technologies such as non-thermal plasma have an advantage of having low energy consumption but the reactor configuration makes it limited for practical application while ultrasonic oxidation has a high removal efficiency but low energy transfer (Zhang et al., 2020d).

2.3.1. Photocatalysis

Heterogeneous semiconductor photocatalysis is a type of advanced oxidation processes (AOP's) that is used in the degradation of recalcitrant organic pollutants in wastewater (Ji et al., 2013). The photocatalytic process was derived from natural photosynthesis where plants capture sunlight energy for growth through the oxidation of water and the reduction of CO_2 (Fujishima et al., 2000). This phenomenon is similar to photocatalysis where a semi-conductor material suspended in an aqueous medium is illuminated and absorbs photons with energies higher than its bandgap thereby resulting in the production of photogenerated holes and electrons on the surface of the catalyst (Molinari et al.,

2020). A semi-conductor material while accelerating the solar photo reaction should not take part or be consumed in the reaction (Lee and Park, 2013). This reduction-oxidation technology leads to the formation of reactive species that can degrade pollutants into water and carbon-dioxide (Byrne et al., 2018). The general photocatalytic mechanism is illustrated in Figure 2.3 and Equation 2.1 – Equation 2.4 (Banerjee et al., 2014) when TiO_2 is used as a photocatalyst. When light with photonic energy matches or exceed that of a semi-conductor,

1. Electrons are excited from the valence band to the conduction band creating a hole in the valence band (Equation 2.1)
2. The valence band (VB) holes and excited conduction band (CB) electrons can recombine, releasing heat and no reaction taking place (Equation 2.2),
3. They can also take part in a redox reaction with water, oxygen and organic compounds leading to the formation of reactive radicals and subsequent mineralization of the pollutant (Equation 2.3 and Equation 2.4).

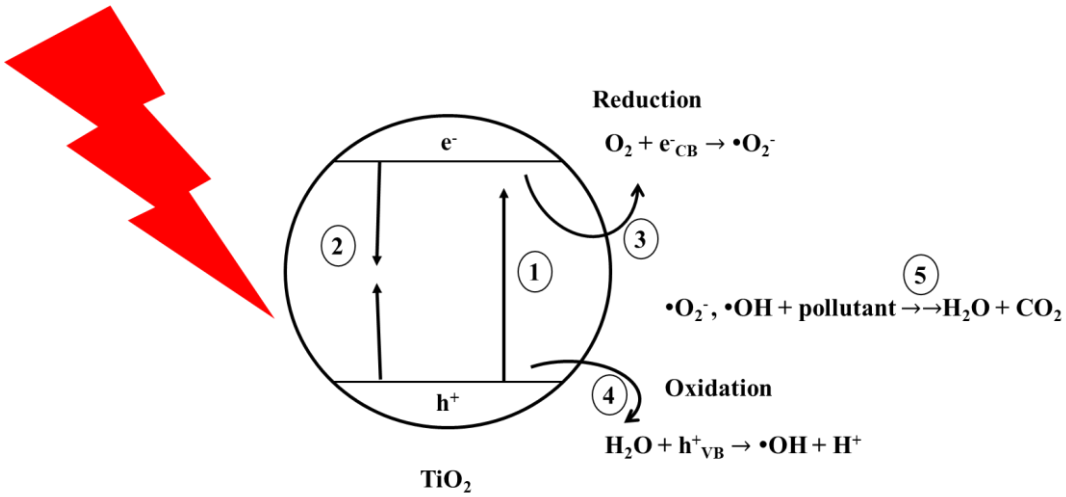

Figure 2.3: TiO_2 photocatalytic mechanism under UV light irradiation (adapted from (Al-Mamun et al., 2019))

$$\text{Semiconductor} + hv \rightarrow h^+_{VB} + e^-_{CB} \quad (2.1)$$

$$e^-_{CB} + h^+_{VB} \rightarrow \text{energy} \quad (2.2)$$

$$h^{+}_{VB} + H_2O \rightarrow \bullet OH + H^{+} \quad (2.3)$$

$$e^{-}_{CB} + O_2 \rightarrow \bullet O_2^{-} \quad (2.4)$$

Researchers continue to investigate other semi-conductor materials for photocatalysis. Commonly used photocatalysts such as TiO_2 (first discovered in the late 1960s by Fujishima and Honda (1972) have various advantages such as its large surface area to volume ratio (Ochiai and Fujishima, 2012), high photocatalytic efficiency and anti-bacteria properties (Zhang et al., 2003), low cost and high stability, non-toxic and biologically inactive (Humayun et al., 2018). It also has various drawbacks. It can only be activated under ultraviolet light irradiation as a result of its wide bandgap and weak separation of carrier causing higher recombination of electron-hole pairs (Humayun et al., 2018). This has resulted in its reduced practical application in the removal of organic pollutants (Liu et al., 2012). The sun is the most abundant source of energy with visible light constituting about 45% of the solar spectrum, near-infrared light is 50% while ultraviolet light is only about 5% of the spectrum (Molinari et al., 2020). This has led to the continuous study in the improvement of semi-conductor materials to shift their light absorption capabilities into the visible light region for the sole purpose of tapping the already abundant resource for water treatment. The photocatalytic process becomes cheaper and more environmentally friendly for industrial practical applications. Over the years, there have been different strategies for synthesizing photocatalyst materials for the enhancement of photocatalytic activity. These aim to improve the separation of electron-hole pair, inhibit recombination and shift the bandgap into the visible light absorption range. These strategies include band engineering through metal and non-metal doping, surface sensitization, co-catalyst coupling and the formation of heterojunctions (Tahir et al., 2020). In addition to these strategies, a good photocatalyst is characterized by a high degradation efficiency, low cost, suitable band gap, good recyclability and chemical stability (Tahir et al., 2020).

2.3.2. Catalyst band engineering

2.3.2.1. Surface sensitization, metal and non-metal doping

Approaches such as impurity doping, defect control and sensitization through organic dyes have been used to improve the visible light responsiveness of a semi-conductor material. Doping impurities on the surface of the semi-conductor enhance the photo activity through the introduction of localized electronic states causing a shift in the optical absorbance of the semi-conductor materials (Wen et al., 2015). Previous studies have doped metal nanoparticles (NPs) on TiO_2 (Yousef et al., 2015). Au, Pd, Ag and Pt are examples of metals that have been loaded on the surface of TiO_2 (Lei et al., 2014, Pol et al., 2016, Nguyen et al., 2018, Mohammed, 2020). This loading improves the photocatalytic activity of the photocatalyst by either shifting the Fermi levels which indicate improved electron transfer or by utilizing the properties of metals such as Ag and Au to improve photocatalytic activity due to their localized surface plasmonic resonance (LSPR) (Park et al., 2013). This improves the visible light absorption of the photocatalyst and sometimes, the added noble metals acts as trapping sites for electrons, hence, improving photocatalytic efficiency. On the other hand, dopants such as carbon, nitrogen, sulphur and fluorine could act as recombination sites of the photogenerated holes and electrons and therefore reduce the efficiency of the photocatalyst (Saison et al., 2013).

2.3.2.2. Co-catalyst coupling

A strategy that has been employed in optimizing the photocatalytic activity of a semi-conductor is modifying it with a co-catalyst to improve the photocatalytic efficiency. de Moraes et al. (2021) designed a tin(IV) oxide and carbon xerogel

composite co-catalyst. The addition of the carbon structure to the tin oxide improved the photocatalytic activity due to the increased surface area and high absorption in visible light. Carbon black (CB) was also used as a co-catalyst to enhance the stability and improve the photocatalytic activity of ZnO nanoparticles (Chang and Hsu, 2020). The photocatalytic efficiency of the CB/ZnO was nearly double that of ZnO alone as a photocatalyst. Fang et al. (2019) verified that a binary photocatalyst consisting of CdS and alkalized Ti_3C_2 nano-sheets acting as a co-catalyst resulted in higher degradation efficiency of rhodamine B (82%).

2.3.2.3. Heterojunctions

Creating a heterojunction photocatalyst takes advantage of the intrinsic properties of two or more materials. This enables the combination to have several advantages over a single-component photocatalyst. Chen et al. (2019) highlighted these four advantages namely; (1) Accelerating the separation of electron-hole pairs, (2) reduction of recombination as a result of increased conduction rate, (3) longer life span of electron carriers and (4) higher activity and stability. A heterojunction is therefore defined as band alignment resulting from the interface of different semi-conductor materials with unidentical band structures.

Low et al. (2017) discussed the five various types of heterojunctions that can be synthesized for use in water treatment. These are conventional heterojunctions that are classified into three groups namely Type I (Stradling gap), type II (staggered gap) and type III (broken gap). Other types of heterojunctions are p-n heterojunction, surface heterojunction, Z-scheme heterojunction and semiconductor/graphene heterojunctions.

Figure 2.4 depicts the schematic illustration of (a) type-II heterojunction, (b) direct z-scheme and (c) all-solid-state- Z scheme. In type II heterojunction, there is a transfer of electrons from photocatalyst I (PC I) to the conduction band of photocatalyst II (PC II). This effectively separates the photogenerated charges in the semiconductor spatially. Direct Z-scheme utilizes an electric charge transfer between the electrons in the CB of PC II and the holes in the valence band of PC I (Li et al., 2021b) while the all-solid-state Z-scheme involves a charge mediator. These mediators ensure that reductive electrons and oxidative holes in the reactive sites remain to participate in the reactions by creating a pathway for the generated electrons in PC II to recombine with the holes in PC I (Zhang et al., 2020c). Table 2.1 shows examples of various photocatalytic heterojunctions that have been previously studied.

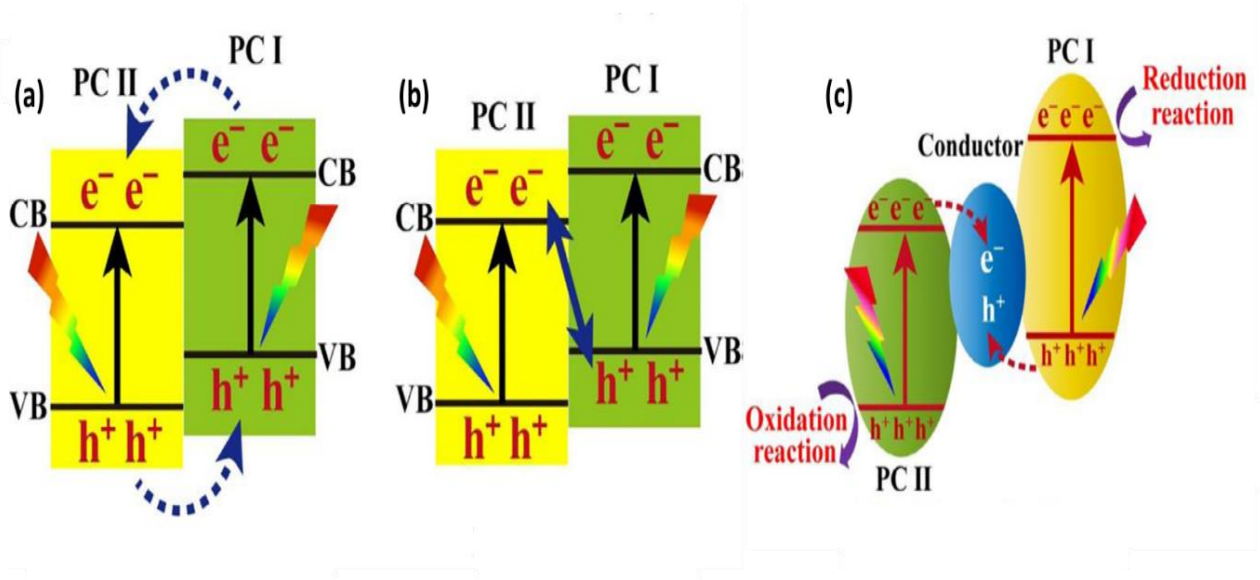

Figure 2.4: (a) Schematic illustration of type-II heterojunction, (b) Schematic illustration of Direct Z-scheme and (c) schematic illustration of all-solid-state-Z-Scheme (Xu et al., 2018)

Table 2.1: Recently synthesized photocatalysts for pollutant degradation

Photocatalyst	Synthesis method	Pollutant degraded	Conditions	Reference
Ni-ZnO/S-g-C_3N_4	Doping/heterojunction	Methyl Blue (MB)	Direct sunlight 100 mg in 100 mL	(Bahadur et al., 2021)
Ag/Ag(I)-TiO_2	Metal doping	Methyl Orange (MO)	350 W Xe lamp 0.05 g in 10 mL	(Liu et al., 2012)
Ag-$AgVO_3$/g-C_3N_4	Z-scheme heterojunction	Ciprofloxacin	500 W halogen lamp 0.1 g in 100 mL	(Samsudin et al., 2020)
Ag_3VO_4/$BiVO_4$	Z-scheme	Bisphenol S	500W Xe lamp 0.02g in 50 mL	(Zhao et al., 2019b)
Cu_0-doped TiO_2	Metal doping	MR RB5 RO16	250 W 0.025 g in 70 mL	(Yousef et al., 2015)
BiOI/p-g-C_3N_4	p-n	MB	300 W 10mg/L	(Jiang et al., 2013)
$Bi_2Fe_4O_9$/Bi_2WO_6	Z-scheme	RhB	300 W 0.03g in 0.1L	(Li et al., 2018)
Bi_2O_3/Bi_2SiO_5	p-n	MB	500 W	(Lu et al., 2018)

		Phenol 2,4-dichlorophenol	100 mg in 50 ml	
$LaVO_4/TiO_2$	Coupling	Benzene	500 W 1.2 g in 20 cm^3/min	(Huang et al., 2009)
$ZnIn_2S_4/BiPO_4$	Type II heterojunction	Tetracycline	300 W 15 mg in 50 mL	(Lu et al., 2019)
Palladium-doped TiO_2	Doping	Methylene blue Methyl orange	100 W 20 mg/L	(Nguyen et al., 2018)
$CoP/ZnSnO_3$	Co-catalyst	Tetracycline	500 W 25 mg in 50 mL	(Chen et al., 2021b)
$LaCoO_3/g\text{-}C_3N_4$	Co-catalyst	Methyl orange	300 W Xe lamp 50 mg in 150 mL	(Luo et al., 2018)

2.3.3. Silver and Bismuth-based photocatalyst

To enhance the conversion of solar energy, plasmonic photocatalysts are used for their efficient light absorbance and containment of surface plasmons (Wang et al., 2017a). This strong light absorption is achieved through the excitation of localized surface plasmon resonances (LSPR) which can be activated by visible and ultraviolet irradiation to generate carriers that can improve reaction rates and pathways (Zhang et al., 2017). Commonly used plasmonic materials are noble metal nanoparticles such as silver (Ag), gold (Au), copper (Cu) and platinum (Pt) due to the production of highly mobile charge carriers and their possession of good optical absorption in the solar spectrum and excellent photoactivity in the visible light region (Zada et al., 2019). The introduction of these noble metals improves the photocatalytic activity of the composite photocatalysts by acting as an electron sink with the ability to inject the photogenerated electrons into the conduction band of the co-catalyst thereby ensuring efficient separation of the generated reactive species (Shiraishi et al., 2019). When activated by visible light, silver can generate electrons and holes that participate in the photocatalysis process, allowing it to play multiple roles as an electron trapper and visible light inducer (Zhang et al., 2022).

Various studies have also presented several types of silver halide-based (AgX, X = Cl, Br, I) photocatalysts which are hybridized on a photoactive or photoinactive substrate (An et al., 2016). This ensures that Ag ions in the AgX matrix formulate into metallic Ag which has good SPR effects and the generated Ag nanoparticles can also be confined in the AgCl matrix thereby avoiding inactivation and reunion during the reaction process (Sun et al., 2020). In the synthesis of binary AgX/ZnO (X = Cl, Br, I) for the degradation of organic pollutants, Phongarthit et al. (2020) recorded a photocatalytic efficiency where AgCl/ZnO had a degradation efficiency higher than AgBr/ZnO and AgI/ZnO in the visible light degradation of

bisphenol A. Also, ZnO only could not degrade the pollutants under the same conditions. Ag/AgCl-based photocatalysts are also formed as a result of the photoreduction of AgCl during light irradiation (Adenuga et al., 2020). Ternary photocatalyst materials such as Bi_2MoO_6/Ag-AgCl (Li et al., 2020a), Ag/AgCl/TiO_2 (Liang et al., 2018), Ag/AgCl/Ti^{3+}-TiO_2 (Yu et al., 2021), Ag/AgCl/GO (Liu et al., 2017) amongst others have been synthesized to harness the properties of Ag/AgCl-based photocatalysts. Li et al. (2020a) in their study prove that the formation of Ag nanoparticles acts as an electron-transfer mediator thereby promoting the photodegradation activity of the synthesized composite material.

Bismuth materials have attracted attention in recent times for their suitable characteristics that make them a good candidate for application in photocatalysis. They have a unique layered framework, electronic band structures that can be adjusted and their potential for visible light responsiveness is advantageous for photocatalytic activity (Zhang et al., 2021). They are non-toxic, resistant to corrosion and chemically stable (Di et al., 2017). Different forms of bismuth-based photocatalysts such as $BiVO_4$, Bi_2MoO_6, Bi_2WO_6, $BiFeO_3$, BiOX (X = Cl, Br, I), etc., (A et al., 2018) has been synthesized in recent years for environmental applications. Bismuth oxyhalides such as BiOX which is an important Bi-based material have gathered attention due to its tetragonal matlockite structure that offers sufficient space for the polarization of atoms and orbitals which excites the formation of internal electric fields (Yang et al., 2018).

The modification of BiOCl into non-stoichiometric forms $Bi_xO_yX_z$ gives a structure that is similar to BiOX with an elevated conduction band potential (Jin et al., 2019). $Bi_{24}O_{31}Cl_{10}$ is produced through the thermal decomposition of BiOCl at temperatures above 600°C (Shabani et al., 2018, Fu et al., 2020, Li et al., 2014, Jin et al., 2018). The compound is a non-stoichiometric oxide of BiOCl

with more O and fewer Cl atoms, it has high chemical and physical stability and a narrow bandgap (2.78 eV) (Kang et al., 2020a) in comparison to BiOCl (3.19 – 3.6 eV) (Li et al., 2014) thereby improving its visible-light absorption potential. The abundant oxygen has a potential to promote degradation through the activation of molecular oxygen to form superoxide radicals (Jin et al., 2015). The efficiency of a photocatalyst is measured by its (i) absorption in light, (ii) separation of charge and (iii) photocatalytic reaction(Yao et al., 2021).

Studies have shown that neat $Bi_{24}O_{31}Cl_{10}$ has low photocatalytic activity under visible light irradiation as a result of its high electron-hole recombination rate (Song et al., 2018, Kang et al., 2020a). Kang et al. (2020b) synthesized a ternary heterojunction photocatalyst – MoS_2/g-C_3N_4/$Bi_{24}O_{31}Cl_{10}$ – in the visible light decomposition of tetracycline and report a 5.38 fold degradation of TC over the ternary composite in comparison to $Bi_{24}O_{31}Cl_{10}$ only. Shabani et al. (2019) also synthesized BiOCl-$Bi_{24}O_{31}Cl_{10}$/rGO for the solar degradation of ofloxacin. The results showed a degradation efficiency of 67.9% for $Bi_{24}O_{31}Cl_{10}$ and 81.2% for the ternary photocatalyst after 60 min. Therefore, band engineering is used to prepare heterojunction photocatalysts to overcome the intrinsic disadvantage of a single-component photocatalyst (Fang et al., 2020).

As seen in Figure 2.5**,** over the last six years, there has been growing interest in research into the combination of silver and bismuth-based materials for photocatalysts applications. Different variations of these composite catalysts have been reported in literature such as β-Bi2O_3/Ag_2O for tetracycline degradation (Wu et al., 2022), AgI/Ag/Bi_3TaO_7 for the degradation of sulfamethoxazole (Ren et al., 2018), Ag/AgCl/BiOCl for visible-light-driven tetracycline degradation (Wu et al., 2021), etc. It shows the potential for future practical application of such combinations.

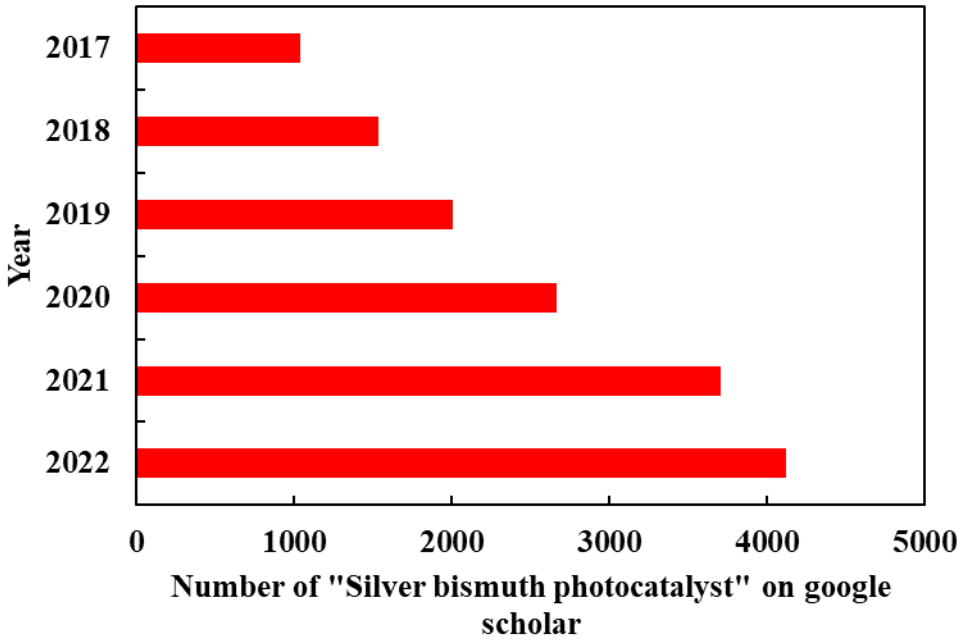

Figure 2.5: Number of "Silver bismuth photocatalysts" mentioned on google scholar in the last six years

2.3.4. Factors affecting the removal of organics from wastewater using photocatalysis

Various factors affect the successful application of photocatalysis in wastewater treatment. This includes the pH of the aqueous solution, the initial concentration of pollutants as well as the photocatalyst dosage. Other factors include light intensity, particle size and shape, reactor configurations and the presence of interfering ions.

2.3.4.1. pH

An important factor to be considered in the application of photocatalysis in water treatment is the pH of the solution. The acidity or the basicity of the aqueous solution affects the reaction happening on the surface of the photocatalyst. This

in turn could promote which of the reactive species will dominate during the reaction process (Gopinath et al., 2020). Also, it has an impact on the adsorption of the contaminant on the surface of the photocatalyst as adsorption is expected to result in higher photocatalytic activity (Chen et al., 2020). For example, when Titania is subjected to an alkaline or acidic medium, the following reactions in Equation 2.5 and Equation 2.6 occur showing that it remains positively charged in an acidic solution and negatively charged in the basic medium (Kumar, 2017):

$$TiOH + H^+ \rightarrow TiOH_2^+ \quad (2.5)$$

$$TiOH + OH^- \rightarrow TiO^- + H_2O \quad (2.6)$$

The potential of the photocatalyst to form aggregates is also a function of the pH of the solution as well as dictating the position of the conduction and valence bands (Ahmed et al., 2020).

2.3.4.2. Initial pollutant concentration

The initial concentration of the pollutant is another important factor that affects photocatalytic activity. There is a potential for "reactant overloading" on the photocatalyst surface (Khaki et al., 2017). This happens because of competition for active sites on the photocatalyst surface and the concentration of pollutants (Hasanpour and Hatami, 2020). Hassani et al. (2020) in their study investigated the effect of the initial concentration on the degradation of Direct Orange 26 (DO26) dye and reported a reduced degradation efficiency as the concentration of DO26 increased. This is because oxidizing agents are more readily available at lower DO26 concentrations, resulting in higher degradation efficiency. In another study by Rawat and Singh (2022), the degradation efficiency was not affected as the concentration of crystal violet dye (CV) increased until a certain point before a slight decrease was measured. They noted that a limited amount of

catalyst with increasing initial concentration results in a limited generation of reactive species. Also, the active sites are covered due to the adsorption of the pollutants on the surface of the photocatalyst as a result of increased concentration.

2.3.4.3. Effect of the photocatalyst dosage

The photocatalyst loading influences the overall performance of the system during degradation studies. A lower concentration of photocatalyst loading ensures that the surface of the material is adequately exposed which enables the pollutants access to photo-generated species (Carbajo et al., 2018). While increasing the dosage increases the active sites available until a certain point, a continuous increase in dosage could result in the aggregation of particles thereby preventing light penetration, which in turn reduces the photodegradation rate (Kiwaan et al., 2020). A high dosage results in huge opacity and consequent light scattering resulting in less penetration of light (Palanisamy et al., 2020). Hence, optimization studies need to be carried out to determine the optimal dosage of photocatalyst for practical application.

2.3.4.4. Other factors

Light intensity is another factor that affects the degradation efficiency during the photocatalytic process. In their review, Reza et al. (2015) state that at low light intensities, a linear increase in rate is measured as the light intensity increases, whereas at intermediate light intensities, beyond a certain value, the rate is half order. At high light intensities, the reaction rate will only reach a certain level due to the limitation on the number of reactive sites. The size and shape of the photocatalyst particle are other factors that influence photocatalytic activity. A particle size decrease results in a higher surface area, which causes an increased

photocatalytic activity due to increased available active sites and an increase in the charge carrier rate. Although, if the particle gets too small, there would be a high rate of recombination because of increased activity (Weldegebrieal, 2020). The morphology of the photocatalyst is also an important factor as it determines the catalyst contact area, charge migration and light absorption (Gu et al., 2022). The morphologies that have been explored include flower-like (Zhu et al., 2021, Ma et al., 2021b), nanorods (Zhang et al., 2020b), nanosheets (Hu et al., 2020), nanoparticles (Reddy et al., 2019), nanoplates (Deng et al., 2019), nanotubes (Yan et al., 2020), hollow microspheres (Abazari et al., 2019), sponge-like (Feng et al., 2020). This means that modifying the morphologies of materials not only improves their adsorption behaviour but could also promote the separation of photogenerated charge (Xiong and Tang, 2021).

Another major component that affects photocatalytic efficiency is the photoreactor configuration. The reactor needs to be designed in such a way that the collection of the emitted light is maximized on the semi-conductor surface (Sacco et al., 2020). It is therefore important that for an ideal photocatalytic efficiency, the reactor should have a high mass transfer speed, reaction surface area and kinetic rate (Koe et al., 2019). Reactor types are mainly summarized into two types namely slurry photocatalytic reactors which consist of suspended photocatalyst particles and fixed bed type reactors involving the immobilization of photocatalyst on reactor walls or spherical glass beads (Ahmed and Haider, 2018). Since salts are always present in an aqueous solution, it is also important to consider their effect on photocatalytic activity. Various ions can have promoting or hindering effects depending on the mechanism. In the study by Dugandžić et al. (2017) for the photodegradation of nicosulfuron, the result show an inhibiting effect by sulphate due to competitive adsorption during the reaction as well as reaction with holes and hydroxyl radicals while the reaction was faster in the presence of sodium ions.

2.4. Toxic organic compounds

Non-biodegradable organic contaminants in wastewater such as herbicides and antibiotics stem from large-scale farms, pharmaceutical industries and hospitals (Tang et al., 2021a). Rapid growth and development in the economy due to the increasing population and the development of more industries has led to environmental pollution especially that of water (Misra et al., 2020). Discharge from industries, agricultural discharge and human activities greatly contribute to the presence of contaminants in wastewater bodies (Deblonde et al., 2011). These organic pollutants when present in water sources pose a serious threat to human and marine life due to their toxicity (Baig et al., 2019). These carcinogenic and endocrine-disrupting compounds find their way into the food thereby inducing serious health challenges to human life while having short and long-term effects on aquatic life and wildlife (Manoli et al., 2019).

2.4.1. Pharmaceuticals (Tetracycline)

Pharmaceutically active compounds (PhACs) continue to pose high risks to human health and aquatic life and are referred to as emerging contaminants in water environments with conventional water treatment processes being unable to remove them sufficiently (Cai et al., 2018, Naghdi et al., 2018). Tetracycline (Figure 2.6), one of the most commonly used antibiotics, is used to treat bacterial infections in humans and animals (Jin et al., 2020). These compounds enter the water environment and wastewater treatment plants through domestic water systems. Tetracycline is not easily absorbed in the animal metabolism and as such, a high percentage (75%) is excreted into the environment (Dai et al., 2019). It has a hydrophilic nature and low volatility that enables it to persist in an aquatic environment. It enables the development of microorganisms that are resistant to antibiotics thereby harming human health (Daghrir and Drogui, 2013). Its

accumulation in the environment leads to its collection in the food chain impacting human health through endocrine disruption, joint disease and nervous system defects (Xu et al., 2021). In bacteria reproduction, tetracycline can inhibit the synthesis of bacterial proteins by binding with aa-tRNA site A on the 30S submit thereby preventing the growth and reproduction of bacteria (Liao et al., 2021). As shown in Table 2.2, various technologies such as adsorption, catalysis and oxidation processes, among others, have been used in the remediation of these compounds.

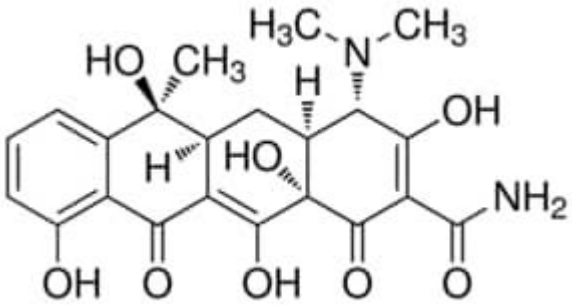

Figure 2.6: Chemical structure of tetracycline

Table 2.2: Techniques used in the removal of tetracycline from wastewater

Method	Technique	Reference
Oxidation process	Chlortetracycline degradation through persulfate oxidation, Fe^{2+} and ZVI as catalysts.	(Pulicharla et al., 2018)
Adsorption	Adsorption of tetracycline on carbon nanotubes and Fe.	(Xiong et al., 2018)
Catalysis	Tetracycline hydrochloride degradation using Fe^{0}-activated persulfate supported with mesoporous carbon.	(Jiang et al., 2018)
Photocatalysis	UV photocatalytic degradation of TC using TiO_2(P25) simultaneously combined with hydrodynamic cavitation.	(Wang et al., 2017b)
Photocatalysis	Photocatalysis using Fe-based metal organic frameworks combined with heterogenous AOP in the visible light degradation of TC hydrochloride.	(Zhang et al., 2019)
Photocatalysis	Visible light degradation of TC using $BiVO_4/TiO_2$/RGO	(Wang et al., 2019d)
Electrochemical oxidation	TC degradation through electrochemical oxidation with a Ti/Ti_4O_7 anode	(Wang et al., 2018c)

Photocatalysis	Visible light photocatalytic degradation of TC using synthesized $AgBr/Bi_2WO_6$.	(Huang et al., 2019)
Electro-oxidation	TC degradation by electro-peroxydisulfate using Fe_3O_4.	(Tang et al., 2021a)
Adsorption	TC removal through Fe/graphene	(Alatalo et al., 2019)
Adsorption	TC removal using biochar derived from sawdust.	(Zhou et al., 2017)
Photocatalysis	Visible light degradation of TC using Iron-based metal-organic framework.	(Wang et al., 2018b)
Photocatalysis	Visible light degradation of TC using low-cost red mud wastes.	(Shi et al., 2020b)
Photo-electro-Fenton	TC degradation in an electrolysis cell using a Fe_3O_4-graphite cathode.	(Liu et al., 2013)
Photocatalysis	Visible light degradation of tetracycline using TiO_2	(Wu et al., 2020)

2.4.2. Herbicide (2,4-dichlorophenoxy acetic acid (2,4-D))

2,4-D is posed as the 3rd most-used herbicide worldwide even though its use is prohibited in many countries (Samir et al., 2015). 2,4-D is a chlorinated hydrocarbon (Figure 2.7) commonly used in farmland for the control of leaf weeds and grasses. It is widely known to be carcinogenic and mutagenic, with low biodegradability in the environment (Leon-Fernandez et al., 2019, Alikhani et al., 2021). 2,4-D is included in the WHO Recommended Classification of Pesticides by Hazard (WHO Class II) and rated in category 4 as having an LD50 of 300 – 2000 mg/kg in the Globally Harmonized System of Classification and Labelling of Chemicals (GHS). 2,4-D is a moderately persistent chemical that is highly soluble in water and it has been reported that 91.7% eventually end up in water (Islam et al., 2018). Previous reports have shown that 2,4-D caused poisonings in humans with incidents such as vomiting, diarrhea, abdominal pain and other peripheral neuromuscular effects (Li et al., 2017a). Marouani et al. (2017) investigated the effect of 2,4-D on the reproductive parameters of male rats. They found a decrease in weight, a reduction in testosterone as well as increased abnormal spermatozoa pointing to its effect on reproductive health.

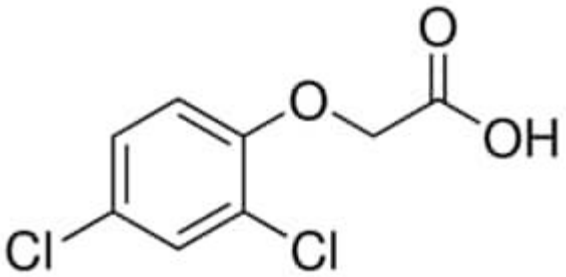

Figure 2.7: Chemical structure of 2,4-dichlorophenoxy acetic acid

The limit of 2,4-D allowed in potable water as set by the World Health Organisation (WHO) and the United States Environmental Protection Agency (USEPA) as 0.1 ppm or less (Trivedi and Mandavgane, 2018). Countries such as

the USA, China, Japan and the European Union have set maximum residue limits for 2,4-D in some food crops and drinking water as seen in Table 2.3. It is advantageous to de-chlorinate chlorinated hydrocarbons as this renders the resulting compound to be less toxic and easily biodegradable (Leon-Fernandez et al., 2019).

Table 2.3: Maximum residue limits for 2,4 dichlorophenoxy acetic acid (Mei et al., 2015)

Product	USA	EU	China	Japan
Rice (mg/kg)	0.5	0.1	-	-
Soybean (mg/kg)	0.02	0.05	0.01	0.05
Wheat (mg/kg)	2	2	2	0.5
Drinking water (µg/L)	100	0.1	30	30

Over the years, researchers have investigated methods for the remediation of 2,4-D from wastewater. Some of these techniques are shown in Table 2.4. The techniques include adsorption, ozonation, biological, bioelectrochemical and photocatalytic methods.

Table 2.4: Techniques used in the removal of 2,4-dichlorophenoxy acetic acid from wastewater

Method	Technique	Reference
Photocatalysis	Degradation of 2,4-D and 2,4-DP using pt-TiO_2 under UV light	(Abdennouri et al., 2015)
Adsorption	2,4-D adsorption using biochars and compared to commercial activated carbon	(Kearns et al., 2014)
Photocatalysis	2,4-D degradation using p25/β-CD	(Safa et al., 2019)
Bioelectrochemical	Dehalogenation of 2,4-D using a microbial fuel cell and a microbial electrolysis cell	(Leon-Fernandez et al., 2019)
Photocatalytic-biological	Photocatalytic UV/TiO_2 experiments followed by biological degradation of 2,4-D	(Samir et al., 2015)
Adsorption	2,4-D removal using carbon and silicon-based adsorbents.	(Arefieva et al., 2015)
Adsorption	Adsorption of 2,4-D onto granular activated carbon	(Ova and Ovez, 2013)
Photolysis and photo-Fenton	Removal of 2,4-D by H_2O_2-induced solar photolysis and photo-Fenton with Fe(III).	(Serra-Clusellas et al., 2018)
Photocatalysis	2,4-D degradation using Ag nanoparticles synthesized through the use of a plant (Cymbopogon nardus).	(Kamarudin et al., 2019)

Adsorption	Adsorption of 2,4-D onto Fly Ash	(Kusmierek and Swiatkowski, 2016)
Photocatalysis	2,4-D photocatalytic degradation using TiO_2 modified with Talc Nanocomposite.	(Ai et al., 2019)
Catalysis/Ozonation	Catalytic degradation of 2,4-D using CuO-Co_3O_4@CeO_2 by peroxymonosulfate	(Li et al., 2020b)
Catalysis/Ozonation	Degradation of 2,4-D using copper/ferrite nanoparticles and ozonation.	(Jaafarzadeh et al., 2017)
Photoelectrochemistry	Photoelectrochemical degradation of 2,4-D using TiO_2-doped nanotubes and formic acid.	(Xu et al., 2020b)
Biodegradation	Degradation of 2,4-D using *Cupriavidus gilardii*	(Wu et al., 2017)

2.4.3. Phenol

Phenol is an organic compound characterized by an attached hydroxyl group (Figure 2.8) which is produced through natural or anthropogenic activities (Mohamad Said et al., 2021). Phenols are found in industrial wastewaters from industries such as oil refining, petrochemicals, pharmaceuticals, coking, etc. and are classified as a major pollutant found in water (Al Bsoul et al., 2021, Liu et al., 2018b). Even at low concentrations, the discharge of phenol into the environment can cause significant damage to the flora and fauna (Vidal and Moraes, 2018). The U.S. Environmental Protection Agency (USEPA) has set the content of phenol in wastewater effluent to be in the range of 0.5 and 1 ppm while the potable water limit is 0.5 ppb (Bin-Dahman and Saleh, 2020). Phenol can affect the nervous and cardiovascular systems through the easy penetration of the skin and its mucus barriers. It also causes severe skin lesions and possible death making it toxic to human health (Dehmani and Abouarnadasse, 2020). Long-term exposure has also been seen to result in muscle weakness, tremors and irregular breathing while more chronic effects include diarrhea, weight loss, and anorexia amongst others (Villegas et al., 2016).

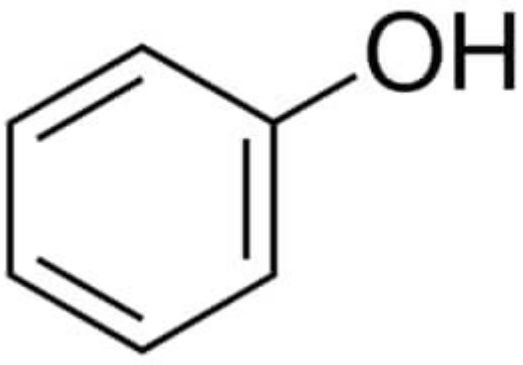

Figure 2.8: Chemical structure of phenol

Various technologies have been used for the removal of phenol from wastewater. These include adsorption, distillation, removal by membrane process, chemical oxidation, biological process and advanced oxidation processes (Villegas et al., 2016). Bin-Dahman and Saleh (2020) studied the adsorption process of phenol using carbon nanotubes (CNT) grafted with polyethylene glycol (PEG). The process was carried out by varying parameters such as adsorbent dosage, pH and contact time. The removal was optimal at pH 4-9 with maximum removal at 20 mg adsorbent dosage and 30 min contact time. Liu et al. (2018b) synthesized a microwave-induced H_2O_2-CuO_x/GAC catalyst for Fenton-like catalytic oxidation of phenol and measured 88.6% phenol removal showing the advantages of combining technologies for higher efficiency. In the study by Vaiano et al. (2018), a Ag/ZnO photocatalyst was synthesized for the degradation of phenol under UV light irradiation with an almost total removal of phenol measured in 180 min. The biodegradation of phenol has also been investigated in the work by Liu et al. (2020) where *Acinetobacter radioresistens* was used. The optimal degradation efficiency was measured at 30°C, pH 6 and 500 mg/L phenol.

2.5. Other uses of photocatalyst

2.5.1. Hydrogen generation from water through water splitting

Hydrogen generation is of utmost importance in the near future as it can be used in fuel cells for the generation of clean energy (Kudo and Miseki, 2009). Various methods explored in the generation of hydrogen include biological hydrogen production, coal hydrogen production, hydrocarbon hydrogen production and water splitting (Li et al., 2021a) from compounds containing hydrogen such as water, biomass and fossil fuels (Chen et al., 2010) but some of these techniques usually require extreme conditions of temperature and pressure. Water splitting is the cheapest and simplest system, however, it is also faced with low practicality

for large-scale applications as it has a low conversion rate (Huck et al., 2020). Efforts continue to rise in the development of strategies for the reduction of global warming such as the development of photocatalytic nanocomposite materials for the evolution of H_2 under solar irradiation. The technique adopted for hydrogen evolution is similar to those utilized in the degradation of organic contaminants in wastewater. After the generation of electron and holes during the irradiation of photocatalyst, the reactive pair takes part in reduction and oxidation reactions with available chemical species resulting in the generation of hydrogen and oxygen as seen in Equation 2.7 to Equation 2.9 (Gopinath and Nalajala, 2021, Yuan et al., 2016) and illustrated in Figure 2.9:

$$H_2O \rightarrow \frac{1}{2} O_2 + H_2 \quad (2.7)$$

$$2H^+ + 2e^- \rightarrow H_2 \quad (2.8)$$

$$2H_2O + 4h^+ \rightarrow 4H^+ + O_2 \quad (2.9)$$

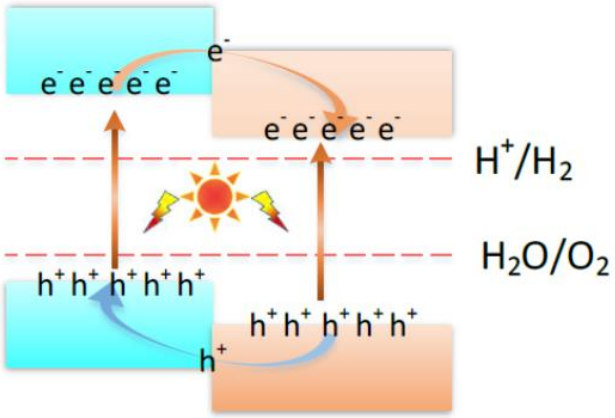

Figure 2.9: Schematic illustration of photocatalytic water splitting (Zhang et al., 2018)

2.5.2. CO_2 conversion into renewable fuels

CO_2 is one of the greenhouse gases contributing to about 60% of global warming (Khan and Tahir, 2019). The excessive use of fossil fuels and industrialization

has resulted in research into potential CO_2 capture, storage and future usage. Simulating artificial photocatalysis for CO_2 reduction is advantageous as not only does it reduce the effects of CO_2, chemicals for future energy supply such as ethanol, methane and methanol are produced (Yuan and Xu, 2015). The photocatalysts play the role of green plants in converting CO_2 into fuel using UV or visible light as illustrated in Figure 2.10 following reaction pathways in Equation 2.10 to Equation 2.15 (Yuan and Xu, 2015, Liu et al., 2015).

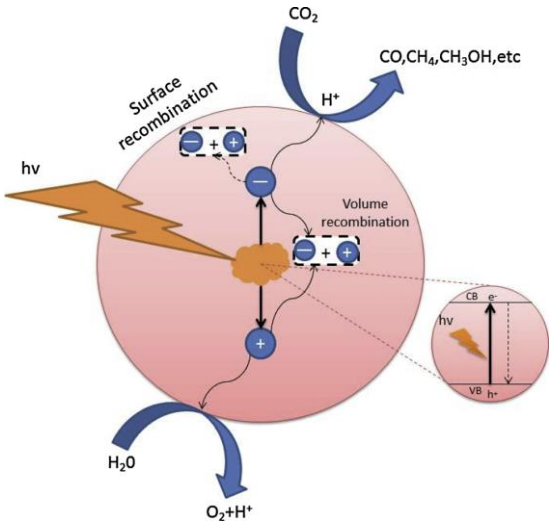

Figure 2.10: Diagram depicting the photocatalytic reduction of CO_2 (Fu et al., 2019)

$$CO_2 \rightarrow CO \rightarrow C\cdot \rightarrow CH_2 \rightarrow CH_4 \quad (2.10)$$

$$CO_2 + 2H^+ + 2e^- \rightarrow CO + H_2O \quad (2.11)$$

$$CO_2 + 8H^+ + 8e^- \rightarrow CH_4 + 2H_2O \quad (2.12)$$

$$CO_2 + 2H^+ + 2e^- \rightarrow HCO_2H \quad (2.13)$$

$$CO_2 + 6H^+ + 6e^- \rightarrow CH_3OH + H_2O \quad (2.14)$$

$$CO_2 + 2H^+ + 4e^- \rightarrow HCHO + H_2O \quad (2.15)$$

CHAPTER 3 – MATERIALS AND METHODS

3.1. Materials and reagents

Materials used in the synthesis process were of analytical grade and used without special treatment. Bismuth (III) nitrate pentahydrate ($Bi(NO_3)_3.5H_2O$), cetyltrimethylammonium chloride (CTAC), tetracycline, 2,4 dichlorophenoxy acetic acid (2,4-D), HPLC grade methanol, 2-propanol, p-benzoquinone and oxalic acid dehydrate were purchased from Sigma Aldrich. Glacial acetic acid, silver nitrate ($AgNO_3$), Phenol, H_2SO_4, NaOH, $NaNO_3$ and trimethylamine were purchased from Glassworld, South Africa. $NaNO_2$, Na_2SO_4, $ZnSO_4.7H_2O$, $MgSO_4.7H_2O$ and NaCl were purchased from Merck SA. HPLC-grade acetonitrile was purchased from VWR chemicals. K_2SO_4 and $CaSO_4.0.5H_2O$ were purchased from SAARCHEM. Deionized water used in this study was from an Elga Purelab Chorus unit except stated otherwise. To investigate the influence of water matrix, the water samples were collected from the Daspoort wastewater treatment plant in Gauteng, South Africa.

3.2. Photocatalyst synthesis

3.2.1. Preparation of $Bi_{24}O_{31}Cl_{10}$

$Bi(NO_3)_3.5H_2O$ (4.85 g) was dissolved in 30 mL water and 15 mL acetic acid. 1 mol (3.2 g) of CTAC was dissolved in 30 mL water. The CTAC solution was added to the bismuth nitrate solution and the mixture was continuously stirred for one hour. The solution was then put in the autoclave for 12 h at 120ºC. The precursor material (BiOCl) was then collected and washed three times with ethanol and three times with water. This was then dried at 80ºC for 4 h. The dried

white particles were calcined in a furnace at 660ºC for 6 h until a light yellow powder was noticed (Wang et al., 2014).

3.2.2. Preparation of $AgCl/Bi_{24}O_{31}Cl_{10}$

The synthesized $Bi_{24}O_{31}Cl_{10}$ (0.2 g) was added to 50 mL of water while being continuously stirred. A 10 mL solution containing 50 mg CTAC was added to the suspension and stirred for 1 h. $AgNO_3$ (27 mg) dissolved in 10 mL water was slowly added into the $Bi_{24}O_{31}Cl_{10}$/CTAC suspension and stirred continuously for 2 h. The collected precipitate was washed with ethanol and water before being dried at 60°C for 8 h. This resulted in 10% AgCl on a mass basis being deposited on the BOC to form a composite photocatalyst. The process was then repeated using different stoichiometric amounts to prepare 20%AgCl/BOC and 50%AgCl/BOC as illustrated in Scheme 3.1 and Equation 3.1 – Equation 3. 4 (Li et al., 2017b).

$$Bi(NO_3)_3 + C_{16}H_{33}(CH_3)_3N\text{-}Cl + H_2O \rightarrow BiOCl + C_{16}H_{33}(CH_3)_3N^+ + 2H^+ + 3NO_3 \quad (3.1)$$

$$BiOCl \xrightarrow{Hv\ 660\ °C} Bi_{24}O_{31}Cl_{10} \quad (3.2)$$

$$Bi_{24}O_{31}Cl_{10} + AgNO_3 \rightarrow Ag^+ \text{-} Bi_{24}O_{31}Cl_{10} + NO^{3-} \quad (3.3)$$

$$Ag^+\text{-}Bi_{24}O_{31}Cl_{10} + C_{16}H_{33}(CH_3)_3N\text{-}Cl \rightarrow AgCl/Bi_{24}O_{31}Cl_{10} + C_{16}H_{33}(CH_3)_3N^+ \quad (3.4)$$

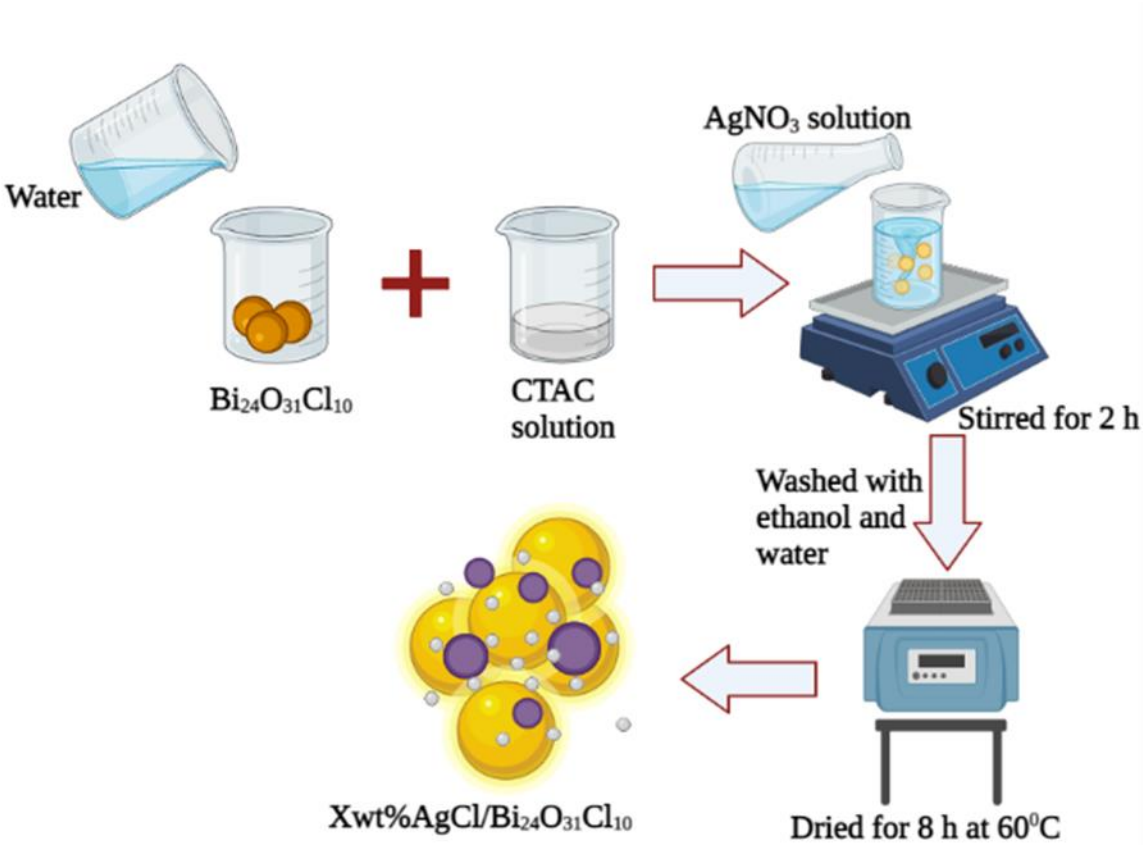

Scheme 3.1: Depiction of Xwt%AgCl/$Bi_{24}O_{31}Cl_{10}$ synthesis

3.3. Characterization techniques

3.3.1. Scanning Electron Microscopy (SEM)/Energy Dispersive Spectroscopy (EDS)

The morphology of the synthesized particles was captured on a Zeiss Crossbeam 540 FEG SEM instrument using the Oxford instruments detector and Aztec 3.0 software SP1. A strip with the samples was attached to an aluminum plate before being coated with carbon. The carbon coater used is a SEM auto-coating unit E2500 (Polaron Equipment Ltd). EDS was also carried out to investigate the elemental analysis and mapping.

3.3.2. X-ray Diffraction (XRD)

XRD analysis was performed using a PANalytical X'Pert Pro powder diffractometer in θ–θ configuration with an X'Celerator detector, variable divergence- and fixed receiving slits with Fe filtered Co-Kα radiation (λ=1.789 A). The mineralogy was determined by selecting the best–fitting pattern from the ICSD database to the measured diffraction pattern, using X'Pert Highscore plus software.

3.3.3. Ultraviolet-visible spectroscopy (UV-VIS)

The optical absorption spectra were recorded using a VWR UV-1600PC Spectrophotometer at an interval of 1 nm from 600 nm to 200 nm. The photocatalyst particles were dispersed in ultrapure water before being transferred into a clean and dry cuvette. Ultrapure water served as blank to ensure that light loss due to absorption and scattering by the solvent is accounted for.

3.3.4. Brunauer-Emmett-Teller (BET)

The nitrogen sorption isotherm and BET surface area were measured on a Micromeritics TriStar II with a liquid nitrogen temperature of 77.350 K. This was done to determine the specific surface area and pore size of the synthesized particles. The samples were dried for 24 h prior to the analysis under pure nitrogen flow to remove all water molecules.

3.3.5. Thermogravimetric analysis (TGA)

This analysis was done using an SDT Q600 instrument with heating in Nitrogen gas from ambient temperature to 800 °C. This was done to investigate the thermal degradation of the synthesized photocatalysts. 5 mg of dried samples were weighed on the hang-down pan.

3.3.6. Photoluminescence (PL)

The PL spectra of the photocatalyst were measured on a Shimadzu RF-6000 Spectro fluorophotometer. Equal amounts of the samples were dispersed in DI water and transferred to a cuvette for analysis in the fluorophotometer. The excitation and emission were carried out at wavelength of 241 nm and 246 nm

3.3.7. Transmission Electron Microscopy (TEM)

The morphologies and structure were further investigated by transmission electron microscopy (TEM) (JEOL JEM 2100F). Samples were placed on a TEM mesh grid and coated with a light layer of carbon for stabilization.

3.4. Degradation studies

Stock solutions (100 mg/L) were prepared by dissolving 0.1 g of 2,4-D and TC in 5 mL of acetonitrile and methanol respectively before being topped with water to the 1 L mark. Phenol stock solutions were prepared directly in DI water. Consequently, dilutions were prepared from these stock solutions to make the required concentrations. Typically, 0.1 g of the synthesized photocatalyst was added to a 200 mL pollutant solution (20 mg/L) and stirred for 30 min in the dark

to achieve the adsorption-desorption equilibrium. The concentration of phenol was varied from 5 mg/L to 30 mg/L while the catalyst dosage was varied from 0.25 g/L to 1 g/L. Thereafter, the suspension was irradiated under six 30 W Fluoro lamps to simulate solar light as illustrated in Figure 3.1. The photocatalytic experiments were carried out in a 400 mL beaker containing a 200 mL solution and a magnetic stirrer to ensure a homogenous solution of pollutant and catalyst. An aliquot of 3 mL samples was collected at 60 min intervals. These aliquots were centrifuged and filtered using a 0.45 µm syringe filter to remove particles before analysis. The unadjusted pH of 2,4-D and TC are 4 and 5.3. The pH of the contaminant was adjusted using 0.1 M H_2SO_4 and NaOH. The batch experiments were carried out in triplicates and the average data is reported.

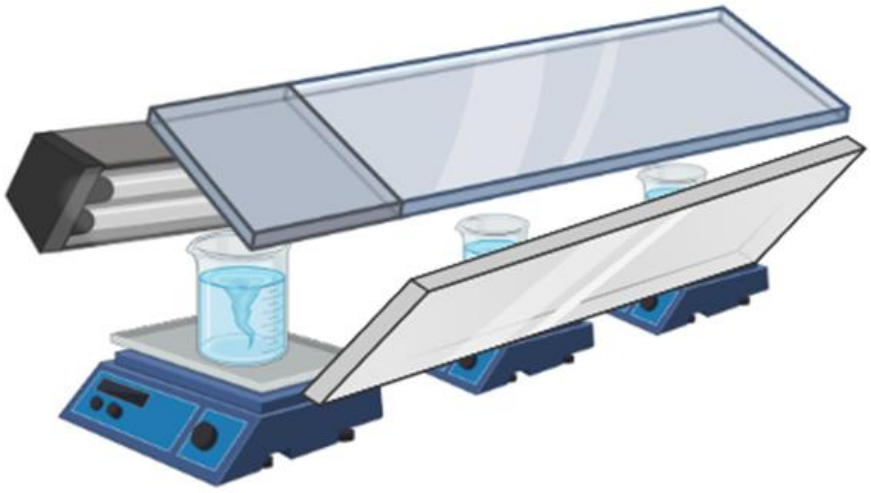

Figure 3.1: Low-wattage experimental set-up

3.5. Analytical techniques

3.5.1. HPLC analysis

The concentration of 2,4-D was quantified on a Waters HPLC with a Waters 2489 UV/VIS detector using a Waters PAH C18 (4.6 x 250 mm, 5 µm) column. The mobile phases consist of two solvents 40% 0.1% acetic acid in water and 60%

methanol. The injection volume was 10 µL at a flow rate of 1 mL/min, the detector wavelength was set at 284 nm and the column temperature at 35°C. Tetracycline was detected using two solvents 47% methanol and 53% 0.01 mol/L oxalic acid. The detector wavelength was set to 355 nm at 10 µL and a flow rate of 1 mL/min with column temperature at 40°C. Phenol was detected using 30% DI water (containing 1% acetic acid) and 70% acetic acid in acetonitrile with 280 nm absorption wavelength, 1.2 mL/min flow rate and injection volume of 10 µL.

3.5.2. Ion Chromatograph

Inorganic ions in the real water samples were quantified using a 940 Professional IC varion ion chromatography (Metrohm, Herisau, Switzerland) with a separation column Metrosep C6-250/4.0 (Metrohm, Switzerland) and C 6 eluent 8 mM oxalic acid (Metrohm, Herisau, Switzerland).

3.5.3. Total organic carbon analysis (TOC)

The mineralization of the organic contaminants was measured using a Shimadzu Total organic carbon TOC-V WP analyzer. The samples were filtered with a 0.45 µm syringe filter to remove particles before being transferred into 40 mL vials. The analysis samples were diluted with one-part sample and three-part DI water. The mobile phase used was a persulfate oxidizer solution and a phosphoric acid solution.

CHAPTER 4 – MATERIAL CHARACTERIZATION

The synthesized materials were characterized using various techniques. This was done to validate the material and investigate them for their material physical characteristics, optical and photonic properties. This chapter describes various characterization techniques such as x-ray diffraction (XRD), scanning electron spectroscopy (SEM), transmission electron microscopy (TEM), ultraviolet-visible spectroscopy (UV-VIS), photoluminescence (PL), Brunauer-Emmert-Teller (BET), and thermogravimetric analysis (TGA).

4.1. X-ray diffraction (XRD)

The crystalline structure and purity of the synthesized materials were investigated using XRD and the spectra are illustrated in Figure 4.1**.** The particles had a high crystallinity with monoclinic $Bi_{24}O_{31}Cl_{10}$ (JCPD No. 75-0877) (Kang et al., 2020a) as indexed in diffraction peaks present at 12.6°, 29°, 34.5°, 36.6°, 35.2°, and 37.5°. It is evident that the characteristic peaks of BOC remain present in the composite photocatalyst, depicting that the assembly of AgCl on the surface of BOC does not change its characteristics. The intensities of the diffraction peaks of BOC reduced as the AgCl content in the composite photocatalyst increased. The presence of AgCl was evidenced by the appearance of new peaks at 30.8° and 37.7° in the composite spectra. A comparison of the spectra for the BiOCl precursor and the calcined BOC revealed a clear phase transformation from the near amorphous BiOCl to a highly crystalline BOC product. The average crystallite size of the photocatalysts could be estimated from the Scherrer formula: $D = K\lambda/\beta\cos\theta$ where D is the crystallite size in nm, K is a constant of 0.9, λ is 0.1789 in nm, β is the width of the line at half-maximum height in radians and θ is the angle of diffraction. The calculated average crystallite size of the

synthesized photocatalyst based on two prominent peaks (12.6° and 47.7°) of BOC is calculated to be 52.5 – 82.8 nm.

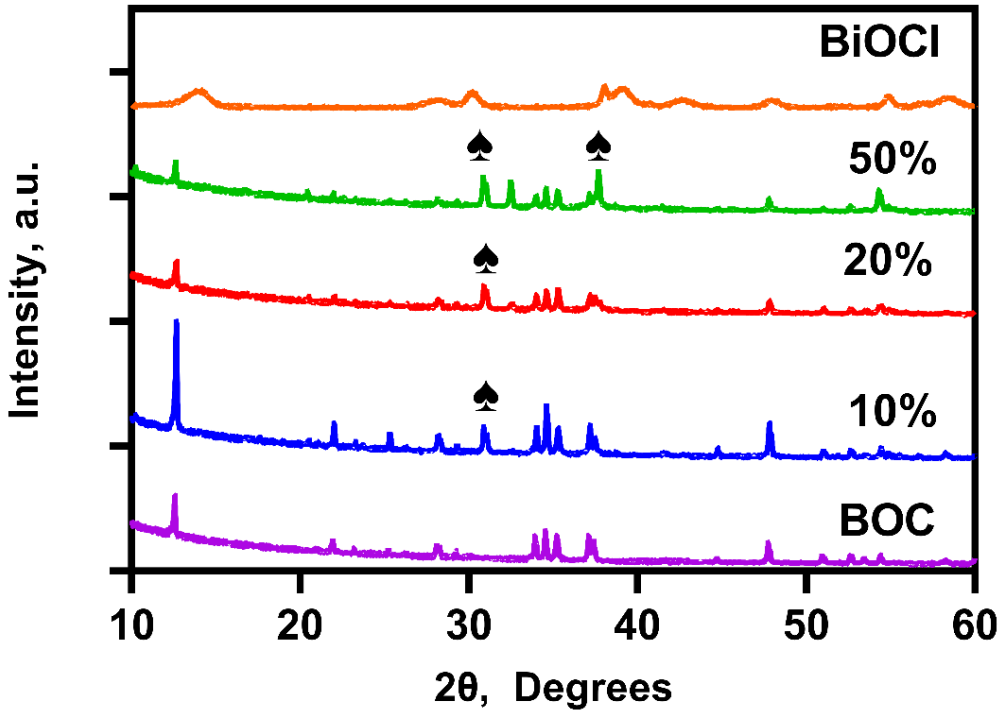

Figure 4.1: XRD spectra of prepared photocatalyst

4.2. Scanning electron microscopy/ Energy dispersive x-ray spectroscopy (SEM/EDS)

Figure 4.2a shows the SEM image of the as-prepared BOC. Clustered, micron-sized, rod-like particles with angular surfaces were observed. Figure 4.2b to Figure 4.2d, reveal that the AgCl precipitated on the surface of the $Bi_{24}O_{31}Cl_{10}$ with near-spherical particles forming agglomerates. As expected, there was a noticeable increase in the density of AgCl particles with an increase in the percentage content with the highest coating observed in the 50%AgCl/BOC composite. This confirms the presence of two different materials in the

synthesized composite material. Nano-sized AgCl particles are seen to be self-assembled on the surface of larger rod-like BOC materials. EDS mapping, spectra and elemental analysis of the synthesized photocatalysts indicated the presence of Bi, O and Cl in the BOC photocatalyst Table 4.1 and Figure 4.3 and the weight ratio of Bi: Cl corresponds to a 2.4/1 molecular ratio showing that BOC was formed (Jin et al., 2018). Xwt%AgCl was loaded on the surface of the BOC using pre-calculated stoichiometric ratios and the elemental mapping is shown in Figure 4.4 to Figure 4.6 depicting the presence and distribution of Ag, Bi, O and Cl in the prepared composite catalyst.

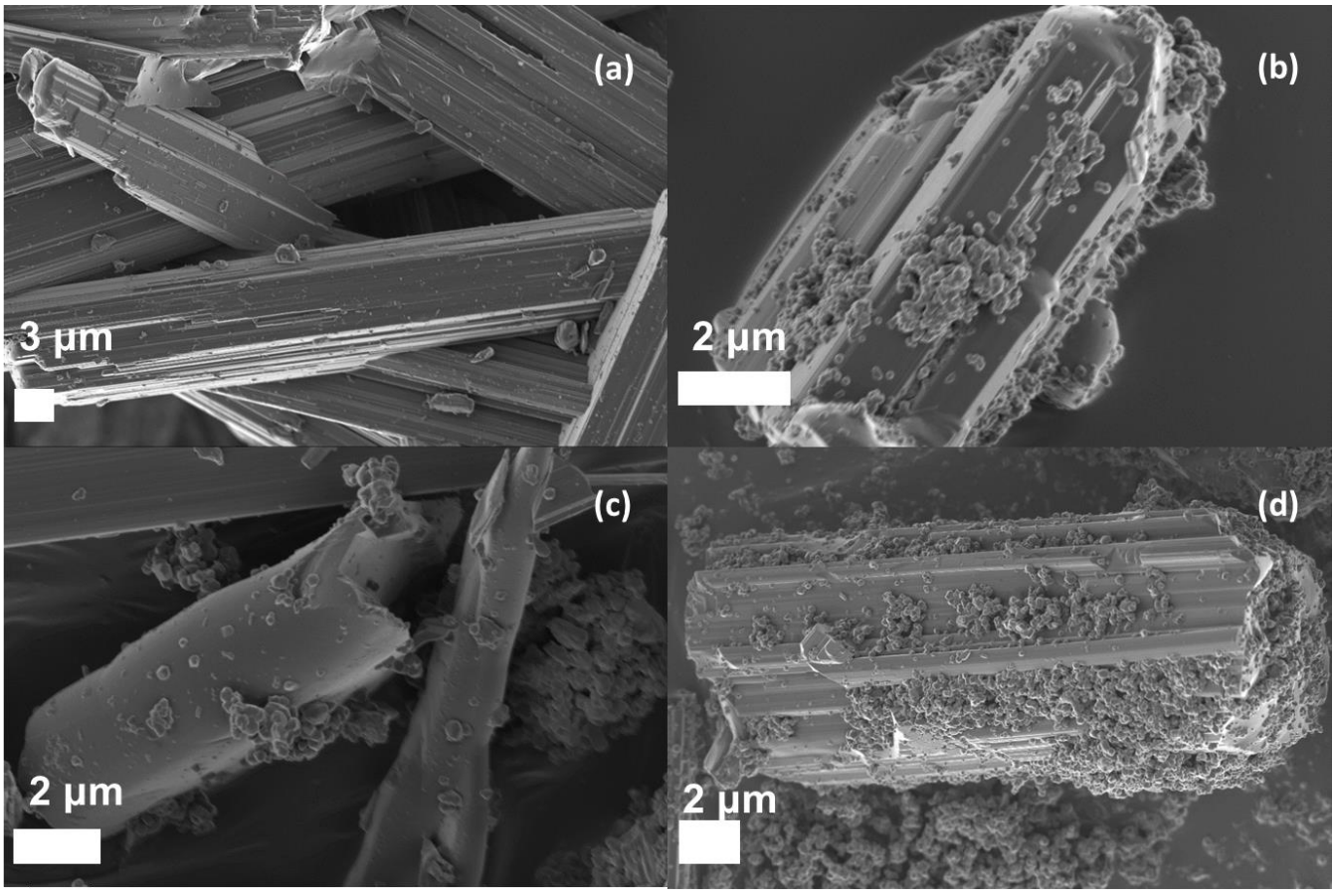

Figure 4.2: SEM image of (a) $Bi_{24}O_{31}Cl_{10}$, (b) 10%AgCl/$Bi_{24}O_{31}Cl_{10}$, (c) 20%AgCl/$Bi_{24}O_{31}Cl_{10}$, and (d) 50%AgCl/$Bi_{24}O_{31}Cl_{10}$

Table 4.1: Elemental analysis of as-prepared $Bi_{24}O_{31}Cl_{10}$

Element	Wt%	Wt% Sigma
O	9.69	
Cl	5.92	0.11
Bi	84.39	0.21
Total:	100.00	

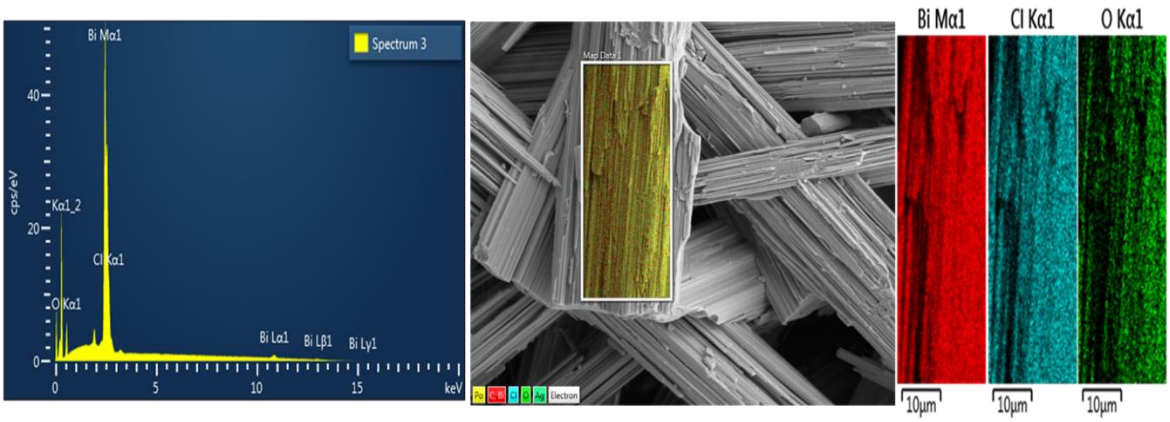

Figure 4.3: SEM-EDS mapping of $Bi_{24}O_{31}Cl_{10}$

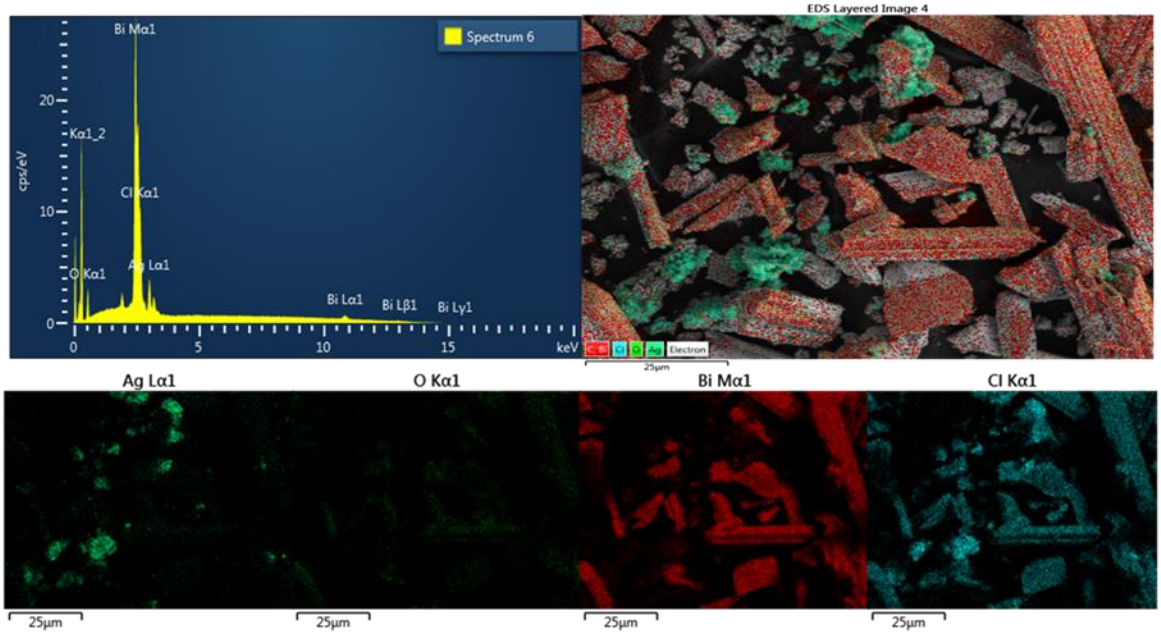

Figure 4.4: SEM-EDS mapping of 10%AgCl/$Bi_{24}O_{31}Cl_{10}$

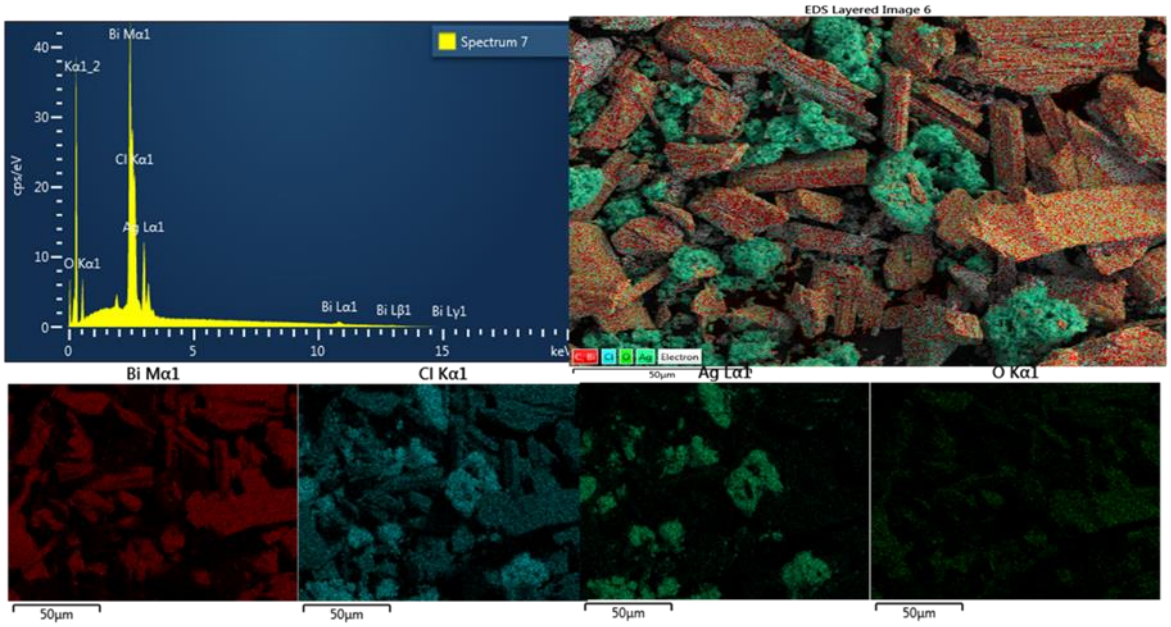

Figure 4.5: SEM-EDS mapping of 20%AgCl/$Bi_{24}O_{31}Cl_{10}$

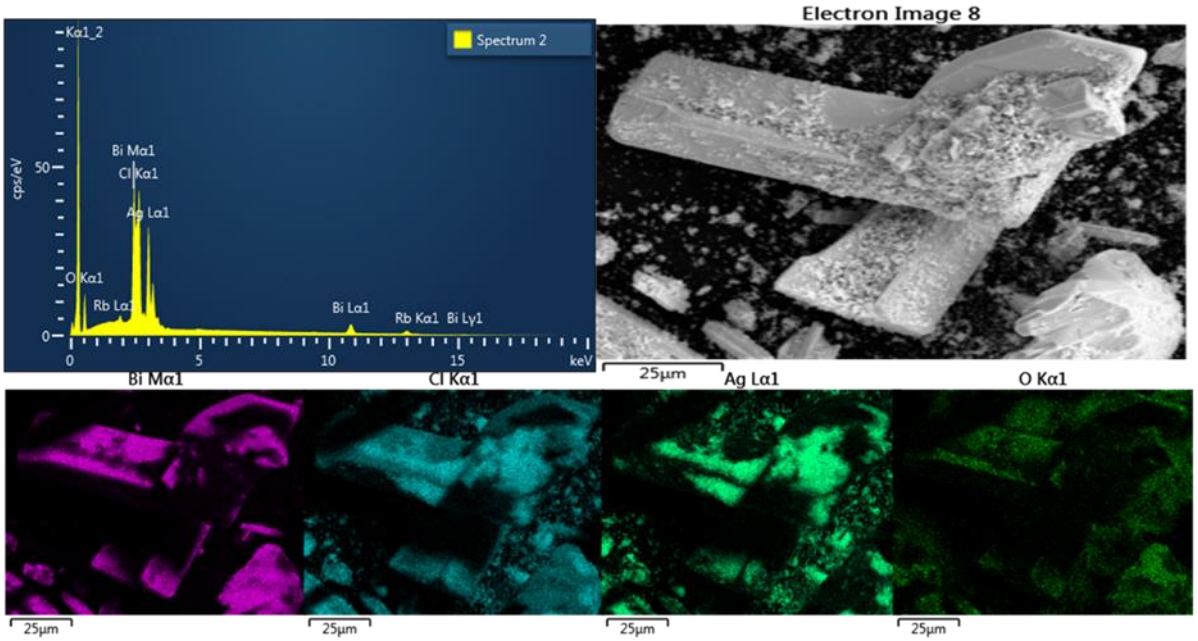

Figure 4.6: SEM-EDS mapping of 50%AgCl/$Bi_{24}O_{31}Cl_{10}$

4.3. Transmission electron microscopy (TEM)

Figure 4.7 **(**a) to (d) show the TEM images of the synthesized $Bi_{24}O_{31}Cl_{10}$, 10%AgCl/$Bi_{24}O_{31}Cl_{10}$, 20%AgCl/$Bi_{24}O_{31}Cl_{10}$ and 50%AgCl/$Bi_{24}O_{31}Cl_{10}$

photocatalyst materials. In Figure 4.7a, micron-sized rod-like $Bi_{24}O_{31}Cl_{10}$ particles can be seen while in Figure 4.7b to Figure 4.7d, the presence of irregular structural morphology was confirmed showing spherical particles being deposited on the surface of the $Bi_{24}O_{31}Cl_{10}$ with the volumes increasing as the percentage amount of AgCl deposited increased.

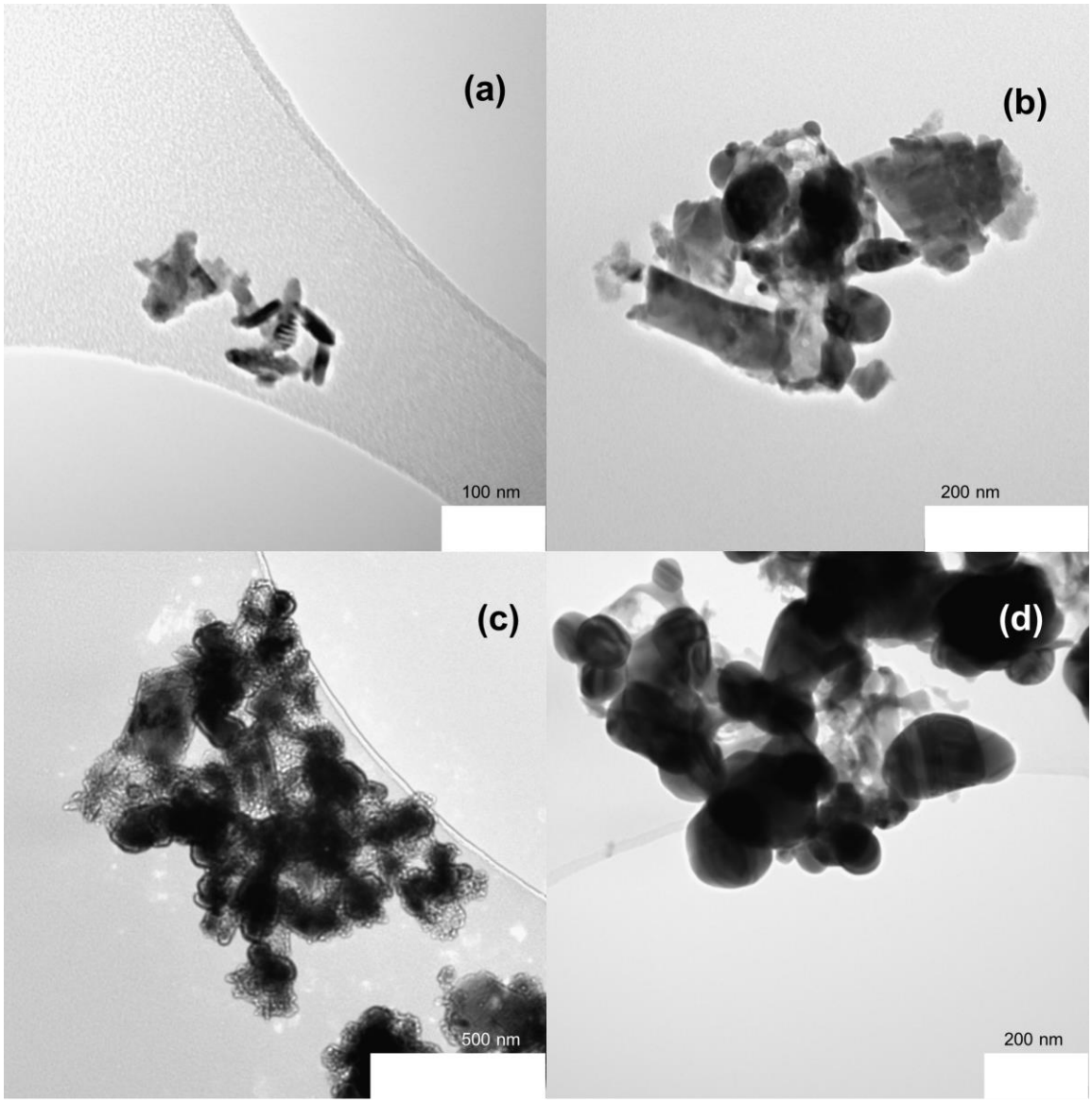

Figure 4.7: TEM image of (a) $Bi_{24}O_{31}Cl_{10}$, (b) 10%AgCl/$Bi_{24}O_{31}Cl_{10}$, (c) 20%AgCl/$Bi_{24}O_{31}Cl_{10}$ and (d) 50%AgCl/$Bi_{24}O_{31}Cl_{10}$

4.4. Ultraviolet-visible spectroscopy (UV-VIS)

It should be noted that the optical properties of a given material are extremely important when selecting an efficient photocatalyst. The light absorption ranges of the synthesized catalysts were investigated using UV-vis analysis. The resulting spectra are presented in Figure 4.8. The pure BOC photocatalyst featured higher adsorption in the ultraviolet light region with minimal adsorption recorded beyond the visible range. The addition of AgCl immediately widened the light adsorption into the visible light absorption region (400 to 600 nm). The increase in visible light adsorption with an increase in wt% of AgCl was attributed to the SPR effects of the silver nanoparticles (Liang et al., 2018). This enabled the synthesized composite photocatalyst, Xwt%AgCl/BOC to absorb visible light and potentially improve its photocatalytic activity. The absorption band edge of BOC was estimated at 420 nm.

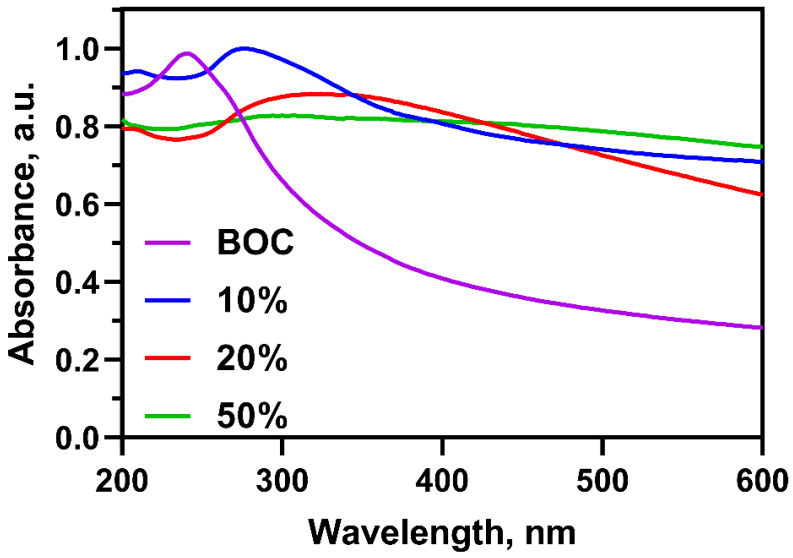

Figure 4.8: UV-Vis spectra of $Bi_{24}O_{31}Cl_{10}$, 10%AgCl/$Bi_{24}O_{31}Cl_{10}$, 20%AgCl/$Bi_{24}O_{31}Cl_{10}$ and 50%AgCl/$Bi_{24}O_{31}Cl_{10}$

4.5. Photoluminescence (PL)

The photoluminescence spectra of the synthesized photocatalysts are shown in Figure 4.9. The intensity of the emission illustrates the rate of electron-hole separation of the synthesized photocatalyst. The higher the intensity, the higher the probability of electron-hole pair recombination ultimately resulting in reduced photocatalytic activity (Ghattavi and Nezamzadeh-Ejhieh, 2020). The intensity of the PL spectra increases in the following order: BOC>10%AgCl/BOC >20%AgCl/BOC>50%AgCl/BOC. This trend showed that assembling different wt% of AgCl on the surface of BOC resulted in improved electron-hole separation which hints towards improved photocatalytic efficiency from the material.

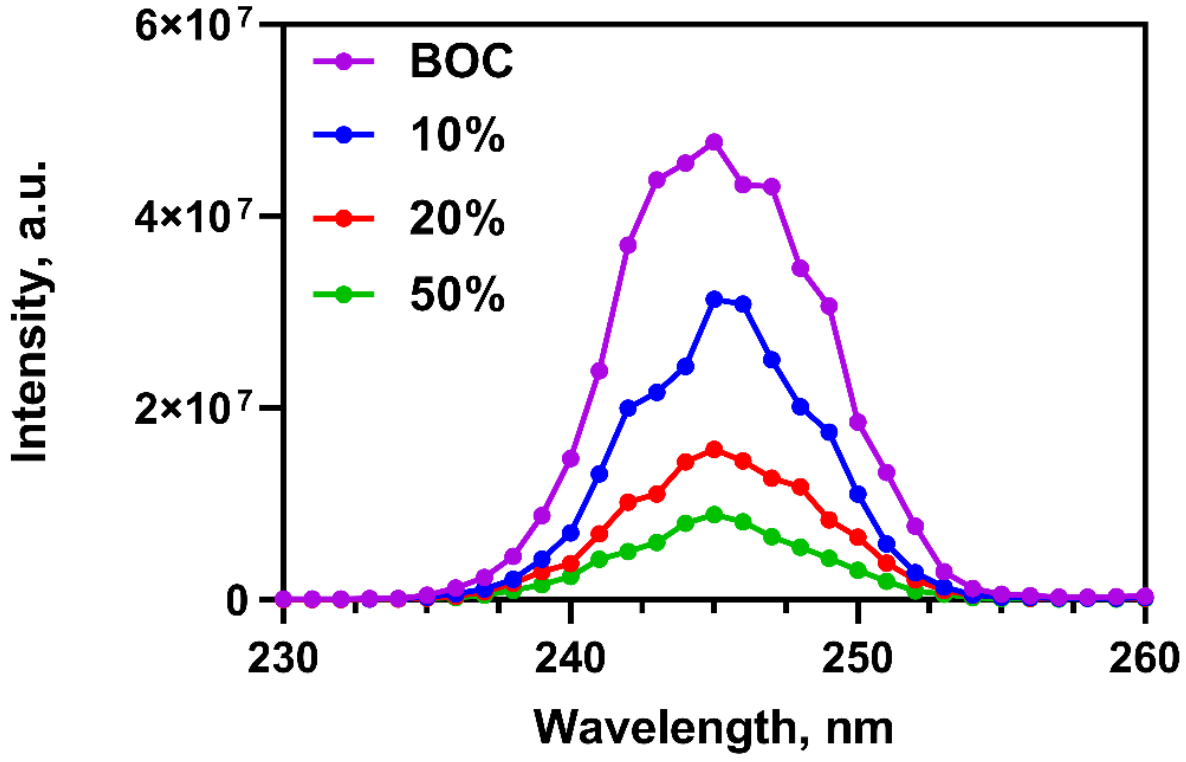

Figure 4.9: Photoluminescence spectra of $Bi_{24}O_{31}Cl_{10}$, 10%AgCl/$Bi_{24}O_{31}Cl1_0$, 20%AgCl/$Bi_{24}O_{31}Cl_{10}$ and 50%AgCl/$Bi_{24}O_{31}Cl_{10}$

4.6. Brunauer-Emmert-Teller (BET)

N_2 desorption-adsorption isotherms of the synthesized photocatalysts are shown in Figure 4.10. BOC has a Brunauer-Emmert-Teller (BET) surface area of 0.0092 m^2/g. After the introduction of AgCl on the surface, the BET surface area increases to 0.55 m^2/g for 10%AgCl/BOC, 1.09 m^2/g for 20%AgCl/BOC and 1.50 m^2/g for 50%AgCl/BOC. The surface area increased with an increasing amount of AgCl. This is advantageous for photocatalysis as the photocatalyst with a higher surface area will have more active sites and therefore exhibit better photocatalytic performance (Wen et al., 2017). The adsorption-desorption isotherms show a type IV isotherm with an H3 hysteresis loop indicating the presence of mesopores on the surface of the photocatalyst.

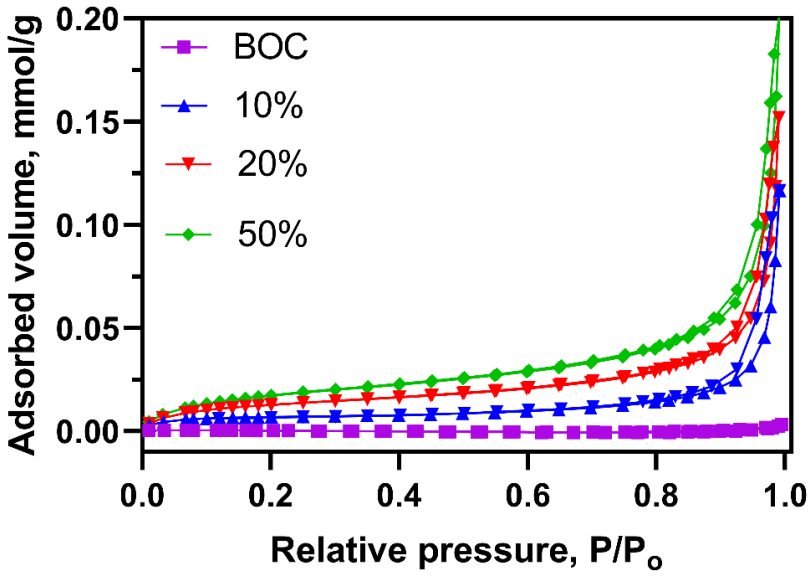

Figure 4.10: N_2 adsorption-desorption isotherm of $Bi_{24}O_{31}Cl_{10}$, 10%AgCl/$Bi_{24}O_{31}Cl1_0$, 20%AgCl/$Bi_{24}O_{31}Cl_{10}$ and 50%AgCl/$Bi_{24}O_{31}Cl_{10}$

4.7. Thermogravimetric analysis (TGA)

Thermogravimetric analysis was performed on the synthesized photocatalyst to determine the thermal stability of $Bi_{24}O_{31}Cl_{10}$ and X%AgCl/$Bi_{24}O_{31}Cl_{10}$ (Figure 4.11). The overall weight loss in the $Bi_{24}O_{31}Cl_{10}$ was 7%. Gradual weight loss in all materials occurred until 600ºC at which 2% weight loss had occurred which is attributed to loss of moisture. The weight loss observed after 600°C was attributed to chlorine ions volatilizing into the air due to heating (Cui et al., 2016). The relatively low mass loss observed in this temperature range reveals the thermal stability of the as-prepared photocatalysts.

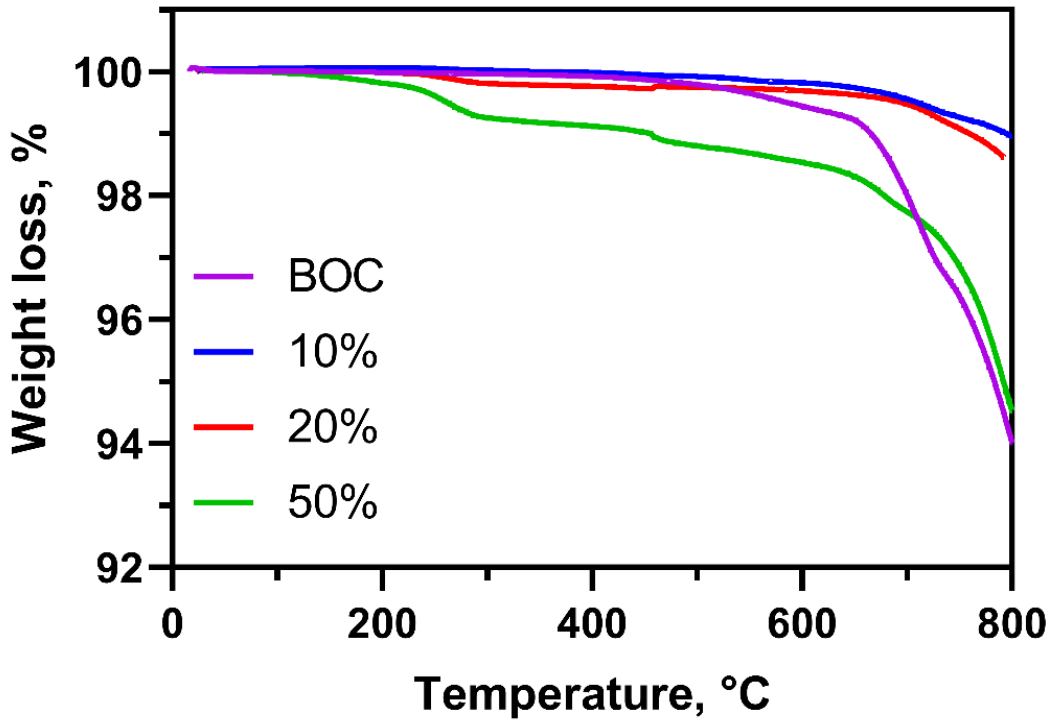

Figure 4.11: TGA curves of $Bi_{24}O_{31}Cl_{10}$, 10%AgCl/$Bi_{24}O_{31}Cl1_0$, 20%AgCl/$Bi_{24}O_{31}Cl_{10}$ and 50%AgCl/$Bi_{24}O_{31}Cl_{10}$

CHAPTER 5 – PHOTOCATALYTIC DEGRADATION STUDIES OF TETRACYCLINE AND 2,4-DICHLOROPHENOXY ACETIC ACID

The efficiency of the synthesized photocatalyst materials was investigated in the degradation of two classes of pollutants – antibiotics and herbicides. The visible light photocatalytic degradation of the catalysts was evaluated in the degradation of tetracycline and 2,4-dichlorophenoxy acetic acid while also investigating the effects of various factors such as the effect of the photocatalyst loading, the effect of initial pollutant loading and the effect of the solution pH. The extent of mineralization and the reusability of the photocatalyst were also investigated. Trapping experiments were carried out to propose a degradation mechanism for the degradation process.

5.1. Photocatalytic degradation of tetracycline

The efficacy of the synthesized photocatalyst materials ($Bi_{24}O_{31}Cl_{10}$, 10%AgCl/$Bi_{24}O_{31}Cl_{10}$, 20%AgCl/$Bi_{24}O_{31}Cl_{10}$ and 50%AgCl/$Bi_{24}O_{31}Cl_{10}$) was evaluated by using 20 mg/L of simulated tetracycline solution under visible light irradiation and a catalyst loading of 0.5 g/L. In Figure 5.1, after 4 h of light irradiation only (photolysis), there was negligible removal of tetracycline. In the same time frame, 10%AgCl/$Bi_{24}O_{31}Cl_{10}$, 20%AgCl/$Bi_{24}O_{31}Cl_{10}$ and 50%AgCl/$Bi_{24}O_{31}Cl_{10}$ measured a degradation efficiency of 55%, 61% and 82% respectively with 50%AgCl/$Bi_{24}O_{31}Cl_{10}$ having the highest removal efficiency. This was 2.2, 2.44 and 3.28 more efficient than using $Bi_{24}O_{31}Cl_{10}$ only (25%). The result shows the effectiveness of combining AgCl and $Bi_{24}O_{31}Cl_{10}$ to form a composite photocatalyst for the visible light degradation of tetracycline.

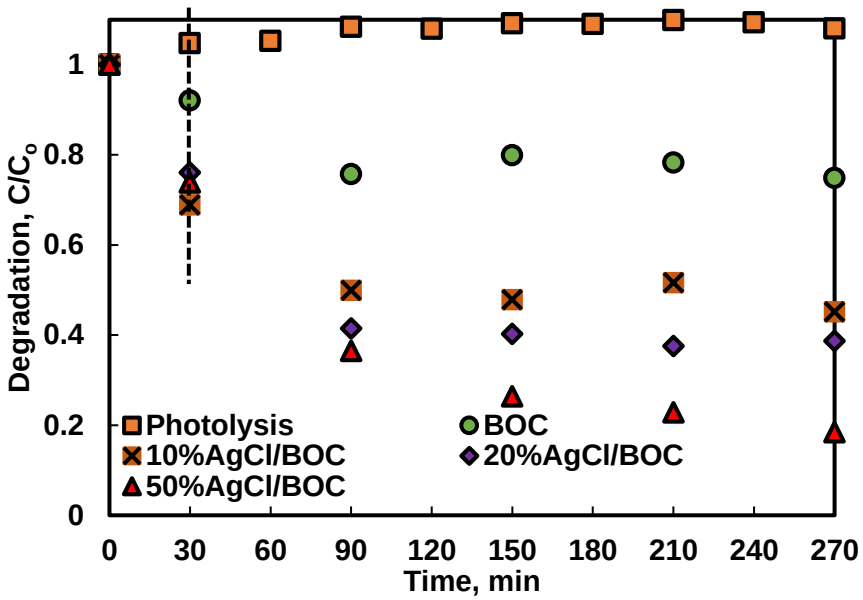

Figure 5.1: Tetracycline degradation in the presence of light-only (photolysis), $Bi_{24}O_{31}Cl_{10}$, 10%AgCl/$Bi_{24}O_{31}Cl_{10}$, 20%AgCl/$Bi_{24}O_{31}Cl_{10}$, 50%AgCl/$Bi_{24}O_{31}Cl_{10}$ at initial conditions (C_0: 20 mg/L, $C_{catalyst}$: 0.5 g/L)

5.1.1. Effect of photocatalyst loading

The effect of photocatalyst loading was investigated in the degradation of tetracycline and the results are presented in Figure 5.2. The degradation efficiency of the photocatalyst measured an initial increase from 64.3% to 81.6% when the catalyst loading increased from 0.25 g/L to 0.5 g/L. The photocatalyst concentration was increased by twofold to 1 g/L, and an additional 3% growth was observed. An increase in catalyst loading generally increases the number of active sites and reactive radicals produced, resulting in enhanced degradation (Zhang et al., 2020a). However, beyond a certain loading, the increased concentration of the photocatalyst results in a turbid suspension. This in turn reduces the amount of light incident on the surface of the photocatalyst as shielding and refraction occur. Also, there could be a possible aggregate of particles as the mass of the photocatalyst increases. This reduces the availability

of active sites and the photodegradation efficiency decreases (Abdellah et al., 2018).

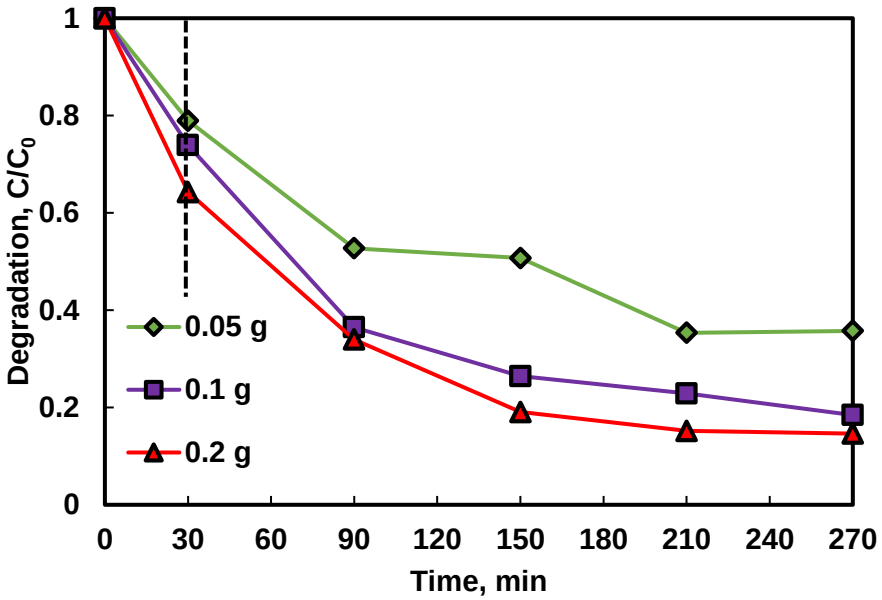

Figure 5.2: Effect of photocatalyst loading on the degradation of tetracycline (Photocatalyst: 50%AgCl/$Bi_{24}O_{31}Cl_{10}$, C_0: 20 mg/L, $C_{catalyst}$: 0.25 g/L, 0.5 g/L, 1 g/L)

5.1.2. Effect of solution pH

The effect of pH on the visible-light photodegradation of tetracycline (Figure 5.3) was investigated at selected pH of 3, 7 and 11 which represents the acidic, neutral and basic conditions and compared to the unadjusted pH of the solution of 5.3. TC degradation demonstrated a faster reaction rate at basic pH conditions of 11 and a slower reaction rate at acidic pH conditions of 3, despite the fact that the overall degradation efficiency beyond 200 minutes was the same. TC has been reported to be an amphoteric molecule as it is cationic at pH less than 3.3, neutral in the pH range of 3.3-7.68 and anionic at pH above 7.68 (Ahmadi et al., 2017, Derikvandi et al., 2021). Therefore, TC will have a significant degradation across

a wider pH range as a result of its unique nature of speciation and characteristics (Cao et al., 2018).

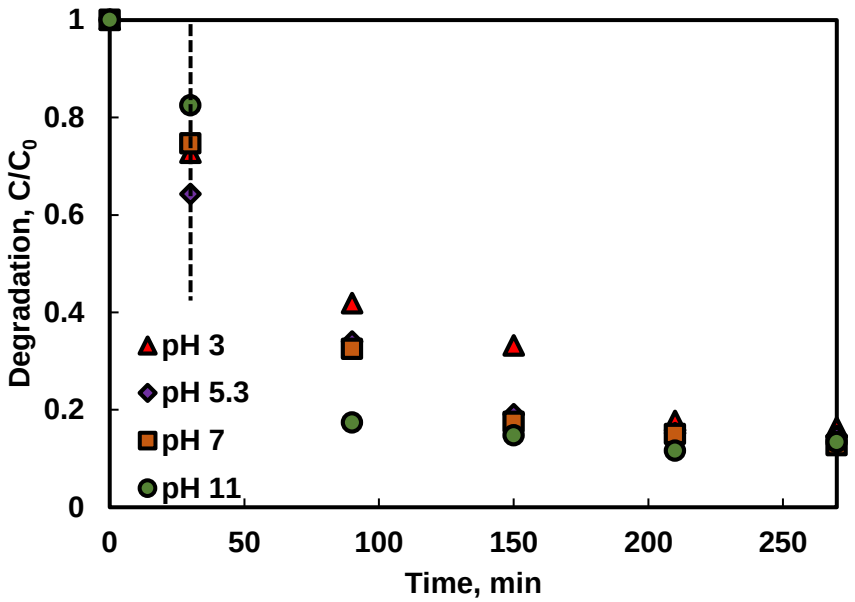

Figure 5.3: Effect of pH on the photocatalytic degradation of tetracycline (Photocatalyst: 50%AgCl/$Bi_{24}O_{31}Cl_{10}$, C_0: 20 mg/L, $C_{catalyst}$: 1 g/L)

5.1.3. Effect of initial pollutant concentration

Further investigations were carried out in Figure 5.4 to study the effect of the initial tetracycline concentration on the photocatalytic degradation efficiency. The tetracycline degradation measured an efficiency of 85%, 78% and 56% at concentrations of 20, 30 and 50 mg/L. The results favour quicker degradation of organic pollutants at lower concentrations. At lower initial concentrations of pollutants, there are more reactive sites to contact the pollutant molecules thereby improving the degradation efficiency (Chang et al., 2019).

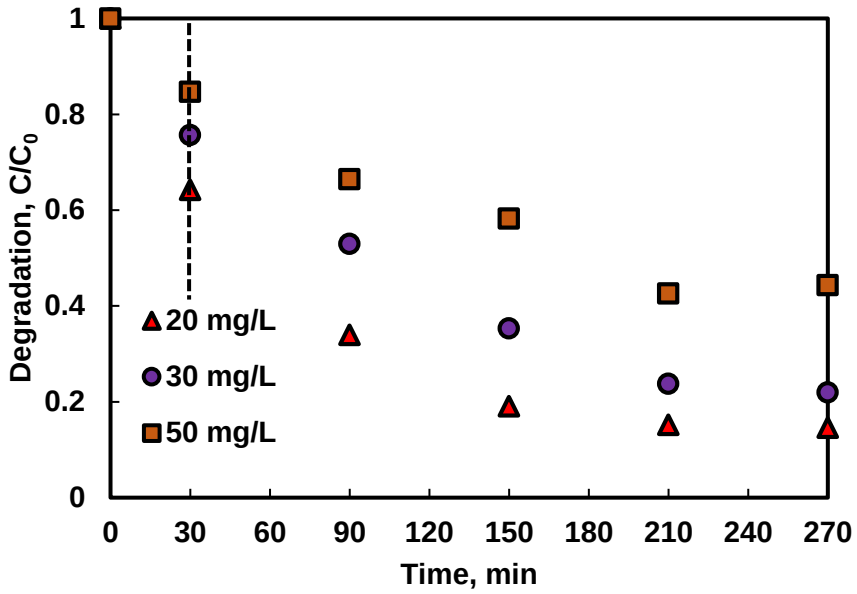

Figure 5.4: Effect of initial pollutant concentration on the degradation of tetracycline (Photocatalyst: 50%AgCl/$Bi_{24}O_{31}Cl_{10}$, C_0: 20 mg/L, 30 mg/L, 50 mg/L, $C_{catalyst}$: 1 g/L)

5.2. Photocatalytic degradation of 2,4-dichlorophenoxy acetic acid (2,4-D)

In Figure 5.5, after 4 h of light irradiation only, 2,4-D showed stability under photolysis conditions. BOC showed minimal removal (3%) of 2,4-D under visible light irradiation. This was attributed to the wide bandgap of BOC and the recombination of photogenerated carriers and as a result, the photocatalytic degradation of 2,4-D was unable to proceed. After 4 h of irradiation, the photodegradation efficiency of 2,4-D using 10%AgCl/BOC, 20%AgCl/BOC and 50%AgCl/BOC were 48%, 54% and 55%, respectively. There was no significant increase in the photodegradation efficiency when 20%AgCl/BOC and 50%AgCl/BOC were used in 2,4-D degradation. As seen from the SEM images, increasing the amount of AgCl nanoparticles on the surface of BOC caused the agglomeration of the particles. This could have inhibited degradation due to the lack of reactive sites and insufficient contact with BOC. The results, therefore, show that to harness the advantage of depositing AgCl with BOC, there is a

maximum amount of AgCl suitable for efficient photodegradation. Also, for the removal of 2,4-D using the synthesized photocatalyst to proceed, light irradiation is of utmost importance. In the rest of this study, 20%AgCl/BOC was used in the degradation of 2,4-D.

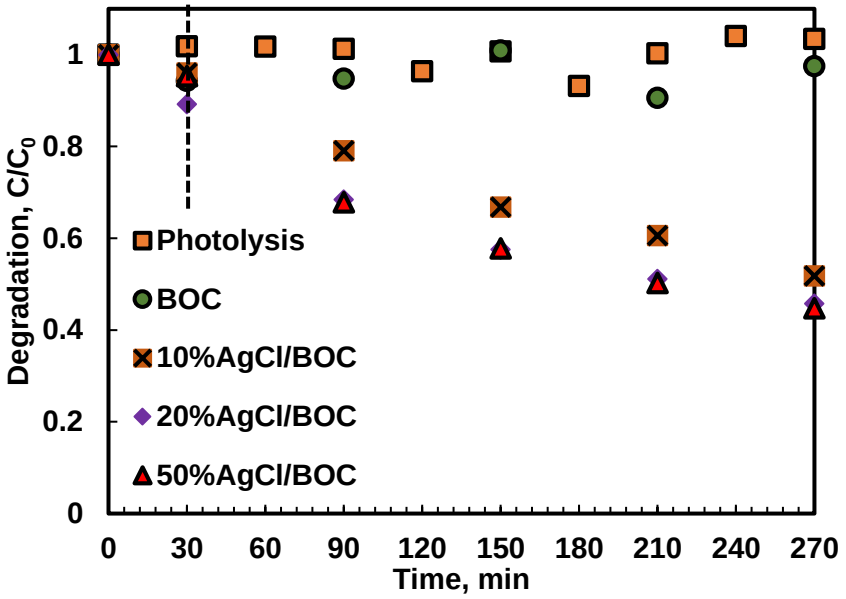

Figure 5.5: 2,4-dichlorophenoxy acetic acid degradation in the presence of light-only (photolysis), $Bi_{24}O_{31}Cl_{10}$, 10%AgCl/$Bi_{24}O_{31}Cl_{10}$, 20%AgCl/$Bi_{24}O_{31}Cl_{10}$, 50%AgCl/$Bi_{24}O_{31}Cl_{10}$ at initial conditions (C_0: 20 mg/L, $C_{catalyst}$: 0.5 g/L)

5.2.1. Effect of photocatalyst loading

The optimum catalyst loading varied depending on the nature of the target pollutant. In Figure 5.6, the degradation efficiency of 2,4-D increased from 31.3% to 54.2% when catalyst loading increased from 0.25 g/L to 0.5 g/L. A further two-fold increase to 1 g/L resulted in decreased degradation efficiency to 38.7%. This increase in photocatalyst dosage resulted in less light incident on the surface of the photocatalyst as well as possible aggregation of materials thereby resulting in a lower degradation efficiency.

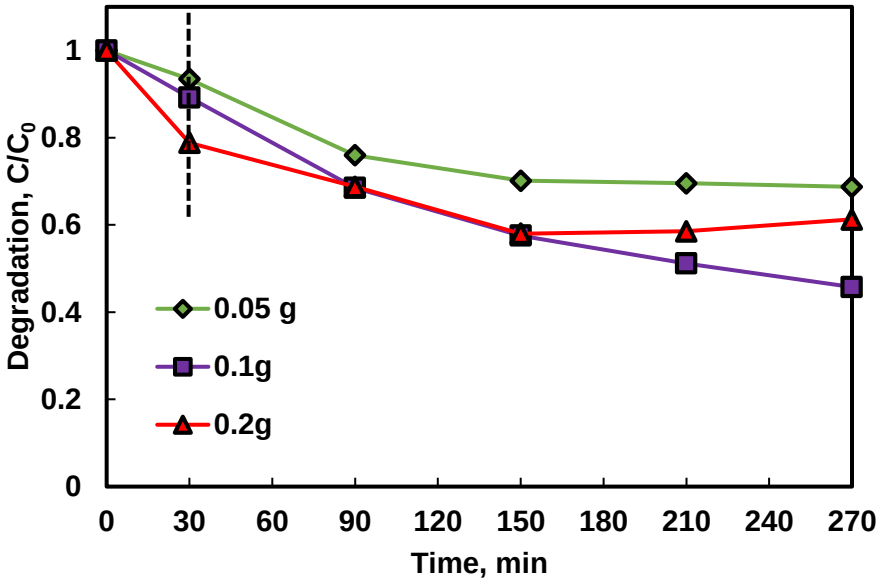

Figure 5.6: Effect of photocatalyst loading on the degradation of 2,4 – dichlorophenoxy acetic acid (Photocatalyst: 20%AgCl/$Bi_{24}O_{31}Cl_{10}$, C_0: 20 mg/L, $C_{catalyst}$: 0.25 g/L, 0.5 g/L, 1 g/L)

5.2.2. Effect of solution pH

The effect of pH in the photocatalytic degradation of 2,4-D was investigated and reported in Figure 5.7. In the degradation of 2,4-D, the optimum degradation of 54% was realized at pH 3 and the unadjusted pH 4. At the neutral pH of 7, degradation efficiency was reduced to 27% while no degradation occurred under alkaline conditions (pH 11). The inhibition in photodegradation observed in the alkaline environment was attributed to the fact that 2,4-D ionizes as anionic in solution (pKa value of 2.64), the photocatalyst's surface charge is negative, resulting in a repulsive force that reduces photodegradation (Adenuga et al., 2021).

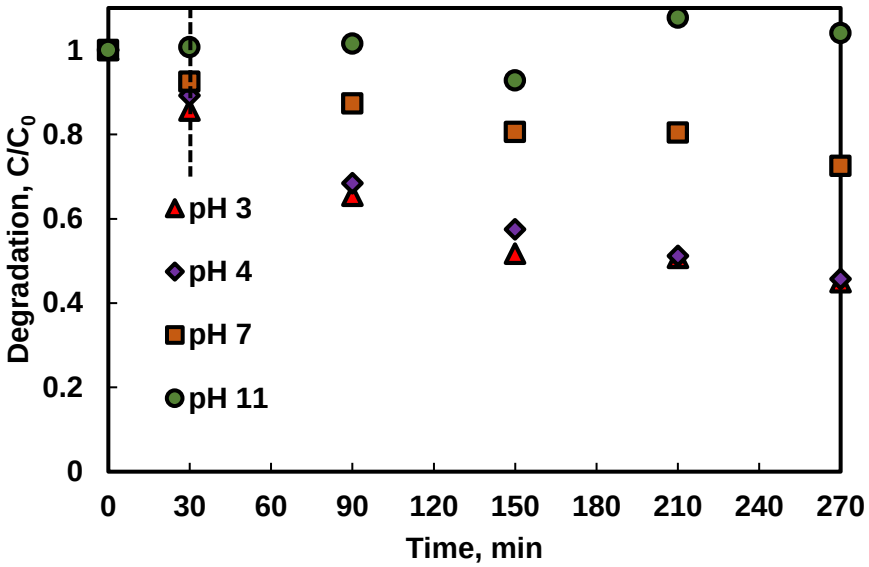

Figure 5.7: Effect of pH in the photocatalytic degradation of 2,4-dichlorophenoxy acetic acid (Photocatalyst: 20%AgCl/$Bi_{24}O_{31}Cl_{10}$, C_0: 20 mg/L, $C_{catalyst}$: 0.5 g/L)

5.2.3. Effect of initial pollutant concentration

The initial concentration of 2,4-D was studied and reported in Figure 5.8 in the range of 10 mg/L – 50 mg/L. The degradation efficiency of 2,4-D showed degradation efficiency of 49%, 54% and 24%, demonstrating a trend of 20 mg/L > 10 mg/L > 50 mg/L. While the concentration of 2,4-D increases, the photocatalyst dosage remained constant. This causes less 2,4-D to be degraded as there are less active sites available to facilitate the degradation process.

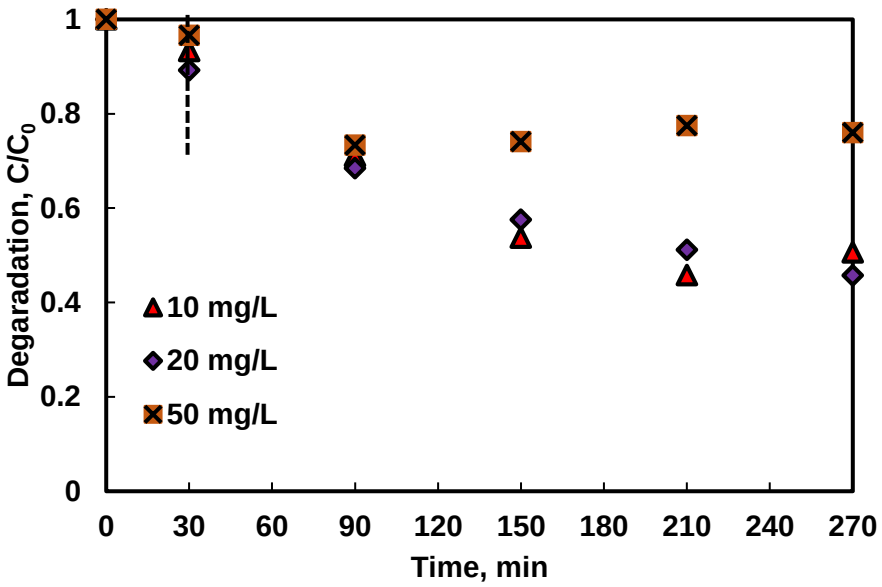

Figure 5.8: Effect of initial pollutant concentration on the degradation of 2,4-dichlorophenoxy acetic acid Effect of initial pollutant concentration on the degradation of tetracycline (Photocatalyst: 20%AgCl/$Bi_{24}O_{31}Cl_{10}$, C_0: 10 mg/L, 20 mg/L, 50 mg/L, $C_{catalyst}$: 0.5 g/L)

5.4. Mineralization

One of the major drivers for the use of advanced oxidation processes such as photocatalysis is their ability to degrade and mineralize target pollutants resulting in environmentally benign reaction products. An analysis of the total organic carbon (TOC) present after treatment gives an indication of the extent of mineralization and points towards the possible formation of intermediate degradation products. In this study, TOC analysis was conducted on tetracycline and 2,4-D after degradation as seen in Figure 5.9**.** TC degradation results indicated that 85.4% had been removed after 4 h, and complete degradation was recorded after 24 h. The measured mineralization rate was 13% and 63% after 4 h and 24 h respectively. Degradation test removals of 54% and 81% for 2,4-D were recorded after 4 and 24 h, respectively. The corresponding TOC removals were 50% and 65% for the same time frames. A possible explanation for the faster

mineralization of 2,4-D in the first 4 hours could be the formation of less complex intermediates when compared to tetracycline since the TOC removal depicts that intermediates were formed during the degradation process. The intermediates produced during the degradation of tetracycline ($C_{22}H_{24}N_2O_8$) could include $C_{22}H_{26}N_2O_9$, $C_{22}H_{23}NO_9$, $C_{12}H_{12}O_4$ and carboxylic acid (Zhong et al., 2019, Li et al., 2019a). Other investigations have also discovered significant 2,4-D intermediate products, including 2,4-dichlorophenol, 2,6-dichlorophenol, 2-chlorohydroquinone, oxalic acid, and glyoxylic acid, among others (Mehralipour and Kermani, 2021, Hama Aziz et al., 2018).

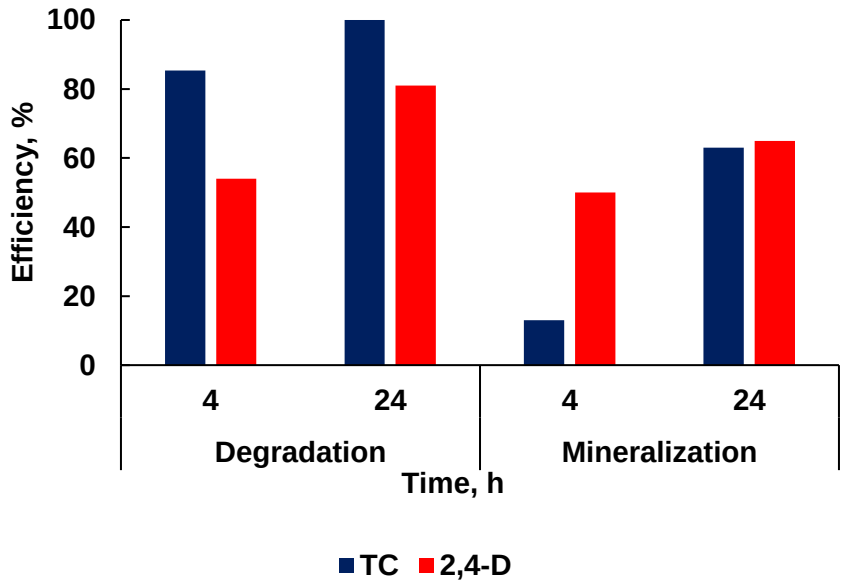

Figure 5.9: Degree of degradation and mineralization of organic pollutants TC and 2,4-D in 4 h and 24 h

5.5. Reusability, Trapping experiments and degradation mechanism

The reusability potential of the as-prepared photocatalyst was presented in Figure 5.10. After each cycle, the photocatalysts were collected and washed with deionized water to remove pollutants from the surface of the photocatalyst. The material was then dried in an oven for 60°C prior to the next cycle. In the

photocatalytic degradation of TC using 50%AgCl/BOC, after three cycles, 79% TC removal was measured. This represents a 6% decrease in efficiency over three cycles, which could be due to particle loss during the washing step prior to reuse. This demonstrates the photocatalyst's reusability and stability.

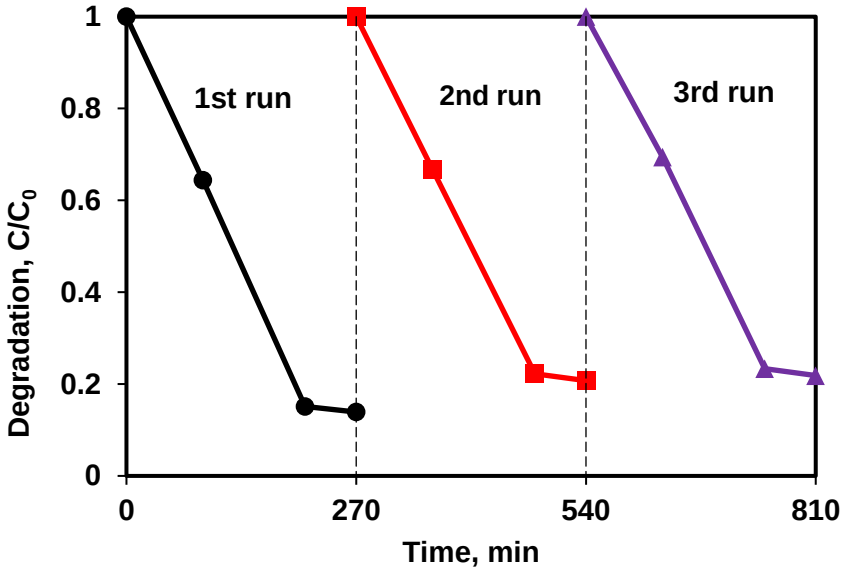

Figure 5.10: Recycle test of 50%AgCl/$Bi_{24}O_{31}Cl_{10}$ in the photocatalytic degradation of tetracycline

The photocatalytic reaction mechanism of the photocatalysts was investigated through capture experiments (Figure 5.11**)**. P-Benzoquinone (BQ), 2-propanol (IPA) and triethanolamine (TEOA) were used as superoxide radical ($^{\bullet}O_2^-$), hydroxyl radical ($^{\bullet}OH$) and hole (h^+) scavengers to investigate their roles in the photocatalytic process (Wang et al., 2020c). The addition of BQ and TEOA to 2,4-D reduced the degradation efficiency by 12% and 52% while the addition of IPA did not suppress the efficiency of the 20%AgCl/BOC. In the degradation of TC using 50%AgCl/BOC, the addition of BQ reduced the degradation efficiency to 63% while IPA and TEOA did not impact the degradation efficiency negatively. The 2,4-D scavenger degradation results show that the main reactive species responsible for the degradation are $^{\bullet}O_2^-$ and h^+ while the dominant reactive

species in TC degradation was the superoxide radical. This difference was attributed to the TC-sensitization, which occurred when TC molecules were absorbed on the surface of the photocatalyst (Zyoud et al., 2019), potentially taking precedence over hole activity during photodegradation. The results also reveal that hydroxyl radicals are not an important reactive agent in this degradation process. A photodegradation mechanism can be proposed for the degradation when Xwt%AgCl/BOC is used in the degradation of organic contaminants in visible light as illustrated in Equation 5.4 to Equation 5.8 and Figure 5.13.

$$\text{AgCl-BOC} \xrightarrow{h\nu} \text{AgCl } (e^-, h^+)/\text{Ag/BOC } (e^-, h^+) \quad (5.4)$$

$$\text{AgCl } (e^-, h^+)/\text{Ag/BOC } (e^-, h^+) \rightarrow \text{AgCl } (e^-) + \text{BOC } (h^+) \quad (5.5)$$

$$\text{BOC } (h^+) + \text{Pollutants} \rightarrow \text{intermediates} \rightarrow CO_2 + H_2O \quad (5.6)$$

$$\text{AgCl } (e^-) + O_2 \rightarrow \text{AgCl} + {}^{\bullet}O_2^- \quad (5.7)$$

$${}^{\bullet}O_2^- + \text{pollutants} \rightarrow \text{products} \quad (5.8)$$

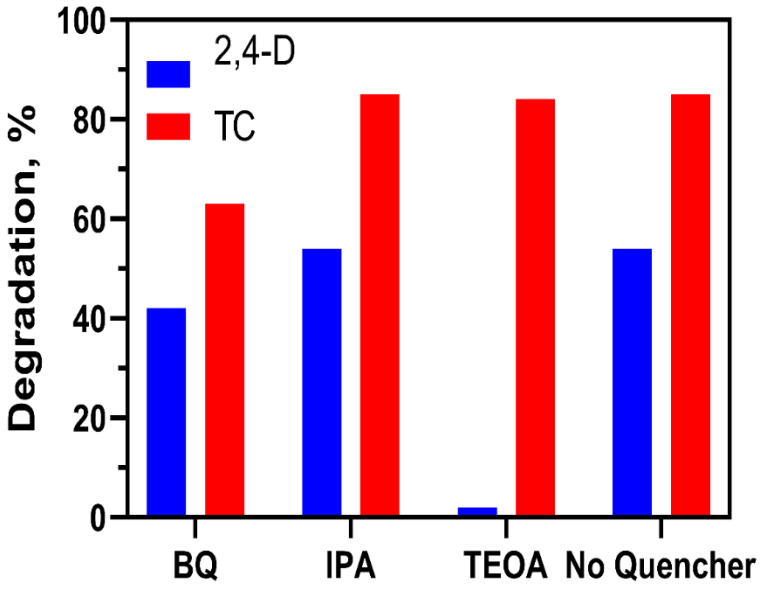

Figure 5.11: Effects of different quenchers on the photocatalytic degradation of 2,4-D and TC

During the irradiation and photodegradation process, Ag^0 is expected to form due to light irradiation and acts as an electron mediator between AgCl and BOC (Li et al., 2020a). This formation was validated and illustrated in Figure 5.12 where a colour change was seen when 50%AgCl/BOC was irradiated by visible light in comparison to being stirred in the dark.

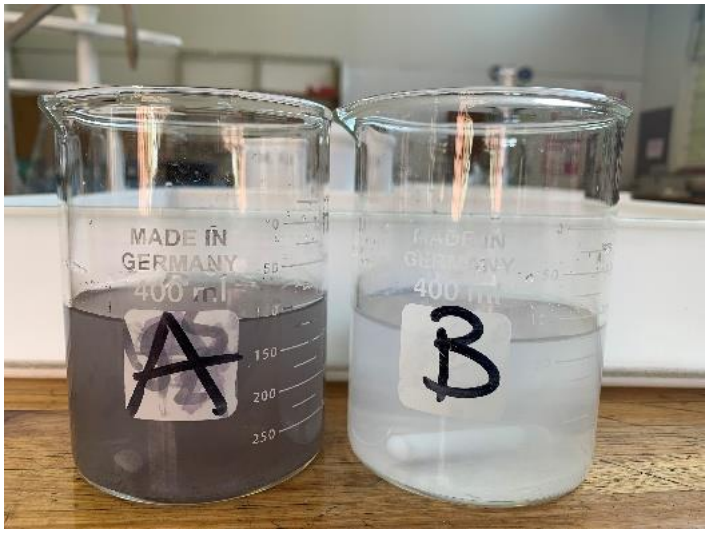

Figure 5.12: (A) 50%AgCl/$Bi_{24}O_{31}Cl_{10}$ irradiated in light and (B) 50%AgCl/$Bi_{24}O_{31}Cl_{10}$ in the dark

This colour is attributed to the formation of Ag^0 photoreduced on the surface of the AgCl during irradiation (Rehan et al., 2018). The formed Ag^0 is photoexcited as a result of its SPR effects (Liu et al., 2018a), thereby transporting electrons from the conduction band (CB) of BOC to that of AgCl while the holes in the valence band of AgCl transferred to that of BOC where it directly degrades the organic contaminants (Wang et al., 2019d). This ensures that the photogenerated carriers are effectively separated. AgCl has a bandgap of 3.26 eV with a valence band and conduction band of +3.20 eV and -0.06 eV (Liu et al., 2018a) while BOC has a valence band and conduction band of +1.49 eV and -1.29 eV. The reduction potential of oxygen $E^0(O_2/{}^{\bullet}O_2)$ is -0.046 eV (Yao and Liu, 2014). The

CB of AgCl being more negative than that of oxygen means that O_2 could be reduced $^{\bullet}O^{2-}$ which is also a reactive species responsible for photodegradation in this study. In the TC mechanism, as a result of TC adsorbed on the surface of BOC, a TC complex is formed (Wu et al., 2020) which can be excited by visible light thereby causing electron transfer from the LUMO of TC to the conduction band of the photocatalyst. This mechanism when compared to the mechanisms described in Figure 2.4 illustrates a similar mechanism to type-II-heterojunction where there is an effective separation of charges. The electrons move from BOC to AgCl while the holes moves from AgCl to BOC thereby reducing recombination. Although, Ag^0 is formed on the surface of AgCl during irradiation, it acts as an electron mediator between CB of BOC and the CB of AgCl.

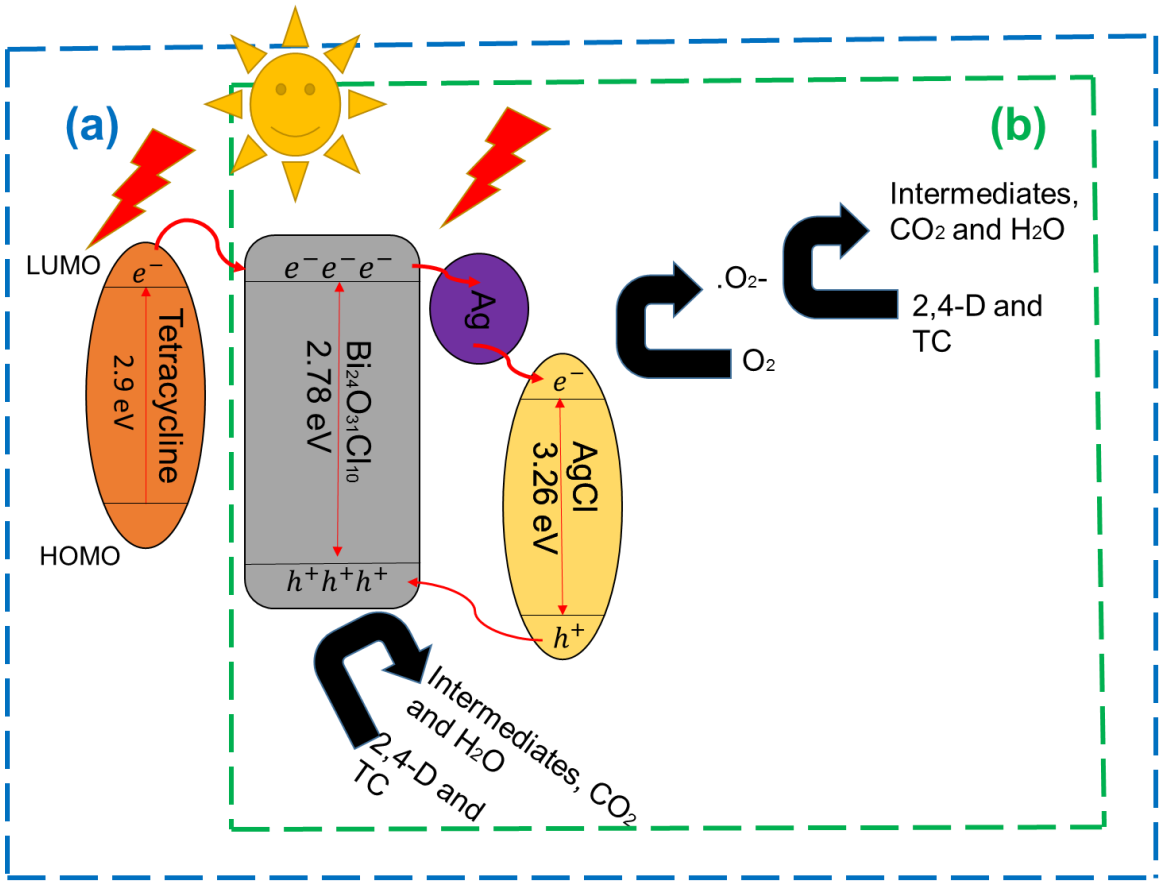

Figure 5.13: Proposed degradation mechanism of Xwt%AgCl/$Bi_{24}O_{31}Cl_{10}$ in the photocatalytic degradation of (a) TC and (b) 2,4-D

5.6. Discussion

The activity and progress of degradation differ in both pollutants. TC is characterized by a yellow colour which has a major absorption range in wavelength 300-430 nm (Zyoud et al., 2017) while 2,4-D is colourless. This enables TC molecules to be sensitized by visible light and be easily adsorbed on the surface of the photocatalysts thereby enhancing photodegradation due to the closeness of the adsorbed contaminants with that of the reactive sites. The degradation of TC in visible light using TiO_2 was reported by Wu et al. (2020), and they note that the visible light absorption of TC causes it to excite electrons which are then transferred from its LUMO to the conduction band of the photocatalyst.

Table 5.1 summarizes the various recently reported $Bi_{24}O_{31}Cl_{10}$-based heterogeneous photocatalysts in comparison with the present study. Six low-wattage (30 W) Fluoro lamps were used to carry out the photodegradation experiments in this study and the efficiency measured in both the degradation of 2,4-D and TC showed great potential when compared to the other studies.

Table 5.1: Comparison of recently reported $Bi_{24}O_{31}Cl_{10}$-based photocatalysts with present study

Photocatalyst	Light source	Pollutant	Degradation	Reference
$AgCl/Bi_{24}O_{31}Cl_{10}$	30 W (6)	2,4-D and TC	54.2% and 82%	This study
MoS_2/g-$C_3N_4/Bi_{24}O_{31}Cl_{10}$	300 W Xe lamp	TC	97.5 %	(Kang et al., 2020a)
$BiOCl/Bi_{24}O_{31}Cl_{10}$	350 W Xe lamp	MO, RhB and 4-CP	74.5%, 98.1% and 88.2%	(Li et al., 2014)
$BiOCl/Bi_{24}O_{31}Cl_{10}$/rGO	400 W halogen lamp	OFL, CIP and LVO	84.8%, 57.2% and 70.7%	(Shabani et al., 2019)
g-C_3N_4/Eu (III) doped $Bi_{24}O_{31}Cl_{10}$	250 W Xe lamp	RhB	91.9%	(Li et al., 2019b)
SnO_2/Bi_2S_3/BiOCl-$Bi_{24}O_{31}Cl_{10}$	Simulated sunlight	RhB	80.8%	(Fenelon et al., 2020)
$Pt/Bi_{24}O_{31}Cl_{10}$	300 W Xe lamp	MO	84%	(Xu et al., 2019)
$AgI/Ag/Bi_{24}O_{31}Cl_{10}$	300 W Xe lamp	MO and phenol	84.3% and 55.1%	(Wang et al., 2019c)
$Ag/Bi_{24}O_{31}Cl_{10}$	240 W Xe lamp	RhB	95.8%	(Song et al., 2018)

5.7. Summary

In summary, a novel AgCl/$Bi_{24}O_{31}Cl_{10}$ composite photocatalyst was developed successfully by loading AgCl nanoparticles on the surface of rod-like $Bi_{24}O_{31}Cl_{10}$ and showed good photodegradation efficiency in the removal of 2,4-D and TC under visible light irradiation. The heterojunction formed improved the photoabsorption of the photocatalyst in the visible light region and improved the separation of photogenerated carriers which was evidenced by the improved photocatalytic activity. Reasonable mineralization of both pollutants at 63% and 65% efficiency was measured. The proposed mechanism suggests that holes and oxygen radicals are the main reactive species responsible for the mineralization of 2,4-D and TC. The results show that this technology can be combined with other technologies for the successful removal of toxic pollutants in wastewater.

CHAPTER 6 – INFLUENCE OF WASTEWATER MATRIX ON THE VISIBLE LIGHT DEGRADATION OF PHENOL

In this chapter, the photocatalytic activity of 50%AgCl/$Bi_{24}O_{31}Cl_{10}$ photocatalyst was investigated on the degradation of phenol spiked in secondary wastewater treatment plant effluent collected from a wastewater treatment plant (WWTP) in Pretoria, South Africa. This was then compared to the degradation of the same compound in DI water. The experimental design was done using the Taguchi method L16 orthogonal tray with three factors (pH, initial phenol concentration and photocatalyst dosage) and four levels. The effects of individual anion components such as Cl^-, NO_3^-, NO_2^-, SO_4^{2-} and cations such as Ca^{2+}, Mg^{2+}, Zn^{2+} and K^+ were investigated.

6.1. Raw water source used in the experiments

The collected effluent water was analysed and reported in Table 6.1. It shows the physical and chemical properties of the collected water. The samples were spiked with a varying concentration (5, 10, 20 and 30 mg/L) of phenol.

Table 6.1: The effluent characteristics of the Daspoort WWTP, Pretoria, South Africa

Parameters	Formula	Value
pH		7
Floride (mg/L)	F^-	0.21
Chloride (mg/L)	Cl^-	48.24
Nitrite (mg/L)	NO_2^-	0.97
Bromide (mg/L)	Br^-	0.15
Nitrate (mg/L)	NO_3^-	14.11
Sulfate (mg/L)	SO_4^{2-}	56.70
Phosphate (mg/L)	PO_4^{3-}	0.39
Lithium (mg/L)	Li^+	0.03
Sodium (mg/L)	Na^+	54.79
Ammonium (mg/L)	NH_4^+	9.27
Manganese (mg/L)	Mn^{2+}	0.07
Magnesium (mg/L)	Mg^{2+}	13.98
Potassium (mg/L)	K^+	11.71
Calcium (mg/L)	Ca^{2+}	30.10
Strontium (mg/L)	Sr^{2+}	0.08

6.2. Experimental design and Analysis of Variance (ANOVA)

Design of experiment (DOE) was performed to determine the optimal conditions for the degradation of phenol using AgCl/$Bi_{24}O_{31}Cl_{10}$ photocatalyst in an aqueous solution of spiked WWTP secondary effluent. The Taguchi L16 (4^3) method was applied while using the Minitab software. The “Larger is better” case was used for the Signal-to-noise (S/N) ratio to define the optimal conditions. The effects of

pH, phenol concentration and photocatalyst dose were investigated with four levels in Table 6.2. The bigger is better function is determined by Equation 6.1:

$$S/N = -10 \log \left(\frac{1}{n}\sum_{i=1}^{n}\frac{1}{Y_i^2}\right) \quad (6.1)$$

Where S/N is the response average for each factor and Yi is the removal of the i^{th} experiment. The degradation efficiency response as a function of time was calculated using Equation 6.2:

$$\text{Degradation efficiency (\%)} = \frac{(C_0 - C_t)}{C_0} \times 100 \quad (6.2)$$

Where C_0 and C_t are the concentrations of phenol at t = 0 and t respectively.

Table 6.2: Photodegradation factors and their levels using the Taguchi method

Factor	Level 1	Level 2	Level 3	Level 4
pH	3	5	7	9
Phenol concentration (mg/L)	5	10	20	30
Photocatalyst dose (g/L)	0.25	0.5	0.75	1

6.3. Degradation studies

The degradation studies following the design of experiment and their responses are reported in Table 6.3 while the signal S/N ratio table for the larger is better case is shown in Table 6.4

Table 6.3: Experimental design and response using Taguchi method L16

No	pH	Phenol concentration (mg/L)	Photocatalyst dose (g/L)	Degradation (%)
1	3	5	0.25	7
2	3	10	0.5	2
3	3	20	0.75	2
4	3	30	1	6
5	5	5	0.5	57
6	5	10	0.25	13
7	5	20	1	7
8	5	30	0.75	9
9	7	5	0.75	80
10	7	10	1	53
11	7	20	0.25	11
12	7	30	0.25	20
13	9	5	1	84
14	9	10	0.75	50
15	9	20	0.5	23
16	9	30	0.25	10

Table 6.4: Order of parameters influencing the photocatalytic degradation of phenol

Level	pH	Phenol concentration	Photocatalyst dose
1	11.13	32.14	20.00
2	23.35	24.19	23.60
3	29.85	17.75	24.29
4	29.92	20.17	26.36
Delta	18.80	14.40	6.36
Rank	1	2	3

The results show that the most important factor determining the degradation efficiency of phenol is pH. The second-ranked factor is the initial phenol concentration and photocatalyst dosage ranks third. pH is an important factor affecting the degradation rate due to its effects on the chemical properties of the pollutant, the surface of the photocatalyst and the reaction kinetics (Moradi et al., 2021). The photocatalytic degradation of phenol at an acidic aqueous solution of 3 using AgCl/$Bi_{24}O_{31}Cl_{10}$ photocatalyst was not supported. The concentration of hydroxyl ion reduces in an acidic medium due to the concentration of proton and this ion is required for the formation of hydroxyl radicals which might be a reactive species aiding degradation (Norouzi et al., 2020). The effects of initial concentration were investigated between 5 mg/L and 30 mg/L. At the highest phenol concentrations, the degradation efficiency was 20% or less while the highest degradation efficiencies were measured at lower concentrations. This phenomenon has been previously confirmed by other studies (Ahmadpour et al., 2020, Sayadi et al., 2019) as a possible increased interaction between the pollutant and the reactive species at lower pollutant concentration as compared to when the pollutant concentration is higher. This results in limited active sites available for

photocatalysis to take place as more organic material is adsorbed on the surface of the photocatalyst material while a limited amount of photons reaches the surface of the photocatalyst (Rafiq et al., 2021). Therefore, the results present a potential for application in the removal of pollutants at low-level concentrations. In these experiments, while pH and initial contaminant concentration were of more significance, photocatalyst dosage is another factor that affects the photodegradation efficiency. Experiments 9 and 13 from Table 6.3 were carried out at photocatalyst dosages of 0.75 g/L and 1 g/L. High photocatalyst dosage enhanced photodegradation through the presence of more reactive sites and the availability of radical's production (Zhao et al., 2018). It is also known that an excessive amount of photocatalyst will reduce the intensity of penetrating light hence reducing the rate of photodegradation (Kiwaan et al., 2020). Figure 6.1 illustrates the mean of S/N ratios and levels of the three factors investigated. The optimal phenol concentration value was at level 1, while that of pH and photocatalyst dosage was at level 3 and level 4, respectively. This suggests the optimum conditions for the photocatalytic degradation of phenol using the photocatalyst.

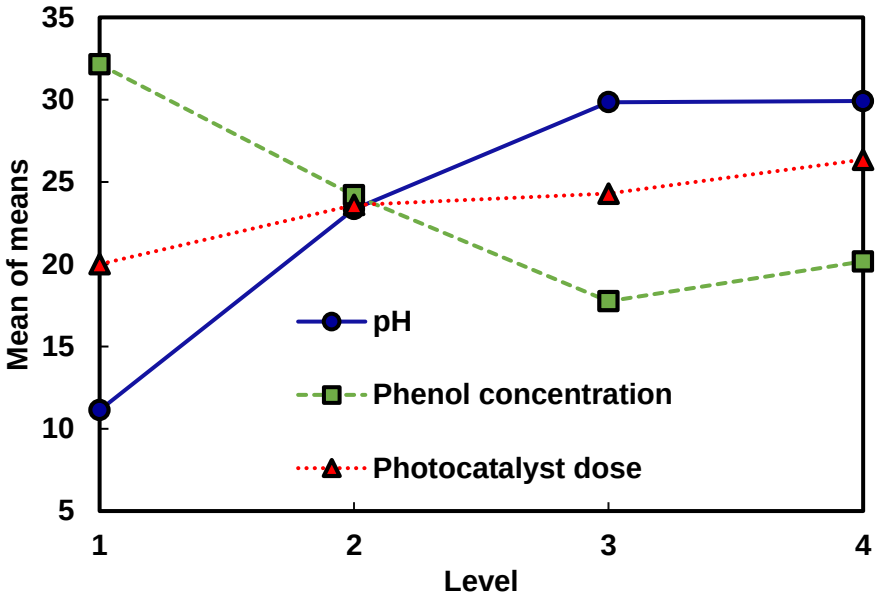

Figure 6.1: Main effects plots of means (pH, phenol concentration and photocatalyst dose)

The analysis of variance (ANOVA) was done to investigate the importance of the selected factors on the degradation of phenol and is reported in Table 6.5. $P \leq 0.0001$ is highly significant; $P \leq 0.01$ is strongly significant; $P \leq 0.05$ is significant; and $P > 0.05$ is not significant (Wang et al., 2019b). Based on Table 6.5 where the ANOVA results are shown, DF = degree of freedom, SS = sum of square, MS =mean of square F-value = Fisher variation ratio and P-value = significant probability value, the P-values conclude that pH and phenol concentration are strongly significant factors for the removal of phenol in a water matrix while the photocatalyst dosage was the least significant. The coefficient of determination $R^2 = 0.9643$ which is greater than 0.95 shows that the model responds to a change in response value in the 96.43% range. The $R_{adj}^2 - R_{pred}^2 = 0.9107 - 0.7459 = 0.1648 < 0.2$ shows reliability of the experiments.

Table 6.5: Analysis of variance for the photocatalytic degradation of phenol

Source	DF	Adj SS	Adj MS	F-Value	P-Value
pH	3	3845.2	1281.75	18.27	0.002
Phenol Concentration	3	5673.3	1891.08	26.95	0.001
Photocatalyst dose	3	1844.2	614.75	8.76	0.013
Error	6	421.0	70.17		
Total	15	11783.7			

The general impact of the wastewater matrix was assessed in the degradation of phenol under visible light irradiation and is reported in Figure 6.2. Experiments were carried out under photolysis and adsorption conditions to investigate the individual effects of light and photocatalyst. The results show negligible phenol removal under photolysis and adsorption conditions, illustrating that light and photocatalysts are required for photocatalytic degradation to take place. After 4 h of light irradiation, photocatalytic degradation of phenol in DI water was 48% while in the water matrix from Daspoort effluent, phenol degradation (Experiment 9 in Table 6.3) was measured at 80%. In this case, the presence of ions promoted degradation when compared to the degradation efficiency in DI water. It is known that various dissolved components in water could either have promotion, inhibitory or neutral effects on the degradation efficiency (Lado Ribeiro et al., 2019). For practical applications, pH, the presence of ions and organics could affect the photocatalytic activity of the semiconductor (Zhao et al., 2019a).

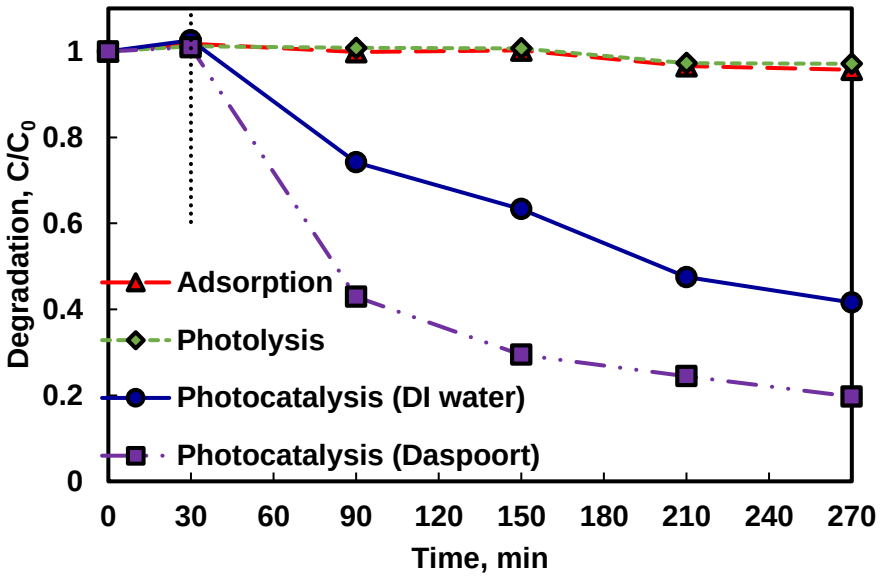

Figure 6.2: Degradation of phenol under different conditions of adsorption, photolysis, and photocatalysis (DI and Daspoort water) (Photocatalyst: 50%AgCl/$Bi_{24}O_{31}Cl_{10}$, C_0: 5 mg/L, $C_{catalyst}$: 0.75 g/L)

The pH of the effluent water enhanced the degradation of the organic pollutant using the photocatalyst. While the pH of the secondary effluent was 7, the pH of deionized water is 5.5. In Table 6.3, degradation at a pH condition below 7 is limited. Moreover, the interfering influence of anions such as Cl^-, SO_4^{2-}, NO_2^- and NO_3^- were selected to investigate the individual influence in DI water. The results of these interactions are reported in Figure 6.3. Sodium salts were used to avoid the various interaction of different cations. Na^+ is known to be at its maximum oxidation state in these salts and as such, will not compete as an h^+ scavenger and also does not influence the surface charge of the photocatalyst at concentrations less than 100 mM (Wang et al., 2015).

After the addition of SO_4^{2-} (Figure 6.3a), at a low sulfate concentration of 20 ppm, the degradation of phenol was neutral while at a higher concentration (50 ppm), there was a reduced effect in the degradation rate. Sulfate has the potential to be adsorbed on the surface of the photocatalysts while also interacting with the

available holes and hydroxyl radicals (Raha and Ahmaruzzaman, 2020). It is important to investigate the effects of nitrates as they are always present in water bodies even at low concentrations. It indicates the presence of water from sources such as livestock waste at high concentrations and may act as a hydroxyl radical to form NO_3•, which is less reactive (Eslami et al., 2020). The addition of nitrates to the photocatalytic reaction (Figure 6.3b) shows that it has an inhibition effect on the degradation efficiency of phenol after 4 h of light irradiation at both 20 and 50 ppm. The degradation efficiency was reduced by 10% when nitrates were introduced. There was total inhibition of degradation when nitrite (Figure 6.3c) was introduced into the photocatalytic system at both 20 ppm and 50 ppm. Wang et al. (2020a) explain that in the presence of NO_2^- the transition n → π* of nitrite easily occurs and NO_2^- is oxidized to HNO_3•$^-$ or $(NO_3$•$)^{2-}$ radical species by the •OH radicals and as such the hydroxyl radicals are not available for degradation. Therefore, for the practical application of phenol removal from wastewater using the photocatalyst, nitrite should be removed before implementing photocatalysis. The wastewater investigated in this study had 0.97 mg/L nitrite present and this could have been too little to effectively inhibit the degradation rate.

Figure 6.3d shows the effects of chloride ions on the degradation of phenol. Cl^- shows a reduction in degradation efficiency in the range of 3% - 6% on the degradation of phenol using AgCl/$Bi_{24}O_{31}Cl_{10}$ as a photocatalyst. Additional Cl^- in the solution has the potential of forming inorganic free radicals Cl• and Cl_2•$^-$ which are also reactive and could promote the degradation of phenol (Wang et al., 2018a). Photocatalytic degradation involving Ag/AgCl – based photocatalysts has reported that Cl• takes part in the degradation process due to its strong oxidizing potential (Wang et al., 2020b, Wu et al., 2019). The concentration of chloride ions in the WWTP effluent used in this study was 48 mg/L and would have had an almost negligible effect on the degradation efficiency.

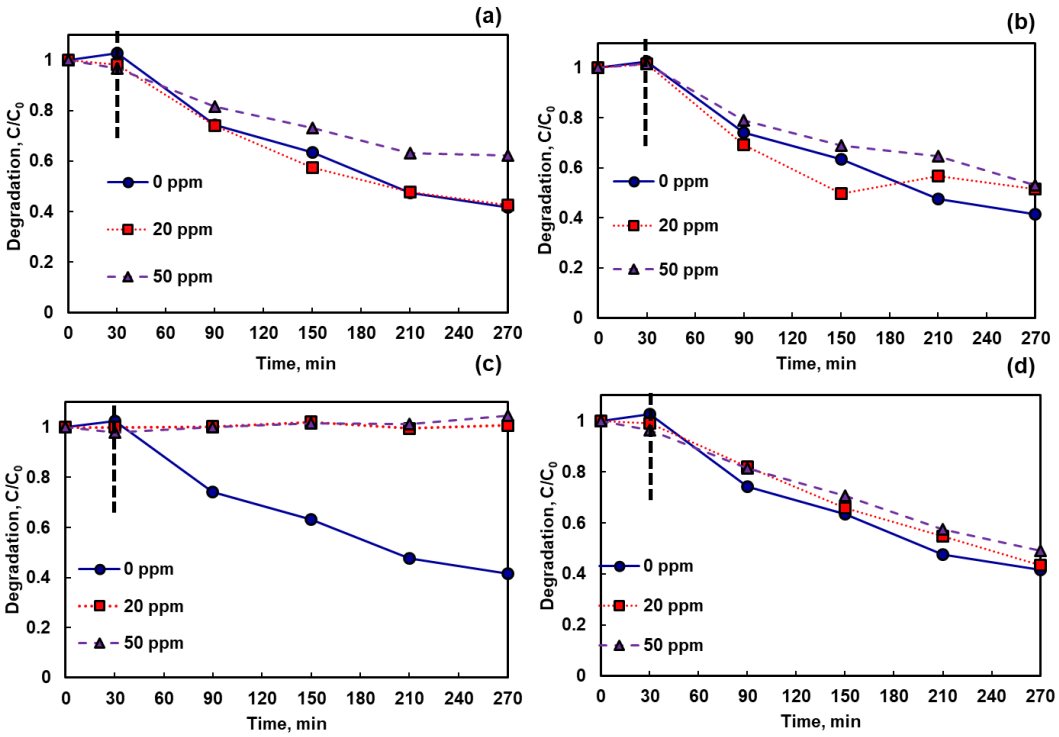

Figure 6.3: Influence of various ions in the removal of phenol (a) SO_4^{2-}, (b) NO_3^-, (c) NO_2^- and (d) Cl^- (Photocatalyst: 50%AgCl/$Bi_{24}O_{31}Cl_{10}$, C_0: 5 mg/L, $C_{catalyst}$: 0.75 g/L)

Sulfate salts of potassium (K_2SO_4), zinc ($ZnSO_4.7H_2O$), calcium ($CaSO_4.0.5H_2O$) and magnesium ($MgSO_4.7H_2O$) were used at concentrations of 20 mg/L and 50 mg/L to investigate the effects of cations in wastewater for the photodegradation of organic pollutants under the same conditions and reported in Figure 6.4(a)-(d). Although it has been previously suggested that these metal ions should not affect degradation as they are already in a stable oxidation state (Dugandžić et al., 2017), the results show that their presence in the wastewater proposes a promotion effect to degradation. Cations present in the wastewater effluent investigated include magnesium, potassium and calcium at concentrations of 13.98, 11.71 and 30.10 mg/L respectively. The results show that the summative effects of these ions promoted the degradation efficiency in the water matrix in comparison to DI water. Gao et al. (2019) confirm that cations such as Ca^{2+} enhance the adsorption

of carbamazepine on the surface of the photocatalyst BiOCl thereby improving the degradation efficiency.

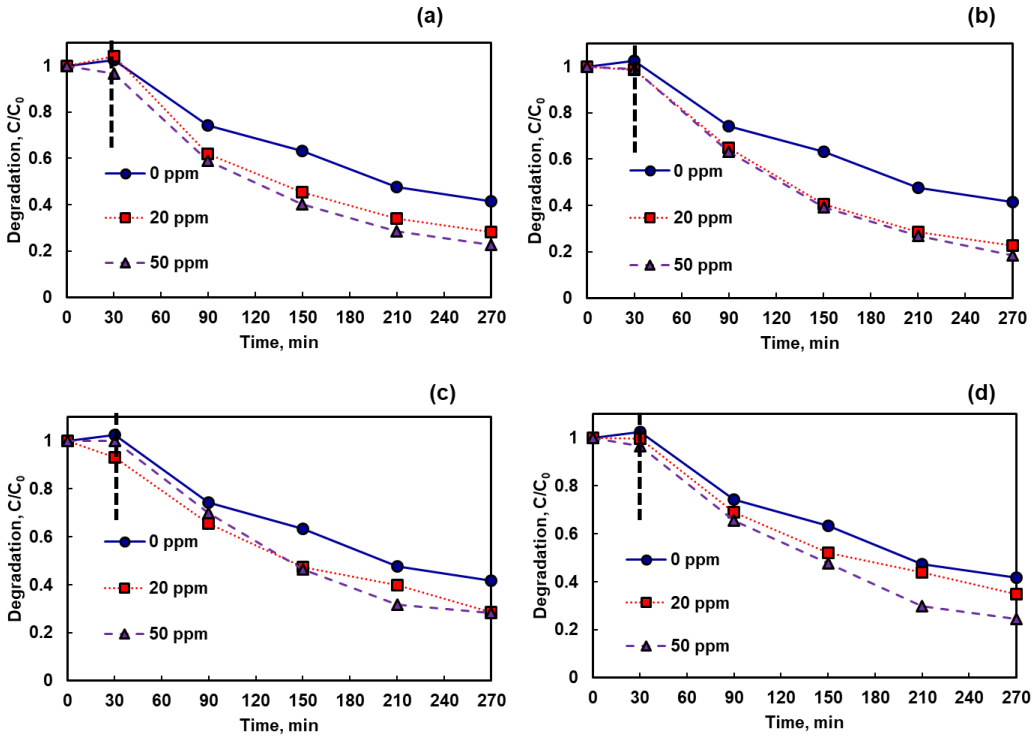

Figure 6.4: Influence of various ions in the removal of phenol (a) Mg^{2+}, (b) Ca^{2+}, (c) Zn^{2+} and (d) K^{+} (Photocatalyst: 50%AgCl/$Bi_{24}O_{31}Cl_{10}$, C_0: 5 mg/L, $C_{catalyst}$: 0.75 g/L)

6.4. Catalyst stability

The reusability of the photocatalyst in the degradation of phenol was estimated through three consecutive cycles. After each cycle, the photocatalysts were collected and washed with deionized water to remove pollutants from the surface of the photocatalyst. The material was then dried in an oven for 60°C prior to the next cycle. The recycling experiments were carried out in similar conditions to experiment 9 in Table 6.3.

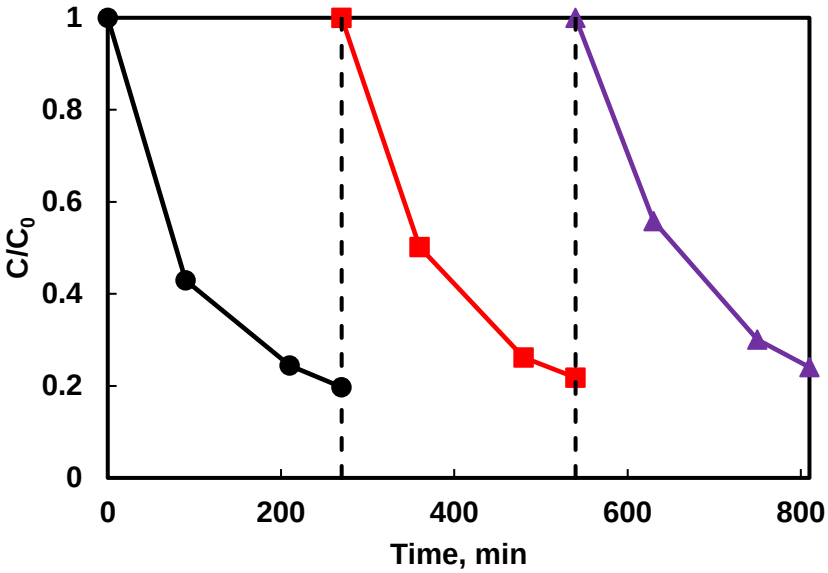

Figure 6.5: Successive photocatalytic degradation of phenol by $AgCl/Bi_{24}O_{31}Cl_{10}$ under visible light irradiation

As shown in Figure 6.5, the degradation efficiency reduced from 80% in cycle 1 to 75% in cycle 3. This points to the relative stability and reusability of the synthesized composite photocatalyst. This agrees with other studies where AgCl-based photocatalysts have been utilized. (Raizada et al., 2020b) in their study examined the stability of their photocatalyst BiOBr/PSCN/Ag/AgCl in the degradation of phenol and measured a reduction of 98% to 90% even after seven cycles. In the evaluation performance of $Ag/AgCl@Ti^{3+}$-TiO_2 for the degradation of tetracycline, Yu et al. (2021) in their study also identify that no inactivation phenomenon is recorded and the slight reduction in activity after three cycles could be attributed to the loss of material or the leaching of Ag from the composite. It should be noted that the material was easily separated from the suspension which also bodes well with its recyclability.

6.5. Comparison with previous studies on the degradation of pollutants in wastewater

Lei et al. (2020) in their study investigated the antibiotics degradation rate in the presence of water matrices. They found that Cl^- and SO_4^{2-} act as radical scavengers and can absorb photons at 245 nm and as such reduce the degradation rate of the antibiotics. Wang et al. (2020d) in their work proved that divalent cations (Mg^{2+} and Ca^{2+}) improved the removal efficiency of Naproxen. This is because these identified cations improved the absorption of the pollutant on the surface of the photocatalyst. In the photodegradation of levofloxacin using a ternary magnetic photocatalyst Ag_3PO_4/rGO/$CoFe_2O_4$ (Hu et al., 2021), Cl^- reduced the degradation efficiency due to its adsorptive competition with the pollutants on the photocatalyst surface while sulfates had zero effect on the degradation rate. Jiménez-Salcedo et al. (2021) compared the photocatalytic degradation of sodium diclofenac using g-C_3N_4 nanosheets in both ultrapure water and tap water under visible light and natural sunlight conditions. Under both light conditions, their result shows a higher degradation of sodium diclofenac in tap water as compared to ultrapure water and the cause was attributed to the presence of "chloride ions of salts".

When investigating the effect of water quality on the degradation of tetracycline while using BVO/FTO@rGO photocatalysts, Yang et al. (2020) reported a decrease in degradation in the presence of SO_4^{2-}, Cl^- and CO_3^- while the degradation was promoted only in the presence of Cr^{6+}. Their work proposes that while Cr^{6+} and tetracycline consume electrons and holes, recombination is inhibited thereby promoting degradation. The anions consume free radicals while also converting them to radicals with lesser oxidizing power thereby reducing the photodegradation efficiency. In the removal of phenolic contaminants using bismuth-modified TiO_2 photocatalyst (Tang et al., 2021b), phenol degradation

was still achieved in the presence of $CaCl_2$, NaCl and KCl while the degradation rate of phenol decreased in the presence of inorganic anions (Cl^-, HCO_3^- and SO_4^{2-}). It is noted that while each component of the water matrix will have its individual effects, the components tend to balance each other thereby having a general effect on degradation or mineralization rate (Náfrádi et al., 2022). Other studies reporting the effects of inorganic ions on the degradation of recalcitrant pollutants are reported in Table 6.6.

Table 6.7 shows the degradation of phenol using various photocatalysts under different reaction conditions. Parameters such as pH, light source, and initial pollutant concentration have been shown to influence the rate of degradation. For example, Chang et al. (2018) measured the highest degradation efficiency in an acidic condition of pH 2 in the presence of Fe_2O_4/TiO_2 while Moradi et al. (2021) reported an optimal pH of 8 when using $FeTiO_3$/GO photocatalyst. Studies carried out using different light sources have shown that excellent degradation efficiency is measured in photocatalytic degradation carried out under UV and high wattage visible light irradiation in a shorter period. It is known that the rate of degradation increases with a decrease in wavelength and therefore shorter wavelength leads to quicker degradation (Ahmad et al., 2020). Galedari et al. (2016) degraded 96% of 50 mg/L phenol in 120 min using UVC light irradiation with a $ZnO@SiO_2$ photocatalyst while 41% of the same concentration was degraded in 420 min when using $ZnO/Ag_2CO_3/Ag_2O$ in Rosman et al. (2018) study. Hayati and co-workers (2018) degraded phenol at 60 mg/L initial concentration in 160 min using ZnO/TiO_2@rGO photocatalyst while Mohamed et al. (2019) degraded a lower concentration (10 mg/L) in a shorter period of 20 min using PAN-CNT/TiO_2-NH_2 photocatalyst. In our study, low-wattage visible light was used to simulate the degradation experiments. For potential practical application, photocatalytic materials that can be activated under low-wattage light and natural sunlight are preferred.

Table 6.6: Summary of different photocatalysts reported for the degradation of organic pollutants in the presence of different ions in wastewater/real-water samples

Photocatalysts	Pollutant	Promoted effect	Neutral Effect	Inhibited effect	Reference
Co_3O_4-Bi_2O_3	Bisphenol A	High Cl^-	-	H_2PO_4 and CO_3^{2-}	(Hu et al., 2018)
UV/TiO_2	Metronidazole	Glucose	-	Fe^{3+}, H_2PO_4, Ca^{2+}, Mg^{2+}, Cl^-, SO_4^{2-}, NO_3^-, HCO_3^-	(Tran et al., 2019)
UVA-LED/TiO_2/persulfate	Ibuprofen	-	-	Cl-, SO_4^{2-}, HCO_3^-	(Ding and Hu, 2020)
g-C_3N_4/$Bi_2O_2CO_3$	Tetracycline	-	-	Cl^-, NO_3^-, CO_3^{2-}, SO_4^{2-}, Mg^{2+}, Fe^{3+}, NH_4^+, Zn^{2+}, Ca^{2+}	(Zhao et al., 2019a)
AgI/UiO-66	Sulfamethoxazole	-	SO_4^{2-} and Cl^-	HCO_3^-	(Wang et al., 2018a)
TiO_2	Sulfamethoxazole	-	-	HPO_4^{2-}, HCO_3^-, SO_4^{2-}, Cl^-, $H_2PO_4^-$	(Yuan et al., 2019)
CQDs/g-C_3N_4	Sulfamethazine	HCO_3^-			(Di et al., 2020)

Cu-CNF/MLCT	CTC-HCl	-	Na^+, K^+	Zn^{2+}, Mg^{2+}, NO_2^-	(Wang et al., 2020a)
NCD_s/TNS-001	DCF	-	Cl^-, SO_4^{2-}, Mg^{2+},	Fe^{3+}, Cu^{2+}	(Wang et al., 2019a)
$Cu_{0.84}Bi_{2.08}O_4$/PDS/Visible light	CIP	-	-	HCO_3^-, PO_4^{3-}, SO_4^{2-}, NO_3^-,	(Tang et al., 2019)
NCD_s-BiOBr/CeO_2	CBZ			SO_4^{2-}, NO_3^-,	(Liang et al., 2020)
$FeTiO_3$/GO	Phenol	-	-	HCO_3^-, Cl^-, SO_4^{2-}	(Moradi et al., 2021)
CeO_2/IK-C_3N4	Acetaminophen	-	-	Cl^-, NO_3^-, SO_4^{2-}, PO_4^{3-}	(Paragas et al., 2021)
Bi_2O_3-Sensitized TiO_2	Tetracycline	-	Cl^-	SO_4^{2-}, NO_3^-	(Shi et al., 2020a)
2D-Bi_4NbO_8Cl	Tetracycline	-	-	CO_3^{2-}, Cl^-, SO_4^{2-}	(Majumdar et al., 2022)
CuO-Cu_2O	Methylene Blue	Low Cl^-	-	SO_4^{2-}, High Cl^-, NO_3^-	(Tavakoli Joorabi et al., 2022)

Floating porous g-C_3N_4	Tetracycline	Cl^-, SO_4^{2-}	-	-	(Tang et al., 2022a)
AgCl/$Bi_{24}O_{31}Cl_{10}$	Phenol	Mg^{2+}, Ca^{2+}, Zn^{2+}, K^+	Cl^-	NO_3^-, NO_2^-, SO_4^{2-},	This study

Table 6.7: Comparison of the photocatalytic degradation of phenol with other studies

Photocatalyst	Phenol concentration (mg/L)	Light source	pH	%	Time	Reference
$FeTiO_3$/GO	50	150 W Xenon	8	100%	150 min	(Moradi et al., 2021)
NCN/Bi_2WO_6	10	300 W Xenon	-	93.1%	5 h	(Zhu and Zhou, 2020)
MgO@Ag/TiO_2	15	150 W Oriel Sol1A system	-	95%	120 min	(Scott et al., 2019)
BiOI/Bi_2WO_6	50	500 W Xenon	-	90.27%	3 h	(Huang et al., 2021)
Fe_3O_4/TiO_2	100	18 W UV	2	99%	150 min	(Chang et al., 2018)
ZnO/TiO_2@rGO	60	150 W Vis	4	91%	160 min	(Hayati et al., 2018)
ZnO/Ag_2CO_3/Ag_2O	50	100 W Vis	-	41%	420 min	(Rosman et al., 2018)
PAN-CNT/TiO_2-NH_2	10	100 W Halogen	5	99.7%	20 min	(Mohamed et al., 2019)
Ag/Ag_3PO_4/WO_3	10	300 W Xenon	7	99%	150 min	(Shi et al., 2019)
ZnO@SiO_2	50	Three 16 W UVC	5.9	96%	120 min	(Galedari et al., 2016)
AgCl/$Bi_{24}O_{31}Cl_{10}$	5	Six 36 W visible	9	84%	240 min	This study

6.6. Summary

The current work was carried out to evaluate the photocatalytic performance of AgCl/$Bi_{24}O_{31}Cl_{10}$ photocatalyst in the degradation of phenol in a secondary effluent from a wastewater treatment plant. The effects of three factors namely pH, initial pollutant concentration and photocatalyst dosage were investigated. The results show that pH is a dominant factor in the photodegradation process, followed by the concentration of pollutants and lastly, the photocatalyst dosage. The performance in the secondary effluent was better when compared to DI water. This was ascribed to the promoting effects of the pH and the presence of ions and other matter in the water matrix. While some ions have promoting effects, others are neutral or inhibit the degradation rate. As such, the total degradation rate is a cumulative response of all the various factors with some weighing more than the other.

CHAPTER 7 – CONCLUSIONS AND RECOMMENDATIONS

7.1. Conclusions

A AgCl/$Bi_{24}O_{31}Cl_{10}$ photocatalyst was identified and synthesized due to the benefits of harnessing the intrinsic properties of both semi-conductor materials and creating a heterojunction photocatalyst. Various techniques were used to characterize the material in order to validate the synthesis method and determine the purity of the photocatalyst. In addition, for the degradation of tetracycline and 2,4-dichlorophenoxy acetic acid, different percentages of silver chloride were deposited on the surface of the $Bi_{24}O_{31}Cl_{10}$ photocatalyst. The results showed that under visible light irradiation, 20%AgCl/$Bi_{24}O_{31}Cl_{10}$ was optimal for 2,4-D degradation and 50%AgCl/$Bi_{24}O_{31}Cl_{10}$ was optimal for TC degradation.

The effects of major factors that could affect photodegradation efficiency were investigated, including the pH of the solution, initial pollutant concentration and photocatalyst dosage. The results show that TC can degrade over a wider pH range, whereas 2,4-D degrades better at acidic pH. The behaviour of both pollutants indicates that the technology is more efficient at lower initial pollutant concentrations. The study also suggests that when using photocatalysis technology, the optimal dosage of semi-conductor material should be investigated to avoid photocatalyst aggregation in the solution, which reduces system efficiency. The material also demonstrated effective mineralization potential of the pollutant studied after 24 hours of irradiation, measuring 63% and 65% for TC and 2,4-D respectively, indicating the formation of intermediates.

The trapping experiments show that while superoxide radicals and holes are the reactive species responsible for degrading 2,4-D, superoxide radicals are responsible for TC degradation. This aids to propose a mechanism whereby Ag^0,

which is generated during irradiation serves as an electron mediator between both photocatalyst components transporting electrons from the conduction band of $Bi_{24}O_{31}Cl_{10}$ to the CB of AgCl. The separation of the electron-hole pairs enables a more efficient degradation process.

The final objective of the study involved evaluating the effectiveness of the synthesized materials in actual water samples. Since a lot of studies involved research in DI water conditions, it is far removed from the realities of environmentally relevant systems. Therefore, it was important to investigate the efficiency of the material in real water samples. The results show a higher efficiency in the degradation of phenol in the water matrix in comparison to DI Water. This is because while some ions have an inhibiting effect, others could have a promoting effect. The cumulative effect of these components promoted the degradation process.

Visible-light photocatalysis has promising socioeconomic implications. This is due to the inherent benefit of using solar energy to remove recalcitrant organic pollutants from wastewater. It results in significantly reduced energy costs when compared to ultraviolet light irradiation. Sunlight is also a universal resource, which could result in lower water costs, particularly in communities where energy supply is scarce. Although, all results were established on a laboratory scale in this study where a low-wattage visible light was simulated, it is important to confirm these hypothesis through pilot tests. The total cost of the technology will be influenced by key factors such as reactor design and other operating conditions. However, other studies have showed a potential of upto a third in the reduction of expenses when switching from an electricity photoreactor to solar energy (Isawi et al., 2021).

7.2. Recommendations

While major milestones were achieved in this study, other aspects could be recommended for future studies.

1. An investigation should be done to identify a degradation pathway for the selected contaminants and their intermediates. This is to ensure that the intermediates being formed are not more toxic than the parent material.

2. It is also important to consider the photocatalysts' potential for applications other than water treatment. The research could be expanded to include the simultaneous degradation of organic contaminants while producing hydrogen or the conversion of CO_2 to renewable fuels.

REFERENCES

A, M., J, M., ASHOKKUMAR, M. & ARUNACHALAM, P. 2018. A review on BiVO 4 photocatalyst: Activity enhancement methods for solar photocatalytic applications. *Applied Catalysis A: General,* 555**,** 47-74.

ABAZARI, R., MAHJOUB, A. R., SHARIATI, J. & NORUZI, S. 2019. Photocatalytic wastewater purification under visible light irradiation using bismuth molybdate hollow microspheres with high surface area. *Journal of Cleaner Production,* 221**,** 582-586.

ABDELLAH, M., NOSIER, S., EL-SHAZLY, A. & MUBARAK, A. 2018. Photocatalytic decolorization of methylene blue using TiO2/UV system enhanced by air sparging. *Alexandria engineering journal,* 57**,** 3727-3735.

ABDENNOURI, M., ELHALIL, A., FARNANE, M., TOUNSADI, H., MAHJOUBI, F. Z., ELMOUBARKI, R., SADIQ, M., KHAMAR, L., GALADI, A., BAÂLALA, M., BENSITEL, M., EL HAFIANE, Y., SMITH, A. & BARKA, N. 2015. Photocatalytic degradation of 2,4-D and 2,4-DP herbicides on Pt/TiO2 nanoparticles. *Journal of Saudi Chemical Society,* 19**,** 485-493.

ADENUGA, D., SKOSANA, S., TICHAPONDWA, S. & CHIRWA, E. 2021. Synthesis of a plasmonic AgCl and oxygen-rich Bi24O31Cl10 composite heterogeneous catalyst for enhanced degradation of tetracycline and 2,4-dichlorophenoxy acetic acid. *RSC Advances,* 11**,** 36760-36768.

ADENUGA, D. O., TICHAPONDWA, S. M. & CHIRWA, E. M. N. 2020. Facile synthesis of a Ag/AgCl/BiOCl composite photocatalyst for visible – light – driven pollutant removal. *Journal of Photochemistry and Photobiology A: Chemistry*, 401.

AGRAWAL, A., PANDEY, R. S. & SHARMA, B. 2010. Water Pollution with Special Reference to Pesticide Contamination in India. *Journal of Water Resource and Protection,* 02**,** 432-448.

AHMAD, K., GHATAK, H. R. & AHUJA, S. M. 2020. A review on photocatalytic remediation of environmental pollutants and H2 production through water splitting: A sustainable approach. *Environmental Technology & Innovation,* 19**,** 100893.

AHMADI, M., MOTLAGH, H. R., JAAFARZADEH, N., MOSTOUFI, A., SAEEDI, R., BARZEGAR, G. & JORFI, S. 2017. Enhanced photocatalytic degradation of tetracycline and real pharmaceutical wastewater using MWCNT/TiO2 nano-composite. *Journal of environmental management,* 186**,** 55-63.

AHMADPOUR, N., SAYADI, M. H., SOBHANI, S. & HAJIANI, M. 2020. Photocatalytic degradation of model pharmaceutical pollutant by novel magnetic TiO2@ZnFe2O4/Pd nanocomposite with enhanced photocatalytic activity and stability under solar light irradiation. *Journal of Environmental Management,* 271**,** 110964.

AHMED, A., USMAN, M., YU, B., DING, X., PENG, Q., SHEN, Y. & CONG, H. 2020. Efficient photocatalytic degradation of toxic Alizarin yellow R dye from industrial wastewater using biosynthesized Fe nanoparticle and study of factors affecting the degradation rate. *Journal of Photochemistry and Photobiology B: Biology,* 202**,** 111682.

AHMED, S. N. & HAIDER, W. 2018. Heterogeneous photocatalysis and its potential applications in water and wastewater treatment: a review. *Nanotechnology,* 29**,** 342001.

AI, M., QIN, W., XIA, T., YE, Y., CHEN, X. & ZHANG, P. 2019. Photocatalytic Degradation of 2,4-Dichlorophenol by TiO2 Intercalated Talc Nanocomposite. *International Journal of Photoenergy,* 2019**,** 1-11.

AKHIL, D., LAKSHMI, D., SENTHIL KUMAR, P., VO, D.-V. N. & KARTIK, A. 2021. Occurrence and removal of antibiotics from industrial wastewater. *Environmental Chemistry Letters,* 19**,** 1477-1507.

AKKARI, M., ARANDA, P., BELVER, C., BEDIA, J., BEN HAJ AMARA, A. & RUIZ-HITZKY, E. 2018. ZnO/sepiolite heterostructured materials for solar photocatalytic degradation of pharmaceuticals in wastewater. *Applied Clay Science,* 156**,** 104-109.

AL-MAMUN, M. R., KADER, S., ISLAM, M. S. & KHAN, M. Z. H. 2019. Photocatalytic activity improvement and application of UV-TiO2 photocatalysis in textile wastewater treatment: A review. *Journal of Environmental Chemical Engineering,* 7**,** 103248.

AL BSOUL, A., HAILAT, M., ABDELHAY, A., TAWALBEH, M., AL-OTHMAN, A., AL-KHARABSHEH, I. N. & AL-TAANI, A. A. 2021. Efficient removal of phenol compounds from water environment using Ziziphus leaves adsorbent. *Science of The Total Environment,* 761**,** 143229.

ALATALO, S.-M., DANESHVAR, E., KINNUNEN, N., MEŠČERIAKOVAS, A., THANGARAJ, S. K., JÄNIS, J., TSANG, D. C. W., BHATNAGAR, A. & LÄHDE, A. 2019. Mechanistic insight into efficient removal of tetracycline from water by Fe/graphene. *Chemical Engineering Journal,* 373**,** 821-830.

ALIKHANI, N., FARHADIAN, M., GOSHADROU, A., TANGESTANINEJAD, S. & ESKANDARI, P. 2021. Photocatalytic degradation and adsorption of herbicide 2,4-dichlorophenoxyacetic acid from aqueous solution using TiO2/BiOBr/Bi2S3 nanostructure stabilized on the activated carbon under visible light. *Environmental Nanotechnology, Monitoring & Management,* 15**,** 100415.

AN, C., WANG, S., SUN, Y., ZHANG, Q., ZHANG, J., WANG, C. & FANG, J. 2016. Plasmonic silver incorporated silver halides for efficient photocatalysis. *Journal of Materials Chemistry A,* 4**,** 4336-4352.

ANH, H. Q., LE, T. P. Q., DA LE, N., LU, X. X., DUONG, T. T., GARNIER, J., ROCHELLE-NEWALL, E., ZHANG, S., OH, N. H., OEURNG, C.,

EKKAWATPANIT, C., NGUYEN, T. D., NGUYEN, Q. T., NGUYEN, T. D., NGUYEN, T. N., TRAN, T. L., KUNISUE, T., TANOUE, R., TAKAHASHI, S., MINH, T. B., LE, H. T., PHAM, T. N. M. & NGUYEN, T. A. H. 2021. Antibiotics in surface water of East and Southeast Asian countries: A focused review on contamination status, pollution sources, potential risks, and future perspectives. *Sci Total Environ,* 764**,** 142865.

AREFIEVA, O. D., ZEMNUKHOVA, L. A., MORGUN, N. P., RYBIN, V. G., TSVETNOV, M. A., KOVSHUN, A. A. & PANASENKO, A. E. 2015. Removal of (2,4-Dichlorophenoxy) Acetic Acid from Aqueous solutions using low-cost sorbents. *Air, Soil and Water Research* 8**,** 59-65.

ATEIA, M., ALALM, M. G., AWFA, D., JOHNSON, M. S. & YOSHIMURA, C. 2020. Modeling the degradation and disinfection of water pollutants by photocatalysts and composites: A critical review. *Science of The Total Environment,* 698**,** 134197.

BABU, D. S., SRIVASTAVA, V., NIDHEESH, P. V. & KUMAR, M. S. 2019. Detoxification of water and wastewater by advanced oxidation processes. *Science of The Total Environment,* 696.

BAHADUR, A., IQBAL, S., ALSAAB, H. O., AWWAD, N. S. & IBRAHIUM, H. A. 2021. Designing a novel visible-light-driven heterostructure Ni–ZnO/S-g-C3N4 photocatalyst for coloured pollutant degradation. *RSC Advances,* 11**,** 36518-36527.

BAIG, N., IHSANULLAH, SAJID, M. & SALEH, T. A. 2019. Graphene-based adsorbents for the removal of toxic organic pollutants: A review. *Journal of Environmental Management,* 244**,** 370-382.

BANERJEE, S., PILLAI, S. C., FALARAS, P., O'SHEA, K. E., BYRNE, J. A. & DIONYSIOU, D. D. 2014. New Insights into the Mechanism of Visible Light Photocatalysis. *J Phys Chem Lett,* 5**,** 2543-54.

BI, C., CAO, J., LINA, H., WANG, Y. & CHEN, S. 2016. Enhanced photocatalytic activity of Bi12O17Cl2 through loading Pt quantum dots as a highly efficient electron capturer. *Applied Catalysis B: Environmental,* 195**,** 132-140.

BIN-DAHMAN, O. A. & SALEH, T. A. 2020. Synthesis of carbon nanotubes grafted with PEG and its efficiency for the removal of phenol from industrial wastewater. *Environmental Nanotechnology, Monitoring & Management,* 13.

BYRNE, C., SUBRAMANIAN, G. & PILLAI, S. C. 2018. Recent advances in photocatalysis for environmental applications. *Journal of Environmental Chemical Engineering,* 6**,** 3531-3555.

CAI, Z., DWIVEDI, A. D., LEE, W.-N., ZHAO, X., LIU, W., SILLANPÄÄ, M., ZHAO, D., HUANG, C.-H. & FU, J. 2018. Application of nanotechnologies for removing pharmaceutically active compounds from water: development and future trends. *Environmental Science: Nano,* 5**,** 27-47.

CAO, J., XIONG, Z. & LAI, B. 2018. Effect of initial pH on the tetracycline (TC) removal by zero-valent iron: Adsorption, oxidation and reduction. *Chemical Engineering Journal,* 343**,** 492-499.

CARBAJO, J., TOLOSANA-MORANCHEL, A., CASAS, J. A., FARALDOS, M. & BAHAMONDE, A. 2018. Analysis of photoefficiency in TiO2 aqueous suspensions: Effect of titania hydrodynamic particle size and catalyst loading on their optical properties. *Applied Catalysis B: Environmental,* 221**,** 1-8.

CESCON, A. & JIANG, J.-Q. 2020. Filtration Process and Alternative Filter Media Material in Water Treatment. *Water,* 12**,** 3377.

CHAI, W. S., CHEUN, J. Y., KUMAR, P. S., MUBASHIR, M., MAJEED, Z., BANAT, F., HO, S.-H. & SHOW, P. L. 2021. A review on conventional and novel materials towards heavy metal adsorption in wastewater treatment application. *Journal of Cleaner Production,* 296**,** 126589.

CHANG, F., WU, F., YAN, W., JIAO, M., ZHENG, J., DENG, B. & HU, X. 2019. Oxygen-rich bismuth oxychloride Bi12O17Cl2 materials: construction, characterization, and sonocatalytic degradation performance. *Ultrasonics sonochemistry,* 50**,** 105-113.

CHANG, J., ZHANG, Q., LIU, Y., SHI, Y. & QIN, Z. 2018. Preparation of Fe3O4/TiO2 magnetic photocatalyst for photocatalytic degradation of phenol. *Journal of Materials Science: Materials in Electronics,* 29**,** 8258-8266.

CHANG, Y.-C. & HSU, C.-C. 2020. Synergetic effect of carbon black as co-catalyst for enhanced visible-light photocatalytic activity and stability on ZnO nanoparticles. *Solid State Sciences,* 107.

CHEN, D., CHENG, Y., ZHOU, N., CHEN, P., WANG, Y., LI, K., HUO, S., CHENG, P., PENG, P., ZHANG, R., WANG, L., LIU, H., LIU, Y. & RUAN, R. 2020. Photocatalytic degradation of organic pollutants using TiO2-based photocatalysts: A review. *Journal of Cleaner Production,* 268**,** 121725.

CHEN, D., LI, B., PU, Q., CHEN, X., WEN, G. & LI, Z. 2019. Preparation of Ag-AgVO3/g-C3N4 composite photo-catalyst and degradation characteristics of antibiotics. *Journal of Hazardous Materials,* 373**,** 303-312.

CHEN, G., WU, G., LI, N., LU, X., ZHAO, J., HE, M., YAN, B., ZHANG, H., DUAN, X. & WANG, S. 2021a. Landfill leachate treatment by persulphate related advanced oxidation technologies. *J Hazard Mater,* 418**,** 126355.

CHEN, Q., YAO, Y., LI, X., LU, J., ZHOU, J. & HUANG, Z. 2018. Comparison of heavy metal removals from aqueous solutions by chemical precipitation and characteristics of precipitates. *Journal of Water Process Engineering,* 26**,** 289-300.

CHEN, X., SHEN, S., GUO, L. & MAO, S. S. 2010. Semiconductor-based Photocatalytic Hydrogen Generation. *Chemical Reviews* 110**,** 6503-6570.

CHEN, X., YANG, Y., KE, Y., CHEN, C. & XIE, S. 2022. A comprehensive review on biodegradation of tetracyclines: Current research progress and prospect. *Science of The Total Environment,* 814**,** 152852.

CHEN, Z., CHU, X., HUANG, X., SUN, H., CHEN, L. & GUO, F. 2021b. Fabrication of visible-light driven CoP/ZnSnO3 composite photocatalyst for high-efficient photodegradation of antibiotic pollutant. *Separation and Purification Technology,* 257.

CHENG, D., NGO, H. H., GUO, W., CHANG, S. W., NGUYEN, D. D., LIU, Y., WEI, Q. & WEI, D. 2020. A critical review on antibiotics and hormones in swine wastewater: Water pollution problems and control approaches. *Journal of Hazardous Materials,* 387**,** 121682.

CRINI, G. & LICHTFOUSE, E. 2018. Advantages and disadvantages of techniques used for wastewater treatment. *Environmental Chemistry Letters,* 17**,** 145-155.

CUI, P., WANG, J., WANG, Z., CHEN, J., XING, X., WANG, L. & YU, R. 2016. Bismuth oxychloride hollow microspheres with high visible light photocatalytic activity. *Nano Research,* 9**,** 593-601.

DAGHRIR, R. & DROGUI, P. 2013. Tetracycline antibiotics in the environment: a review. *Environmental Chemistry Letters,* 11**,** 209-227.

DAI, Y., LIU, M., LI, J., YANG, S., SUN, Y., SUN, Q., WANG, W., LU, L., ZHANG, K., XU, J., ZHENG, W., HU, Z., YANG, Y., GAO, Y. & LIU, Z. 2019. A review on pollution situation and treatment methods of tetracycline in groundwater. *Separation Science and Technology,* 55**,** 1005-1021.

DE MORAES, N. P., GOES, C. M., ROCHA, R. D. S., GOUVÊA, M. E. V., DE SIERVO, A., SILVA, M. L. C. P. D. & RODRIGUES, L. A. 2021. Tannin-based carbon xerogel as a promising co-catalyst for photodegradation processes based on solar light: a case study using the tin (IV) oxide/carbon xerogel composite. *Chemical Engineering Communications***,** 1-13.

DE OLIVEIRA, M., FRIHLING, B. E. F., VELASQUES, J., FILHO, F. J. C. M., CAVALHERI, P. S. & MIGLIOLO, L. 2020. Pharmaceuticals residues and xenobiotics contaminants: Occurrence, analytical techniques and sustainable alternatives for wastewater treatment. *Science of The Total Environment,* 705**,** 135568.

DEBLONDE, T., COSSU-LEGUILLE, C. & HARTEMANN, P. 2011. Emerging pollutants in wastewater: A review of the literature. *International Journal of Hygiene and Environmental Health,* 214**,** 442-448.

DEHMANI, Y. & ABOUARNADASSE, S. 2020. Study of the adsorbent properties of nickel oxide for phenol depollution. *Arabian Journal of Chemistry,* 13**,** 5312-5325.

DENG, F., LU, X., LUO, Y., WANG, J., CHE, W., YANG, R., LUO, X., LUO, S. & DIONYSIOU, D. D. 2019. Novel visible-light-driven direct Z-scheme CdS/CuInS2 nanoplates for excellent photocatalytic degradation

performance and highly-efficient Cr(VI) reduction. *Chemical Engineering Journal,* 361**,** 1451-1461.

DERIKVANDI, H., VOSOUGH, M. & NEZAMZADEH-EJHIEH, A. 2021. A novel double Ag@ AgCl/Cu@ Cu2O plasmonic nanostructure: experimental design and LC-Mass detection of tetracycline degradation intermediates. *International Journal of Hydrogen Energy,* 46**,** 2049-2064.

DI, G., ZHU, Z., DAI, Q., ZHANG, H., SHEN, X., QIU, Y., HUANG, Y., YU, J., YIN, D. & KÜPPERS, S. 2020. Wavelength-dependent effects of carbon quantum dots on the photocatalytic activity of g-C3N4 enabled by LEDs. *Chemical Engineering Journal,* 379**,** 122296.

DI, J., XIA, J., LI, H., GUO, S. & DAI, S. 2017. Bismuth oxyhalide layered materials for energy and environmental applications. *Nano Energy,* 41**,** 172-192.

DING, H. & HU, J. 2020. Degradation of ibuprofen by UVA-LED/TiO2/persulfate process: Kinetics, mechanism, water matrix effects, intermediates and energy consumption. *Chemical Engineering Journal,* 397**,** 125462.

DOTTO, G. L. & MCKAY, G. 2020. Current scenario and challenges in adsorption for water treatment. *Journal of Environmental Chemical Engineering,* 8**,** 103988.

DUGANDŽIĆ, A. M., TOMAŠEVIĆ, A. V., RADIŠIĆ, M. M., ŠEKULJICA, N. Ž., MIJIN, D. Ž. & PETROVIĆ, S. D. 2017. Effect of inorganic ions, photosensitisers and scavengers on the photocatalytic degradation of nicosulfuron. *Journal of Photochemistry and Photobiology A: Chemistry,* 336**,** 146-155.

ESLAMI, A., MEHDIPOUR, F., LIN, K.-Y. A., SHARIFI MALEKSARI, H., MIRZAEI, F. & GHANBARI, F. 2020. Sono-photo activation of percarbonate for the degradation of organic dye: The effect of water matrix and identification of by-products. *Journal of Water Process Engineering,* 33.

EVANS, A. E. V., MATEO-SAGASTA, J., QADIR, M., BOELEE, E. & IPPOLITO, A. 2019. Agricultural water pollution: key knowledge gaps and research needs. *Current Opinion in Environmental Sustainability,* 36**,** 20-27.

FANG, H., PAN, Y., YIN, M. & PAN, C. 2019. Enhanced visible light photocatalytic activity of CdS with alkalized Ti3C2 nano-sheets as co-catalyst for degradation of rhodamine B. *Journal of Materials Science: Materials in Electronics,* 30**,** 14954-14966.

FANG, X., CHEN, J. & ZHAN, J. 2020. Heterojunction photocatalyst for organic degradation: Superior photocatalytic activity through the phase and interface engineering. *Ceramics International,* 46**,** 23245-23256.

FENELON, E., BUI, D.-P., TRAN, H. H., YOU, S.-J., WANG, Y.-F., CAO, T. M. & VAN PHAM, V. 2020. Straightforward Synthesis of

SnO2/Bi2S3/BiOCl–Bi24O31Cl10 Composites for Drastically Enhancing Rhodamine B Photocatalytic Degradation under Visible Light. *ACS Omega,* 5**,** 20438-20449.

FENG, C., CHEN, Z., JING, J., SUN, M., TIAN, J., HAN, J., LI, W. & MA, L. 2020. Synthesis of a novel three-dimensional sponge-like microporous CdS film with high photoelectrochemical performance and stability. *Journal of Electroanalytical Chemistry,* 874.

FENG, Z., YU, J., SUN, D. & WANG, T. 2016. Visible-light-driven photocatalysts Ag/AgCl dispersed on mesoporous Al2O3 with enhanced photocatalytic performance. *J Colloid Interface Sci,* 480**,** 184-190.

FÓNAGY, O., SZABÓ-BÁRDOS, E. & HORVÁTH, O. 2021. 1,4-Benzoquinone and 1,4-hydroquinone based determination of electron and superoxide radical formed in heterogeneous photocatalytic systems. *Journal of Photochemistry and Photobiology A: Chemistry,* 407**,** 113057.

FU, S.-M., LI, G.-S., WEN, X., FAN, C.-M., LIU, J.-X., ZHANG, X.-C. & LI, R. 2020. Effect of calcination temperature on microstructure and photocatalytic activity of BiOX (X=Cl, Br). *Transactions of Nonferrous Metals Society of China,* 30**,** 765-773.

FU, Z., YANG, Q., LIU, Z., CHEN, F., YAO, F., XIE, T., ZHONG, Y., WANG, D., LI, J., LI, X. & ZENG, G. 2019. Photocatalytic conversion of carbon dioxide: From products to design the catalysts. *Journal of CO2 Utilization,* 34**,** 63-73.

FUJISHIMA, A. & HONDA, K. 1972. Electrochemical photolysis of water at a semiconductor electrode. *Nature,* 238.

FUJISHIMA, A., RAO, T. N. & TRYK, D. A. 2000. Titanium dioxide photocatalysis. *Journal of Photochemistry and Photobiology C: Photochemistry Reviews* 1**,** 1-21.

GALEDARI, N. A., RAHMANI, M. & TASBIHI, M. 2016. Preparation, characterization, and application of ZnO@SiO2 core–shell structured catalyst for photocatalytic degradation of phenol. *Environmental Science and Pollution Research,* 24**,** 12655-12663.

GANGU, K. K., MADDILA, S. & JONNALAGADDA, S. B. 2019. A review on novel composites of MWCNTs mediated semiconducting materials as photocatalysts in water treatment. *Science of The Total Environment,* 646**,** 1398-1412.

GAO, W., RAN, C., WANG, M., LI, L., SUN, Z. & YAO, X. 2016. The role of reduction extent of graphene oxide in the photocatalytic performance of Ag/AgX (X = Cl, Br)/rGO composites and the pseudo-second-order kinetics reaction nature of the Ag/AgBr system. *Physical Chemistry Chemical Physics,* 18**,** 18219-18226.

GAO, X., GUO, Q., TANG, G., PENG, W., LUO, Y. & HE, D. 2019. Effects of inorganic ions on the photocatalytic degradation of carbamazepine. *Journal of Water Reuse and Desalination,* 9**,** 301-309.

GAUTAM, P., KUMAR, S. & LOKHANDWALA, S. 2019. Advanced oxidation processes for treatment of leachate from hazardous waste landfill: A critical review. *Journal of Cleaner Production,* 237**,** 117639.

GHATTAVI, S. & NEZAMZADEH-EJHIEH, A. 2020. A visible light driven AgBr/g-C3N4 photocatalyst composite in methyl orange photodegradation: Focus on photoluminescence, mole ratio, synthesis method of g-C3N4 and scavengers. *Composites Part B: Engineering,* 183**,** 107712.

GOPINATH, C. S. & NALAJALA, N. 2021. A scalable and thin film approach for solar hydrogen generation: a review on enhanced photocatalytic water splitting. *Journal of Materials Chemistry A,* 9**,** 1353-1371.

GOPINATH, K. P., MADHAV, N. V., KRISHNAN, A., MALOLAN, R. & RANGARAJAN, G. 2020. Present applications of titanium dioxide for the photocatalytic removal of pollutants from water: A review. *J Environ Manage,* 270**,** 110906.

GOU, J., LI, X., ZHANG, H., GUO, R., DENG, X., CHENG, X., XIE, M. & CHENG, Q. 2018. Synthesis of silver/silver chloride/exfoliated graphite nano-photocatalyst and its enhanced visible light photocatalytic mechanism for degradation of organic pollutants. *Journal of Industrial and Engineering Chemistry,* 59**,** 99-107.

GU, Y., GUO, B., YI, Z., WU, X., ZHANG, J. & YANG, H. 2022. Synthesis of a Self-assembled Dual Morphologies Ag-NPs/SrMoO
4
Photocatalyst with LSPR Effect for the Degradation of Methylene Blue Dye. *ChemistrySelect,* 7.

GUO, Y., BAI, L., TANG, X., HUANG, Q., XIE, B., WANG, T., WANG, J., LI, G. & LIANG, H. 2018. Coupling continuous sand filtration to ultrafiltration for drinking water treatment: Improved performance and membrane fouling control. *Journal of Membrane Science,* 567**,** 18-27.

HADDOUT, S., PRIYA, K. L., HOGUANE, A. M. & LJUBENKOV, I. 2020. Water Scarcity: A Big Challenge to Slums in Africa to Fight against COVID-19. *Science & Technology Libraries,* 39**,** 281-288.

HAMA AZIZ, K. H., MIESSNER, H., MUELLER, S., MAHYAR, A., KALASS, D., MOELLER, D., KHORSHID, I. & RASHID, M. A. M. 2018. Comparative study on 2,4-dichlorophenoxyacetic acid and 2,4-dichlorophenol removal from aqueous solutions via ozonation, photocatalysis and non-thermal plasma using a planar falling film reactor. *Journal of Hazardous Materials,* 343**,** 107-115.

HASAN, M. K., SHAHRIAR, A. & JIM, K. U. 2019. Water pollution in Bangladesh and its impact on public health. *Heliyon,* 5**,** e02145.

HASANPOUR, M. & HATAMI, M. 2020. Photocatalytic performance of aerogels for organic dyes removal from wastewaters: Review study. *Journal of Molecular Liquids,* 309.

HASSANI, A., FARAJI, M. & EGHBALI, P. 2020. Facile fabrication of mpg-C3N4/Ag/ZnO nanowires/Zn photocatalyst plates for photodegradation of dye pollutant. *Journal of Photochemistry and Photobiology A: Chemistry,* 400.

HAYATI, F., ISARI, A. A., FATTAHI, M., ANVARIPOUR, B. & JORFI, S. 2018. Photocatalytic decontamination of phenol and petrochemical wastewater through ZnO/TiO2 decorated on reduced graphene oxide nanocomposite: influential operating factors, mechanism, and electrical energy consumption. *RSC Advances,* 8**,** 40035-40053.

HEEBNER, A. & ABBASSI, B. 2022. Electrolysis catalyzed ozonation for advanced wastewater treatment. *Journal of Water Process Engineering,* 46.

HOU, X., WANG, Z., CHEN, J., WANG, J., LU, Q. & WU, D. 2021. Facile construction of silver-based solid solution heterophase for efficient visible-light-driven photocatalytic degradation of tetracycline. *Chemical Engineering Journal,* 414**,** 128915.

HU, K., LI, R., YE, C., WANG, A., WEI, W., HU, D., QIU, R. & YAN, K. 2020. Facile synthesis of Z-scheme composite of TiO2 nanorod/g-C3N4 nanosheet efficient for photocatalytic degradation of ciprofloxacin. *Journal of Cleaner Production,* 253.

HU, L., ZHANG, G., LIU, M., WANG, Q. & WANG, P. 2018. Enhanced degradation of Bisphenol A (BPA) by peroxymonosulfate with Co3O4-Bi2O3 catalyst activation: Effects of pH, inorganic anions, and water matrix. *Chemical Engineering Journal,* 338**,** 300-310.

HU, Z., GE, M. & GUO, C. 2021. Efficient removal of levofloxacin from different water matrices via simultaneous adsorption and photocatalysis using a magnetic Ag3PO4/rGO/CoFe2O4 catalyst. *Chemosphere,* 268**,** 128834.

HUANG, D., LI, J., ZENG, G., XUE, W., CHEN, S., LI, Z., DENG, R., YANG, Y. & CHENG, M. 2019. Facile construction of hierarchical flower-like Z-scheme AgBr/Bi2WO6 photocatalysts for effective removal of tetracycline: Degradation pathways and mechanism. *Chemical Engineering Journal,* 375**,** 121991.

HUANG, H., LI, D., LIN, Q., ZHANG, W., SHAO, Y., CHEN, Y., SUN, M. & FU, X. 2009. Efficient Degradation of Benzene over LaVO4/TiO2 Nanocrystalline Heterojunction Photocatalyst under Visible Light Irradiation. *Environmental Science and Technology,* 43**,** 4164-4168.

HUANG, X., GUO, Q., YAN, B., LIU, H., CHEN, K., WEI, S., WU, Y. & WANG, L. 2021. Study on photocatalytic degradation of phenol by BiOI/Bi2WO6 layered heterojunction synthesized by hydrothermal method. *Journal of Molecular Liquids,* 322**,** 114965.

HUCK, M., RING, L., KÜPPER, K., KLARE, J., DAUM, D. & SCHÄFER, H. 2020. Water splitting mediated by an electrocatalytically driven cyclic

process involving iron oxide species. *Journal of Materials Chemistry A,* 8**,** 9896-9910.

HUMAYUN, M., RAZIQ, F., KHAN, A. & LUO, W. 2018. Modification strategies of TiO2 for potential applications in photocatalysis: a critical review. *Green Chemistry Letters and Reviews,* 11**,** 86-102.

IKE, I. A., LINDEN, K. G., ORBELL, J. D. & DUKE, M. 2018. Critical review of the science and sustainability of persulphate advanced oxidation processes. *Chemical Engineering Journal,* 338**,** 651-669.

ISAWI, H., ABDELAZIZ, M. O., ABO ZEED, D., EL-KHOLY, R. A., EL-NOSS, M., SAID, M. M., EL-AASSAR, A.-H. M. & SHAWKY, H. A. 2021. Semi industrial continuous flow photoreactor for wastewater purification in some polluted areas: Design, Manufacture, and Socio-economic impacts. *Environmental Nanotechnology, Monitoring & Management,* 16.

ISLAM, F., WANG, J., FAROOQ, M. A., KHAN, M. S. S., XU, L., ZHU, J., ZHAO, M., MUNOS, S., LI, Q. X. & ZHOU, W. 2018. Potential impact of the herbicide 2,4-dichlorophenoxyacetic acid on human and ecosystems. *Environ Int,* 111**,** 332-351.

JAAFARZADEH, N., GHANBARI, F. & AHMADI, M. 2017. Efficient degradation of 2,4-Dichlorophenoxyacetic acid by peroxymonosulfate/magnetic copper ferrite nanopartilcles/ozone: A novel combination of advanced oxidation processes. *Chemical Engineering Journal,* 320.

JI, Y., ZHOU, L., FERRONATO, C., SALVADOR, A., YANG, X. & CHOVELON, J.-M. 2013. Degradation of sunscreen agent 2-phenylbenzimidazole-5-sulfonic acid by TiO2 photocatalysis: Kinetics, photoproducts and comparison to structurally related compounds. *Applied Catalysis B: Environmental,* 140-141**,** 457-467.

JIANG, D., CHEN, L., ZHU, J., CHEN, M., SHI, W. & XIE, J. 2013. Novel p–n heterojunction photocatalyst constructed by porous graphite-like C3N4 and nanostructured BiOI: facile synthesis and enhanced photocatalytic activity. *Dalton Transactions,* 42**,** 15726.

JIANG, X., GUO, Y., ZHANG, L., JIANG, W. & XIE, R. 2018. Catalytic degradation of tetracycline hydrochloride by persulfate activated with nano Fe0 immobilized mesoporous carbon. *Chemical Engineering Journal,* 341**,** 392-401.

JIMÉNEZ-SALCEDO, M., MONGE, M. & TENA, M. T. 2021. The photocatalytic degradation of sodium diclofenac in different water matrices using g-C3N4 nanosheets: A study of the intermediate by-products and mechanism. *Journal of Environmental Chemical Engineering,* 9**,** 105827.

JIN, C., LI, W., CHEN, Y., LI, R., HUO, J., HE, Q. & WANG, Y. 2020. Efficient Photocatalytic Degradation and Adsorption of Tetracycline over Type-II Heterojunctions Consisting of ZnO Nanorods and K-Doped Exfoliated g-

C3N4 Nanosheets. *Industrial & Engineering Chemistry Research,* 59**,** 2860-2873.

JIN, X., LV, C., ZHOU, X., YE, L., XIE, H., LIU, Y., SU, H., ZHANG, B. & CHEN, G. 2019. Oxygen Vacancy Engineering of Bi24 O31 Cl10 for Boosted Photocatalytic CO2 Conversion. *ChemSusChem,* 12**,** 2740-2747.

JIN, X., LV, C., ZHOU, X., ZHANG, C., ZHANG, B., SU, H. & CHEN, G. 2018. Realizing the regulated carrier separation and exciton generation of Bi24O31Cl10via a carbon doping strategy. *Journal of Materials Chemistry A,* 6**,** 24350-24357.

JIN, X., YE, L., WANG, H., SU, Y., XIE, H., ZHONG, Z. & ZHANG, H. 2015. Bismuth-rich strategy induced photocatalytic molecular oxygen activation properties of bismuth oxyhalogen: The case of Bi24O31Cl10. *Applied Catalysis B: Environmental,* 165**,** 668-675.

JIN, X., YE, L., XIE, H. & CHEN, G. 2017. Bismuth-rich bismuth oxyhalides for environmental and energy photocatalysis. *Coordination Chemistry Reviews,* 349**,** 84-101.

JOSHIBA, G. J., SENTHIL KUMAR, P., FEMINA, C. C., JAYASHREE, E., RACCHANA, R. & SIVANESAN, S. 2019. Critical review on biological treatment strategies of dairy wastewater. *Desalination and Water Treatment,* 160**,** 94-109.

KAMARUDIN, N. S., JUSOH, R., SETIABUDI, H. D., JUSOH, N. W. C., JAAFAR, N. F. & SUKOR, N. F. 2019. Cymbopogon nardus Mediated Synthesis of Ag Nanoparticles for the Photocatalytic Degradation of 2,4-Dicholorophenoxyacetic Acid. *Bulletin of Chemical Reaction Engineering & Catalysis,* 14.

KANAKARAJU, D., GLASS, B. D. & OELGEMÖLLER, M. 2018. Advanced oxidation process-mediated removal of pharmaceuticals from water: A review. *Journal of Environmental Management,* 219**,** 189-207.

KANAUJIYA, D. K., PAUL, T., SINHAROY, A. & PAKSHIRAJAN, K. 2019. Biological Treatment Processes for the Removal of Organic Micropollutants from Wastewater: a Review. *Current Pollution Reports,* 5**,** 112-128.

KANCHANAMALA DELANKA-PEDIGE, H. M., MUNASINGHE-ARACHCHIGE, S. P., ABEYSIRIWARDANA-ARACHCHIGE, I. S. A. & NIRMALAKHANDAN, N. 2021. Evaluating wastewater treatment infrastructure systems based on UN Sustainable Development Goals and targets. *Journal of Cleaner Production,* 298**,** 126795.

KANG, J., JIN, C., LI, Z., WANG, M., CHEN, Z. & WANG, Y. 2020a. Dual Z-scheme MoS2/g-C3N4/Bi24O31Cl10 ternary heterojunction photocatalysts for enhanced visible-light photodegradation of antibiotic. *Journal of Alloys and Compounds,* 825**,** 153975.

KANG, J., JIN, C., LI, Z., WANG, M., CHEN, Z. & WANG, Y. 2020b. Dual Z-scheme MoS2/g-C3N4/Bi24O31Cl10 ternary heterojunction

photocatalysts for enhanced visible-light photodegradation of antibiotic. *Journal of Alloys and Compounds,* 825.

KEARNS, J. P., WELLBORN, L. S., SUMMERS, R. S. & KNAPPE, D. R. U. 2014. 2,4-D adsorption to biochars: Effect of preparation conditions on equilibrium adsorption capacity and comparison with commercial activated carbon literature data. *Water Research,* 62**,** 20-28.

KHAKI, M. R. D., SHAFEEYAN, M. S., RAMAN, A. A. A. & DAUD, W. 2017. Application of doped photocatalysts for organic pollutant degradation - A review. *J Environ Manage,* 198**,** 78-94.

KHAN, A. A. & TAHIR, M. 2019. Recent advancements in engineering approach towards design of photo-reactors for selective photocatalytic CO2 reduction to renewable fuels. *Journal of CO2 Utilization,* 29**,** 205-239.

KIWAAN, H. A., ATWEE, T. M., AZAB, E. A. & EL-BINDARY, A. A. 2020. Photocatalytic degradation of organic dyes in the presence of nanostructured titanium dioxide. *Journal of Molecular Structure,* 1200.

KOE, W. S., LEE, J. W., CHONG, W. C., PANG, Y. L. & SIM, L. C. 2019. An overview of photocatalytic degradation: photocatalysts, mechanisms, and development of photocatalytic membrane. *Environmental Science and Pollution Research,* 27**,** 2522-2565.

KUDO, A. & MISEKI, Y. 2009. Heterogeneous photocatalyst materials for water splitting. *Chem Soc Rev,* 38**,** 253-78.

KUMAR, A. 2017. A Review on the Factors Affecting the Photocatalytic Degradation of Hazardous Materials. *Material Science & Engineering International Journal,* 1.

KURNIAWAN, S., ABDULLAH, S., IMRON, M., SAID, N., ISMAIL, N., HASAN, H., OTHMAN, A. & PURWANTI, I. 2020. Challenges and Opportunities of Biocoagulant/Bioflocculant Application for Drinking Water and Wastewater Treatment and Its Potential for Sludge Recovery. *International Journal of Environmental Research and Public Health,* 17**,** 9312.

KUSMIEREK, K. & SWIATKOWSKI, A. 2016. Adsorption of 2,4-Dichlorophenoxyacetic Acid from an Aqueous Solution on Fly Ash. *Water Environ Res,* 88**,** 231-8.

LADO RIBEIRO, A. R., MOREIRA, N. F. F., LI PUMA, G. & SILVA, A. M. T. 2019. Impact of water matrix on the removal of micropollutants by advanced oxidation technologies. *Chemical Engineering Journal,* 363**,** 155-173.

LEE, S.-Y. & PARK, S.-J. 2013. TiO2 photocatalyst for water treatment applications. *Journal of Industrial and Engineering Chemistry,* 19**,** 1761-1769.

LEI, J., CHEN, B., ZHOU, L., DING, N., CAI, Z., WANG, L., IN, S.-I., CUI, C., ZHOU, Y., LIU, Y. & ZHANG, J. 2020. Efficient degradation of antibiotics in different water matrices through the photocatalysis of inverse

opal K-g-C3N4: Insights into mechanism and assessment of antibacterial activity. *Chemical Engineering Journal,* 400**,** 125902.

LEI, X. F., XUE, X. X. & YANG, H. 2014. Preparation and characterization of Ag-doped TiO2 nanomaterials and their photocatalytic reduction of Cr(VI) under visible light. *Applied Surface Science,* 321**,** 396-403.

LEON-FERNANDEZ, L. F., VILLASEÑOR, J., RODRIGUEZ, L., CAÑIZARES, P., RODRIGO, M. A. & FERNÁNDEZ-MORALES, F. J. 2019. Dehalogenation of 2,4-Dichlorophenoxyacetic acid by means of bioelectrochemical systems. *Journal of Electroanalytical Chemistry,* 854**,** 113564.

LI, B., LAI, C., ZENG, G., QIN, L., YI, H., HUANG, D., ZHOU, C., LIU, X., CHENG, M., XU, P., ZHANG, C., HUANG, F. & LIU, S. 2018. Facile Hydrothermal Synthesis of Z-Scheme Bi2Fe4O9/Bi2WO6 Heterojunction Photocatalyst with Enhanced Visible Light Photocatalytic Activity. *ACS Applied Materials & Interfaces,* 10**,** 18824-18836.

LI, F.-T., WANG, Q., WANG, X.-J., LI, B., HAO, Y.-J., LIU, R.-H. & ZHAO, D.-S. 2014. In-situ one-step synthesis of novel BiOCl/Bi24O31Cl10 heterojunctions via self-combustion of ionic liquid with enhanced visible-light photocatalytic activities. *Applied Catalysis B: Environmental,* 150-151**,** 574-584.

LI, K., WU, J. Q., JIANG, L. L., SHEN, L. Z., LI, J. Y., HE, Z. H., WEI, P., LV, Z. & HE, M. F. 2017a. Developmental toxicity of 2,4-dichlorophenoxyacetic acid in zebrafish embryos. *Chemosphere,* 171**,** 40-48.

LI, M., LI, D., ZHOU, Z., WANG, P., MI, X., XIA, Y., WANG, H., ZHAN, S., LI, Y. & LI, L. 2020a. Plasmonic Ag as electron-transfer mediators in Bi2MoO6/Ag-AgCl for efficient photocatalytic inactivation of bacteria. *Chemical Engineering Journal,* 382**,** 122762.

LI, S., SUN, J. & GUAN, J. 2021a. Strategies to improve electrocatalytic and photocatalytic performance of two-dimensional materials for hydrogen evolution reaction. *Chinese Journal of Catalysis,* 42**,** 511-556.

LI, W., ZHANG, D., LAN, Y. & GUO, J. 2020b. CuO-Co3O4@CeO2 as a heterogeneous catalyst for efficient degradation of 2,4-dichlorophenoxyacetic acid by peroxymonosulfate. *Journal of Hazardous Materials,* 381.

LI, X., GARLISI, C., GUAN, Q., ANWER, S., AL-ALI, K., PALMISANO, G. & ZHENG, L. 2021b. A review of material aspects in developing direct Z-scheme photocatalysts. *Materials Today,* 47**,** 75-107.

LI, X., ZHU, C., SONG, Y., DU, D. & LIN, Y. 2017b. Solvent co-mediated synthesis of ultrathin BiOCl nanosheets with highly efficient visible-light photocatalytic activity. *RSC Advances,* 7**,** 10235-10241.

LI, Z., GUO, C., LYU, J., HU, Z. & GE, M. 2019a. Tetracycline degradation by persulfate activated with magnetic Cu/CuFe2O4 composite: Efficiency,

stability, mechanism and degradation pathway. *Journal of Hazardous Materials,* 373**,** 85-96.

LI, Z., JIN, C., LV, C., WANG, M., KANG, J., LIU, S., XIE, Y. & ZHU, T. 2019b. Construction of g-C3N4/Eu(III) doped Bi24O31Cl10 heterojunction for the enhanced visible-light photocatalytic performance. *Materials Chemistry and Physics,* 237**,** 121829.

LIANG, L., GAO, S., ZHU, J., WANG, L., XIONG, Y., XIA, X. & YANG, L. 2020. The enhanced photocatalytic performance toward carbamazepine by nitrogen-doped carbon dots decorated on BiOBr/CeO2: Mechanism insight and degradation pathways. *Chemical Engineering Journal,* 391**,** 123599.

LIANG, X., WANG, P., LI, M., ZHANG, Q., WANG, Z., DAI, Y., ZHANG, X., LIU, Y., WHANGBO, M.-H. & HUANG, B. 2018. Adsorption of gaseous ethylene via induced polarization on plasmonic photocatalyst Ag/AgCl/TiO2 and subsequent photodegradation. *Applied Catalysis B: Environmental,* 220**,** 356-361.

LIAO, Q., RONG, H., ZHAO, M., LUO, H., CHU, Z. & WANG, R. 2021. Interaction between tetracycline and microorganisms during wastewater treatment: A review. *Sci Total Environ,* 757**,** 143981.

LIU, H., ZHANG, H., SHEN, P., CHEN, F. & ZHANG, S. 2015. Synergistic Effects in Nanoengineered HNb3O8/Graphene Hybrids with Improved Photocatalytic Conversion Ability of CO2 into Renewable Fuels. *Langmuir,* 32**,** 254-264.

LIU, L., DENG, J., NIU, T., ZHENG, G., ZHANG, P., JIN, Y., JIAO, Z. & SUN, X. 2017. One-step synthesis of Ag/AgCl/GO composite: A photocatalyst of extraordinary photoactivity and stability. *J Colloid Interface Sci,* 493**,** 281-287.

LIU, Q., ZENG, C., AI, L., HAO, Z. & JIANG, J. 2018a. Boosting visible light photoreactivity of photoactive metal-organic framework: Designed plasmonic Z-scheme Ag/AgCl@ MIL-53-Fe. *Applied Catalysis B: Environmental,* 224**,** 38-45.

LIU, R., WANG, P., WANG, X., YU, H. & YU, J. 2012. UV- and Visible-Light Photocatalytic Activity of Simultaneously Deposited and Doped Ag/Ag(I)-TiO2 Photocatalyst. *The Journal of Physical Chemistry C,* 116**,** 17721-17728.

LIU, S., ZHAO, X.-R., SUN, H.-Y., LI, R.-P., FANG, Y.-F. & HUANG, Y.-P. 2013. The degradation of tetracycline in a photo-electro-Fenton system. *Chemical Engineering Journal,* 231**,** 441-448.

LIU, Y., WANG, W., SHAH, S. B., ZANAROLI, G., XU, P. & TANG, H. 2020. Phenol biodegradation by Acinetobacter radioresistens APH1 and its application in soil bioremediation. *Appl Microbiol Biotechnol,* 104**,** 427-437.

LIU, Z., MENG, H., ZHANG, H., CAO, J., ZHOU, K. & LIAN, J. 2018b. Highly efficient degradation of phenol wastewater by microwave induced H2O2-

CuOx/GAC catalytic oxidation process. *Separation and Purification Technology,* 193**,** 49-57.

LOW, J., YU, J., JARONIEC, M., WAGEH, S. & AL-GHAMDI, A. A. 2017. Heterojunction Photocatalysts. *Advanced Materials,* 29**,** 1601694.

LU, C., GUO, F., YAN, Q., ZHANG, Z., LI, D., WANG, L. & ZHOU, Y. 2019. Hydrothermal synthesis of type II ZnIn2S4/BiPO4 heterojunction photocatalyst with dandelion-like microflower structure for enhanced photocatalytic degradation of tetracycline under simulated solar light. *Journal of Alloys and Compounds,* 811.

LU, H., HAO, Q., CHEN, T., ZHANG, L., CHEN, D., MA, C., YAO, W. & ZHU, Y. 2018. A high-performance Bi2O3/Bi2SiO5 p-n heterojunction photocatalyst induced by phase transition of Bi2O3. *Applied Catalysis B: Environmental,* 237**,** 59-67.

LUO, J., ZHOU, X., NING, X., ZHAN, L., MA, L., XU, X., LI, S. & SUN, S. 2018. Utilization of LaCoO3 as an efficient co-catalyst to boost the visible light photocatalytic performance of g-C3N4. *Separation and Purification Technology,* 201**,** 309-317.

MA, D., YI, H., LAI, C., LIU, X., HUO, X., AN, Z., LI, L., FU, Y., LI, B., ZHANG, M., QIN, L., LIU, S. & YANG, L. 2021a. Critical review of advanced oxidation processes in organic wastewater treatment. *Chemosphere,* 275**,** 130104.

MA, M., YANG, Y., CHEN, Y., MA, Y., LYU, P., CUI, A., HUANG, W., ZHANG, Z., LI, Y. & SI, F. 2021b. Photocatalytic degradation of MB dye by the magnetically separable 3D flower-like Fe3O4/SiO2/MnO2/BiOBr-Bi photocatalyst. *Journal of Alloys and Compounds,* 861.

MAJUMDAR, A., GHOSH, U. & PAL, A. 2022. 2D-Bi4NbO8Cl nanosheet for efficient photocatalytic degradation of tetracycline in synthetic and real wastewater under visible-light: Influencing factors, mechanism and degradation pathway. *Journal of Alloys and Compounds,* 900**,** 163400.

MAJUMDER, A., SAIDULU, D., GUPTA, A. K. & GHOSAL, P. S. 2021. Predicting the trend and utility of different photocatalysts for degradation of pharmaceutically active compounds: A special emphasis on photocatalytic materials, modifications, and performance comparison. *J Environ Manage,* 293**,** 112858.

MANOLI, K., MORRISON, L. M., SUMARAH, M. W., NAKHLA, G., RAY, A. K. & SHARMA, V. K. 2019. Pharmaceuticals and pesticides in secondary effluent wastewater: Identification and enhanced removal by acid-activated ferrate(VI). *Water Res,* 148**,** 272-280.

MAO, D., YUAN, J., QU, X., SUN, C., YANG, S. & HE, H. 2019. Size tunable Bi3O4Br hierarchical hollow spheres assembled with {0 0 1}-facets exposed nanosheets for robust photocatalysis against phenolic pollutants. *Journal of Catalysis,* 369**,** 209-221.

MAROUANI, N., TEBOURBI, O., CHERIF, D., HALLEGUE, D., YACOUBI, M. T., SAKLY, M., BENKHALIFA, M. & BEN RHOUMA, K. 2017. Effects of oral administration of 2,4-dichlorophenoxyacetic acid (2,4-D) on reproductive parameters in male Wistar rats. *Environ Sci Pollut Res Int,* 24**,** 519-526.

MECHA, A. C. & CHOLLOM, M. N. 2020. Photocatalytic ozonation of wastewater: a review. *Environmental Chemistry Letters,* 18**,** 1491-1507.

MEHRALIPOUR, J. & KERMANI, M. 2021. Ultrasonic coupling with electrical current to effective activation of Persulfate for 2, 4 Dichlorophenoxyacetic acid herbicide degradation: modeling, synergistic effect, and a by-product study. *Journal of Environmental Health Science and Engineering,* 19**,** 625-639.

MEI, X.-Y., HONG, Y.-Q. & CHEN, G.-H. 2015. Review on Analysis Methodology of Phenoxy Acid Herbicide Residues. *Food Analytical Methods,* 9**,** 1532-1561.

MIKLOS, D. B., REMY, C., JEKEL, M., LINDEN, K. G., DREWES, J. E. & HUBNER, U. 2018. Evaluation of advanced oxidation processes for water and wastewater treatment - A critical review. *Water Res,* 139**,** 118-131.

MISRA, M., CHOWDHURY, S. R. & SINGH, N. 2020. TiO2@Au@CoMn2O4 core–shell nanorods for photo–electrochemical and photocatalytic activity for decomposition of toxic organic compounds and photo reduction of Cr6+ ion. *Journal of Alloys and Compounds,* 824**,** 153861.

MOHAMAD SAID, K. A., ISMAIL, A. F., ABDUL KARIM, Z., ABDULLAH, M. S. & HAFEEZ, A. 2021. A review of technologies for the phenolic compounds recovery and phenol removal from wastewater. *Process Safety and Environmental Protection,* 151**,** 257-289.

MOHAMED, A., NASSER, W. S., KAMEL, B. M. & HASHEM, T. 2019. Photodegradation of phenol using composite nanofibers under visible light irradiation. *European Polymer Journal,* 113**,** 192-196.

MOHAMMED, M. K. A. 2020. Sol-gel synthesis of Au-doped TiO2 supported SWCNT nanohybrid with visible-light-driven photocatalytic for high degradation performance toward methylene blue dye. *Optik,* 223**,** 165607.

MOLINARI, R., LAVORATO, C. & ARGURIO, P. 2020. Visible-Light Photocatalysts and Their Perspectives for Building Photocatalytic Membrane Reactors for Various Liquid Phase Chemical Conversions. *Catalysts,* 10**,** 1334.

MORADI, M., VASSEGHIAN, Y., KHATAEE, A., HARATI, M. & ARFAEINIA, H. 2021. Ultrasound-assisted synthesis of FeTiO3/GO nanocomposite for photocatalytic degradation of phenol under visible light irradiation. *Separation and Purification Technology,* 261.

NÁFRÁDI, M., ALAPI, T., BENCSIK, G. & JANÁKY, C. 2022. Impact of Reaction Parameters and Water Matrices on the Removal of Organic

Pollutants by TiO2/LED and ZnO/LED Heterogeneous Photocatalysis Using 365 and 398 nm Radiation. *Nanomaterials* [Online], 12.

NAGHDI, M., TAHERAN, M., BRAR, S. K., KERMANSHAHI-POUR, A., VERMA, M. & SURAMPALLI, R. Y. 2018. Removal of pharmaceutical compounds in water and wastewater using fungal oxidoreductase enzymes. *Environmental Pollution,* 234**,** 190-213.

NAWROCKI, J. & KASPRZYK-HORDERN, B. 2010. The efficiency and mechanisms of catalytic ozonation. *Applied Catalysis B: Environmental,* 99**,** 27-42.

NGUYEN, C. H., FU, C.-C. & JUANG, R.-S. 2018. Degradation of methylene blue and methyl orange by palladium-doped TiO2 photocatalysis for water reuse: Efficiency and degradation pathways. *Journal of Cleaner Production,* 202**,** 413-427.

NOROUZI, M., FAZELI, A. & TAVAKOLI, O. 2020. Phenol contaminated water treatment by photocatalytic degradation on electrospun Ag/TiO2 nanofibers: Optimization by the response surface method. *Journal of Water Process Engineering,* 37**,** 101489.

OCHIAI, T. & FUJISHIMA, A. 2012. Photoelectrochemical properties of TiO2 photocatalyst and its applications for environmental purification. *Journal of Photochemistry and Photobiology C: Photochemistry Reviews,* 13**,** 247-262.

OVA, D. & OVEZ, B. 2013. 2,4-Dichlorophenoxyacetic acid removal from aqueous solutions via adsorption in the presence of biological contamination. *Journal of Environmental Chemical Engineering,* 1**,** 813-821.

PALANISAMY, V. K., MANOHARAN, K., RAMAN, K. & SUNDARAM, R. 2020. Efficient sunlight-driven photocatalytic behavior of zinc sulfide nanorods towards Rose Bengal degradation. *Journal of Materials Science: Materials in Electronics,* 31**,** 14795-14809.

PARAGAS, L. K. B., DIEN DANG, V., SAHU, R. S., GARCIA-SEGURA, S., DE LUNA, M. D. G., PIMENTEL, J. A. I. & DOONG, R.-A. 2021. Enhanced visible-light-driven photocatalytic degradation of acetaminophen over CeO2/I, K-codoped C3N4 heterojunction with tunable properties in simulated water matrix. *Separation and Purification Technology,* 272**,** 117567.

PARK, H., PARK, Y., KIM, W. & CHOI, W. 2013. Surface modification of TiO2 photocatalyst for environmental applications. *Journal of Photochemistry and Photobiology C: Photochemistry Reviews,* 15**,** 1-20.

PHONGARTHIT, K., AMORNPITOKSUK, P. & SUWANBOON, S. 2020. Photocatalytic degradation of rhodamine B, reactive orange, and bisphenol A under visible light irradiation over AgX/ZnO (X=Cl, Br, I) prepared from green approach. *Optik,* 204**,** 164224.

POL, R., GUERRERO, M., GARCÍA-LECINA, E., ALTUBE, A., ROSSINYOL, E., GARRONI, S., BARÓ, M. D., PONS, J., SORT, J. & PELLICER, E. 2016. Ni-, Pt- and (Ni/Pt)-doped TiO2 nanophotocatalysts: A smart approach for sustainable degradation of Rhodamine B dye. *Applied Catalysis B: Environmental*, 181**,** 270-278.

PULICHARLA, R., DROUINAUD, R., BRAR, S. K., DROGUI, P., PROULX, F., VERMA, M. & SURAMPALLI, R. Y. 2018. Activation of persulfate by homogeneous and heterogeneous iron catalyst to degrade chlortetracycline in aqueous solution. *Chemosphere*, 207**,** 543-551.

QUESADA, H. B., BAPTISTA, A. T. A., CUSIOLI, L. F., SEIBERT, D., DE OLIVEIRA BEZERRA, C. & BERGAMASCO, R. 2019. Surface water pollution by pharmaceuticals and an alternative of removal by low-cost adsorbents: A review. *Chemosphere*, 222**,** 766-780.

RAFIQ, A., IKRAM, M., ALI, S., NIAZ, F., KHAN, M., KHAN, Q. & MAQBOOL, M. 2021. Photocatalytic degradation of dyes using semiconductor photocatalysts to clean industrial water pollution. *Journal of Industrial and Engineering Chemistry*, 97**,** 111-128.

RAHA, S. & AHMARUZZAMAN, M. 2020. Enhanced performance of a novel superparamagnetic g-C3N4/NiO/ZnO/Fe3O4 nanohybrid photocatalyst for removal of esomeprazole: Effects of reaction parameters, co-existing substances and water matrices. *Chemical Engineering Journal*, 395**,** 124969.

RAIZADA, P., SUDHAIK, A., PATIAL, S., HASIJA, V., PARWAZ KHAN, A. A., SINGH, P., GAUTAM, S., KAUR, M. & NGUYEN, V.-H. 2020a. Engineering nanostructures of CuO-based photocatalysts for water treatment: Current progress and future challenges. *Arabian Journal of Chemistry*, 13**,** 8424-8457.

RAIZADA, P., THAKUR, P., SUDHAIK, A., SINGH, P., THAKUR, V. K. & HOSSEINI-BANDEGHARAEI, A. 2020b. Fabrication of dual Z-scheme photocatalyst via coupling of BiOBr/Ag/AgCl heterojunction with P and S co-doped g-C3N4 for efficient phenol degradation. *Arabian Journal of Chemistry*, 13**,** 4538-4552.

RAN, M., WANG, H., CUI, W., LI, J., CHEN, P., SUN, Y., SHENG, J., ZHOU, Y., ZHANG, Y. & DONG, F. 2019. Light-Induced Generation and Regeneration of Oxygen Vacancies in BiSbO4 for Sustainable Visible Light Photocatalysis. *ACS Applied Materials & Interfaces*, 11**,** 47984-47991.

RAWAT, S. & SINGH, J. 2022. Synthesis of nZnO from waste batteries by hydrometallurgical method for photocatalytic degradation of organic pollutants under visible light irradiation. *J Environ Manage*, 318**,** 115518.

REDDY, C. V., REDDY, I. N., REDDY, K. R., JAESOOL, S. & YOO, K. 2019. Template-free synthesis of tetragonal Co-doped ZrO2 nanoparticles for

applications in electrochemical energy storage and water treatment. *Electrochimica Acta,* 317**,** 416-426.

REHAN, M., KHATTAB, T. A., BAROHUM, A., GATJEN, L. & WILKEN, R. 2018. Development of Ag/AgX (X=Cl, I) nanoparticles toward antimicrobial, UV-protected and self-cleanable viscose fibers. *Carbohydr Polym,* 197**,** 227-236.

REN, M., CHEN, J., WANG, P., HOU, J., QIAN, J., WANG, C. & AO, Y. 2018. Construction of silver iodide/silver/bismuth tantalate Z-scheme photocatalyst for effective visible light degradation of organic pollutants. *J Colloid Interface Sci,* 532**,** 190-200.

REZA, K. M., KURNY, A. S. W. & GULSHAN, F. 2015. Parameters affecting the photocatalytic degradation of dyes using TiO2: a review. *Applied Water Science,* 7**,** 1569-1578.

ROSMAN, N., SALLEH, W. N. W., ISMAIL, A. F., JAAFAR, J., HARUN, Z., AZIZ, F., MOHAMED, M. A., OHTANI, B. & TAKASHIMA, M. 2018. Photocatalytic degradation of phenol over visible light active ZnO/Ag2CO3/Ag2O nanocomposites heterojunction. *Journal of Photochemistry and Photobiology A: Chemistry,* 364**,** 602-612.

SACCO, O., VAIANO, V. & SANNINO, D. 2020. Main parameters influencing the design of photocatalytic reactors for wastewater treatment: a mini review. *Journal of Chemical Technology & Biotechnology*.

SAFA, S., MIRZAEI, M., KAZEMI, F., GHANEIAN, M. T. & KABOUDIN, B. 2019. Study of visible-light photocatalytic degradation of 2,4-dichlorophenoxy acetic acid in batch and circulated-mode photoreactors. *J Environ Health Sci Eng,* 17**,** 233-245.

SAISON, T., GRAS, P., CHEMIN, N., CHANÉAC, C., DURUPTHY, O., BREZOVÁ, V., COLBEAU-JUSTIN, C. & JOLIVET, J.-P. 2013. New Insights into Bi2WO6 Properties as a Visible-Light Photocatalyst. *The Journal of Physical Chemistry C,* 117**,** 22656-22666.

SAMIR, R., ESSAM, T., RAGAB, Y. & HASHEM, A. 2015. Enhanced photocatalytic–biological degradation of 2,4 dichlorophenoxyacetic acid. *Bulletin of Faculty of Pharmacy, Cairo University,* 53**,** 77-82.

SAMSUDIN, M. F. R., FREBILLOT, C., KADDOURY, Y., SUFIAN, S. & ONG, W. J. 2020. Bifunctional Z-Scheme Ag/AgVO3/g-C3N4 photocatalysts for expired ciprofloxacin degradation and hydrogen production from natural rainwater without using scavengers. *J Environ Manage,* 270**,** 110803.

SAYADI, M. H., SOBHANI, S. & SHEKARI, H. 2019. Photocatalytic degradation of azithromycin using GO@Fe3O4/ ZnO/ SnO2 nanocomposites. *Journal of Cleaner Production,* 232**,** 127-136.

SCOTT, T., ZHAO, H., DENG, W., FENG, X. & LI, Y. 2019. Photocatalytic degradation of phenol in water under simulated sunlight by an ultrathin MgO coated Ag/TiO2 nanocomposite. *Chemosphere,* 216**,** 1-8.

SERRA-CLUSELLAS, A., DE ANGELIS, L., LIN, C. H., VO, P., BAYATI, M., SUMNER, L., LEI, Z., AMARAL, N. B., BERTINI, L. M., MAZZA, J., PIZZIO, L. R., STRIPEIKIS, J. D., RENGIFO-HERRERA, J. A. & FIDALGO DE CORTALEZZI, M. M. 2018. Abatement of 2,4-D by H2O2 solar photolysis and solar photo-Fenton-like process with minute Fe(III) concentrations. *Water Res,* 144**,** 572-580.

SHABANI, M., HAGHIGHI, M. & KAHFOROUSHAN, D. 2018. One-pot combustion fabrication of grain-like mesoporous intra-heterostructure BixOyClz nanophotocatalyst with substantial solar-light-driven degradation of antibiotic ofloxacin: influence of various fuels. *Catalysis Science & Technology,* 8**,** 4052-4069.

SHABANI, M., HAGHIGHI, M., KAHFOROUSHAN, D. & HAGHIGHI, A. 2019. Sono-solvothermal hybrid fabrication of BiOCl-Bi24O31Cl10/rGO nano-heterostructure photocatalyst with efficient solar-light-driven performance in degradation of fluoroquinolone antibiotics. *Solar Energy Materials and Solar Cells,* 193**,** 335-350.

SHARMA, V., VINOTH KUMAR, R., PAKSHIRAJAN, K. & PUGAZHENTHI, G. 2017. Integrated adsorption-membrane filtration process for antibiotic removal from aqueous solution. *Powder Technology,* 321**,** 259-269.

SHI, H., YANG, S., HAN, C., NIU, Z., LI, H., HUANG, X. & MA, J. 2019. Fabrication of Ag/Ag3PO4/WO3 ternary nanoparticles as superior photocatalyst for phenol degradation under visible light irradiation. *Solid State Sciences,* 96**,** 105967.

SHI, Q., ZHANG, Y., SUN, D., ZHANG, S., TANG, T., ZHANG, X. & CAO, S. 2020a. Bi2O3-Sensitized TiO2 Hollow Photocatalyst Drives the Efficient Removal of Tetracyclines under Visible Light. *Inorganic Chemistry,* 59**,** 18131-18140.

SHI, W., REN, H., LI, M., SHU, K., XU, Y., YAN, C. & TANG, Y. 2020b. Tetracycline removal from aqueous solution by visible-light-driven photocatalytic degradation with low cost red mud wastes. *Chemical Engineering Journal,* 382**,** 122876.

SHIRAISHI, Y., IMAI, J., YASUMOTO, N., SAKAMOTO, H., TANAKA, S., ICHIKAWA, S. & HIRAI, T. 2019. Doping of Nb5+ Species at the Au–TiO2 Interface for Plasmonic Photocatalysis Enhancement. *Langmuir,* 35**,** 5455-5462.

SONG, J., ZHANG, L., YANG, J., HU, J.-S. & HUANG, X.-H. 2018. Ag nanoparticle-decorated biscuit-like Bi24O31Cl10 hierarchical microstructure composed of ultrathin nanoflake with outstanding photocatalytic activity. *Journal of Alloys and Compounds,* 735**,** 660-667.

SRIVASTAVA, A., GUPTA, B., MAJUMDER, A., GUPTA, A. K. & NIMBHORKAR, S. K. 2021. A comprehensive review on the synthesis, performance, modifications, and regeneration of activated carbon for the

adsorptive removal of various water pollutants. *Journal of Environmental Chemical Engineering,* 9**,** 106177.

SUN, D., ZHANG, Y., LIU, Y., WANG, Z., CHEN, X., MENG, Z., KANG, S., ZHENG, Y., CUI, L., CHEN, M., DONG, M. & HU, B. 2020. In-situ homodispersely immobilization of Ag@AgCl on chloridized g-C3N4 nanosheets as an ultrastable plasmonic photocatalyst. *Chemical Engineering Journal,* 384**,** 123259.

TAHIR, M., TASLEEM, S. & TAHIR, B. 2020. Recent development in band engineering of binary semiconductor materials for solar driven photocatalytic hydrogen production. *International Journal of Hydrogen Energy,* 45**,** 15985-16038.

TANG, H., DAI, Z., XIE, X., WEN, Z. & CHEN, R. 2019. Promotion of peroxydisulfate activation over Cu0.84Bi2.08O4 for visible light induced photodegradation of ciprofloxacin in water matrix. *Chemical Engineering Journal,* 356**,** 472-482.

TANG, J., WANG, J., TANG, L., FENG, C., ZHU, X., YI, Y., FENG, H., YU, J. & REN, X. 2022a. Preparation of floating porous g-C3N4 photocatalyst via a facile one-pot method for efficient photocatalytic elimination of tetracycline under visible light irradiation. *Chemical Engineering Journal,* 430**,** 132669.

TANG, S., ZHAO, M., YUAN, D., LI, X., WANG, Z., ZHANG, X., JIAO, T. & KE, J. 2021a. Fe3O4 nanoparticles three-dimensional electro-peroxydisulfate for improving tetracycline degradation. *Chemosphere,* 268**,** 129315.

TANG, W., CHEN, J., YIN, Z., SHENG, W., LIN, F., XU, H. & CAO, S. 2021b. Complete removal of phenolic contaminants from bismuth-modified TiO2 single-crystal photocatalysts. *Chinese Journal of Catalysis,* 42**,** 347-355.

TANG, W., PEI, Y., ZHENG, H., ZHAO, Y., SHU, L. & ZHANG, H. 2022b. Twenty years of China's water pollution control: Experiences and challenges. *Chemosphere,* 295**,** 133875.

TAVAKOLI JOORABI, F., KAMALI, M. & SHEIBANI, S. 2022. Effect of aqueous inorganic anions on the photocatalytic activity of CuO–Cu2O nanocomposite on MB and MO dyes degradation. *Materials Science in Semiconductor Processing,* 139**,** 106335.

TRAN, M. L., FU, C.-C. & JUANG, R.-S. 2019. Effects of water matrix components on degradation efficiency and pathways of antibiotic metronidazole by UV/TiO2 photocatalysis. *Journal of Molecular Liquids,* 276**,** 32-38.

TRIVEDI, N. S. & MANDAVGANE, S. A. 2018. Fundamentals of 2, 4 Dichlorophenoxyacetic Acid Removal from Aqueous Solutions. *Separation & Purification Reviews* 47**,** 337-354.

VAIANO, V., MATARANGOLO, M., MURCIA, J. J., ROJAS, H., NAVÍO, J. A. & HIDALGO, M. C. 2018. Enhanced photocatalytic removal of phenol

from aqueous solutions using ZnO modified with Ag. *Applied Catalysis B: Environmental,* 225**,** 197-206.

VERMA, S., DAVEREY, A. & SHARMA, A. 2017. Slow sand filtration for water and wastewater treatment – a review. *Environmental Technology Reviews,* 6**,** 47-58.

VIDAL, R. R. L. & MORAES, J. S. 2018. Removal of organic pollutants from wastewater using chitosan: a literature review. *International Journal of Environmental Science and Technology,* 16**,** 1741-1754.

VILLEGAS, L. G. C., MASHHADI, N., CHEN, M., MUKHERJEE, D., TAYLOR, K. E. & BISWAS, N. 2016. A Short Review of Techniques for Phenol Removal from Wastewater. *Current Pollution Reports,* 2**,** 157-167.

WANG, C.-Y., ZHANG, X., SONG, X.-N., WANG, W.-K. & YU, H.-Q. 2016. Novel Bi12O15Cl6 Photocatalyst for the Degradation of Bisphenol A under Visible-Light Irradiation. *ACS Applied Materials & Interfaces,* 8**,** 5320-5326.

WANG, C., XUE, Y., WANG, P. & AO, Y. 2018a. Effects of water environmental factors on the photocatalytic degradation of sulfamethoxazole by AgI/UiO-66 composite under visible light irradiation. *Journal of Alloys and Compounds,* 748**,** 314-322.

WANG, D., JIA, F., WANG, H., CHEN, F., FANG, Y., DONG, W., ZENG, G., LI, X., YANG, Q. & YUAN, X. 2018b. Simultaneously efficient adsorption and photocatalytic degradation of tetracycline by Fe-based MOFs. *Journal of Colloid and Interface Science,* 519**,** 273-284.

WANG, D., LI, Y., LI PUMA, G., WANG, C., WANG, P., ZHANG, W. & WANG, Q. 2015. Mechanism and experimental study on the photocatalytic performance of Ag/AgCl @ chiral TiO2 nanofibers photocatalyst: The impact of wastewater components. *Journal of Hazardous Materials,* 285**,** 277-284.

WANG, F., WU, Y., WANG, Y., LI, J., JIN, X., ZHANG, Q., LI, R., YAN, S., LIU, H., FENG, Y., LIU, G. & LV, W. 2019a. Construction of novel Z-scheme nitrogen-doped carbon dots/{0 0 1} TiO2 nanosheet photocatalysts for broad-spectrum-driven diclofenac degradation: Mechanism insight, products and effects of natural water matrices. *Chemical Engineering Journal,* 356**,** 857-868.

WANG, H., ZHANG, J., YUAN, X., JIANG, L., XIA, Q. & CHEN, H. 2020a. Photocatalytic removal of antibiotics from natural water matrices and swine wastewater via Cu(I) coordinately polymeric carbon nitride framework. *Chemical Engineering Journal,* 392**,** 123638.

WANG, J. & CHEN, H. 2020. Catalytic ozonation for water and wastewater treatment: Recent advances and perspective. *Sci Total Environ,* 704**,** 135249.

WANG, J. & WANG, S. 2020. Reactive species in advanced oxidation processes: Formation, identification and reaction mechanism. *Chemical Engineering Journal*, 401.

WANG, J., ZHI, D., ZHOU, H., HE, X. & ZHANG, D. 2018c. Evaluating tetracycline degradation pathway and intermediate toxicity during the electrochemical oxidation over a Ti/Ti4O7 anode. *Water Research*, 137**,** 324-334.

WANG, J. & ZHUAN, R. 2020. Degradation of antibiotics by advanced oxidation processes: An overview. *Sci Total Environ*, 701**,** 135023.

WANG, L., SHANG, J., HAO, W., JIANG, S., HUANG, S., WANG, T., SUN, Z., DU, Y., DOU, S., XIE, T., WANG, D. & WANG, J. 2014. A dye-sensitized visible light photocatalyst-Bi24O31Cl10. *Scientific Reports*, 4.

WANG, N., CHENG, K., XU, Z.-F., LI, P., GENG, G., CHEN, C., WANG, D., CHEN, P. & LIU, M. 2020b. High-performance natural-sunlight-driven Ag/AgCl photocatalysts with a cube-like morphology and blunt edges via a bola-type surfactant-assisted synthesis. *Physical Chemistry Chemical Physics*, 22**,** 3940-3952.

WANG, N., LI, X., YANG, Y., SHANG, Y., ZHUANG, X., LI, H. & ZHOU, Z. 2019b. Combined process of visible light irradiation photocatalysis-coagulation enhances natural organic matter removal: Optimization of influencing factors and mechanism. *Chemical Engineering Journal*, 374**,** 748-759.

WANG, P., CAO, Y., ZHOU, X., XU, C. & YAN, Q. 2020c. Facile construction of 3D hierarchical flake ball-shaped γ-AgI/Bi2WO6 Z-scheme heterojunction towards enhanced visible-light photocatalytic performance. *Applied Surface Science*, 531**,** 147345.

WANG, P., CHEN, J., BAI, Y., YANG, P., DU, Y. & ZHANG, H. 2019c. Preparation of a novel Z-scheme AgI/Ag/Bi24O31Cl10 catalyst with enhanced photocatalytic performance via an Ag0 electron transfer intermediate. *Journal of Materials Science: Materials in Electronics*, 30**,** 10606-10618.

WANG, Q. & YANG, Z. 2016. Industrial water pollution, water environment treatment, and health risks in China. *Environmental Pollution*, 218**,** 358-365.

WANG, S., GAO, Y., MIAO, S., LIU, T., MU, L., LI, R., FAN, F. & LI, C. 2017a. Positioning the Water Oxidation Reaction Sites in Plasmonic Photocatalysts. *Journal of the American Chemical Society*, 139**,** 11771-11778.

WANG, W., HAN, Q., ZHU, Z., ZHANG, L., ZHONG, S. & LIU, B. 2019d. Enhanced photocatalytic degradation performance of organic contaminants by heterojunction photocatalyst BiVO4/TiO2/RGO and its compatibility on four different tetracycline antibiotics. *Advanced Powder Technology*, 30**,** 1882-1896.

WANG, X., JIA, J. & WANG, Y. 2017b. Combination of photocatalysis with hydrodynamic cavitation for degradation of tetracycline. *Chemical Engineering Journal*, 315**,** 274-282.

WANG, Y., JING, B., WANG, F., WANG, S., LIU, X., AO, Z. & LI, C. 2020d. Mechanism Insight into enhanced photodegradation of pharmaceuticals and personal care products in natural water matrix over crystalline graphitic carbon nitrides. *Water Research*, 180**,** 115925.

WELDEGEBRIEAL, G. K. 2020. Synthesis method, antibacterial and photocatalytic activity of ZnO nanoparticles for azo dyes in wastewater treatment: A review. *Inorganic Chemistry Communications*, 120**,** 108140.

WEN, J., LI, X., LIU, W., FANG, Y., XIE, J. & XU, Y. 2015. Photocatalysis fundamentals and surface modification of TiO2 nanomaterials. *Chinese Journal of Catalysis*, 36**,** 2049-2070.

WEN, X.-J., NIU, C.-G., HUANG, D.-W., ZHANG, L., LIANG, C. & ZENG, G.-M. 2017. Study of the photocatalytic degradation pathway of norfloxacin and mineralization activity using a novel ternary Ag/AgCl-CeO 2 photocatalyst. *Journal of Catalysis*, 355**,** 73-86.

WU, J., FANG, X., DONG, H., LIAN, L., MA, N. & DAI, W. 2021. Bimetallic silver/bismuth-MOFs derived strategy for Ag/AgCl/BiOCl composite with extraordinary visible light-driven photocatalytic activity towards tetracycline. *Journal of Alloys and Compounds*, 877.

WU, S., HU, H., LIN, Y., ZHANG, J. & HU, Y. H. 2020. Visible light photocatalytic degradation of tetracycline over TiO2. *Chemical Engineering Journal*, 382**,** 122842.

WU, W., SUN, Y. & ZHOU, H. 2022. In-situ construction of β-Bi2O3/Ag2O photocatalyst from deactivated AgBiO3 for tetracycline degradation under visible light. *Chemical Engineering Journal*, 432**,** 134316.

WU, W., WANG, J., ZHANG, T., JIANG, S., MA, X., ZHANG, G., ZHANG, X., CHEN, X. & LI, B. 2019. Controllable synthesis of Ag/AgCl@MIL-88A via in situ growth method for morphology-dependent photocatalytic performance. *Journal of Materials Chemistry C*, 7**,** 5451-5460.

WU, X., WANG, W., LIU, J., PAN, D., TU, X., LV, P., WANG, Y., CAO, H., WANG, Y. & HUA, R. 2017. Rapid Biodegradation of the Herbicide 2,4-Dichlorophenoxyacetic Acid by Cupriavidus gilardii T-1. *Journal of Agricultural and Food Chemistry*, 65**,** 3711-3720.

XIAO, X., JIANG, J. & ZHANG, L. 2013. Selective oxidation of benzyl alcohol into benzaldehyde over semiconductors under visible light: The case of Bi12O17Cl2 nanobelts. *Applied Catalysis B: Environmental*, 142-143**,** 487-493.

XIONG, L. & TANG, J. 2021. Strategies and Challenges on Selectivity of Photocatalytic Oxidation of Organic Substances. *Advanced Energy Materials*, 11**,** 2003216.

XIONG, W., ZENG, G., YANG, Z., ZHOU, Y., ZHANG, C., CHENG, M., LIU, Y., HU, L., WAN, J., ZHOU, C., XU, R. & LI, X. 2018. Adsorption of tetracycline antibiotics from aqueous solutions on nanocomposite multi-walled carbon nanotube functionalized MIL-53(Fe) as new adsorbent. *Science of The Total Environment,* 627**,** 235-244.

XU, B., GAO, Y., LI, Y., LIU, S., LV, D., ZHAO, S., GAO, H., YANG, G., LI, N. & GE, L. 2020a. Synthesis of Bi3O4Cl nanosheets with oxygen vacancies: The effect of defect states on photocatalytic performance. *Applied Surface Science,* 507**,** 144806.

XU, B., LI, J., LIU, L., LI, Y., GUO, S., GAO, Y., LI, N. & GE, L. 2019. Pt/Bi24O31Cl10 composite nanosheets with significantly enhanced photocatalytic activity under visible light irradiation. *Chinese Journal of Catalysis,* 40**,** 713-721.

XU, L., ZHANG, H., XIONG, P., ZHU, Q., LIAO, C. & JIANG, G. 2021. Occurrence, fate, and risk assessment of typical tetracycline antibiotics in the aquatic environment: A review. *Sci Total Environ,* 753**,** 141975.

XU, Q., ZHANG, L., YU, J., WAGEH, S., AL-GHAMDI, A. A. & JARONIEC, M. 2018. Direct Z-scheme photocatalysts: Principles, synthesis, and applications. *Materials Today,* 21**,** 1042-1063.

XU, X., CAI, J., ZHOU, M., DU, X. & ZHANG, Y. 2020b. Photoelectrochemical degradation of 2,4-dichlorophenoxyacetic acid using electrochemically self-doped Blue TiO2 nanotube arrays with formic acid as electrolyte. *Journal of Hazardous Materials,* 382.

YAN, H., LIU, L., WANG, R., ZHU, W., REN, X., LUO, L., ZHANG, X., LUO, S., AI, X. & WANG, J. 2020. Binary composite MoS2/TiO2 nanotube arrays as a recyclable and efficient photocatalyst for solar water disinfection. *Chemical Engineering Journal,* 401.

YAN, Q., XIE, X., LIU, Y., WANG, S., ZHANG, M., CHEN, Y. & SI, Y. 2019. Constructing a new Z-scheme multi-heterojunction photocataslyts Ag-AgI/BiOI-Bi2O3 with enhanced photocatalytic activity. *Journal of Hazardous Materials,* 371**,** 304-315.

YANG, J., ZHU, M. & DIONYSIOU, D. D. 2021. What is the role of light in persulfate-based advanced oxidation for water treatment? *Water Res,* 189**,** 116627.

YANG, R., ZHU, Z., HU, C., ZHONG, S., ZHANG, L., LIU, B. & WANG, W. 2020. One-step preparation (3D/2D/2D) BiVO4/FeVO4@rGO heterojunction composite photocatalyst for the removal of tetracycline and hexavalent chromium ions in water. *Chemical Engineering Journal,* 390**,** 124522.

YANG, Y., ZHANG, C., LAI, C., ZENG, G., HUANG, D., CHENG, M., WANG, J., CHEN, F., ZHOU, C. & XIONG, W. 2018. BiOX (X=Cl, Br, I) photocatalytic nanomaterials: Applications for fuels and environmental management. *Adv Colloid Interface Sci,* 254**,** 76-93.

YAO, L., YANG, H., CHEN, Z., QIU, M., HU, B. & WANG, X. 2021. Bismuth oxychloride-based materials for the removal of organic pollutants in wastewater. *Chemosphere,* 273.

YAO, X. & LIU, X. 2014. One-pot synthesis of ternary Ag(2)CO(3)/Ag/AgCl photocatalyst in natural geothermal water with enhanced photocatalytic activity under visible light irradiation. *J Hazard Mater,* 280**,** 260-8.

YAZIDI, A., ATROUS, M., EDI SOETAREDJO, F., SELLAOUI, L., ISMADJI, S., ERTO, A., BONILLA-PETRICIOLET, A., LUIZ DOTTO, G. & BEN LAMINE, A. 2020. Adsorption of amoxicillin and tetracycline on activated carbon prepared from durian shell in single and binary systems: Experimental study and modeling analysis. *Chemical Engineering Journal,* 379**,** 122320.

YOUSEF, A., EL-HALWANY, M. M., BARAKAT, N. A. M., AL-MAGHRABI, M. N. & KIM, H. Y. 2015. Cu0- doped TiO2 nanofibers as potential photocatalyst and antimicrobial agent. *Journal of Industrial and Engineering Chemistry,* 26**,** 251-258.

YU, X., HUANG, J., ZHAO, J., LIU, S., XIANG, D., TANG, Y., LI, J., GUO, Q., MA, X. & ZHAO, J. 2021. Efficient visible light photocatalytic antibiotic elimination performance induced by nanostructured Ag/AgCl@Ti3+-TiO2 mesocrystals. *Chemical Engineering Journal,* 403.

YUAN, L., HAN, C., YANG, M.-Q. & XU, Y.-J. 2016. Photocatalytic water splitting for solar hydrogen generation: fundamentals and recent advancements. *International Reviews in Physical Chemistry,* 35**,** 1-36.

YUAN, L. & XU, Y.-J. 2015. Photocatalytic conversion of CO2 into value-added and renewable fuels. *Applied Surface Science,* 342**,** 154-167.

YUAN, R., ZHU, Y., ZHOU, B. & HU, J. 2019. Photocatalytic oxidation of sulfamethoxazole in the presence of TiO2: Effect of matrix in aqueous solution on decomposition mechanisms. *Chemical Engineering Journal,* 359**,** 1527-1536.

ZADA, A., MUHAMMAD, P., AHMAD, W., HUSSAIN, Z., ALI, S., KHAN, M., KHAN, Q. & MAQBOOL, M. 2019. Surface Plasmonic-Assisted Photocatalysis and Optoelectronic Devices with Noble Metal Nanocrystals: Design, Synthesis, and Applications. *Advanced Functional Materials,* 30**,** 1906744.

ZAMORA-LEDEZMA, C., NEGRETE-BOLAGAY, D., FIGUEROA, F., ZAMORA-LEDEZMA, E., NI, M., ALEXIS, F. & GUERRERO, V. H. 2021. Heavy metal water pollution: A fresh look about hazards, novel and conventional remediation methods. *Environmental Technology & Innovation,* 22**,** 101504.

ZHANG, D., LV, S. & LUO, Z. 2020a. A study on the photocatalytic degradation performance of a [KNbO 3] 0.9-[BaNi 0.5 Nb 0.5 O 3− δ] 0.1 perovskite. *RSC Advances,* 10**,** 1275-1280.

ZHANG, D., QI, J., JI, H., LI, S., CHEN, L., HUANG, T., XU, C., CHEN, X. & LIU, W. 2020b. Photocatalytic degradation of ofloxacin by perovskite-type NaNbO3 nanorods modified g-C3N4 heterojunction under simulated solar light: Theoretical calculation, ofloxacin degradation pathways and toxicity evolution. *Chemical Engineering Journal,* 400.

ZHANG, L., KANKI, T., SANO, N. & TOYODA, A. 2003. Development of TiO2 photocatalyst reaction for water purification. *Separation and Purification Technology,* 31**,** 105-110.

ZHANG, L., LI, Y., LI, Q., FAN, J., CARABINEIRO, S. A. C. & LV, K. 2021. Recent advances on Bismuth-based Photocatalysts: Strategies and mechanisms. *Chemical Engineering Journal,* 419.

ZHANG, M., YIN, H.-F., YAO, J.-C., ARIF, M., QIU, B., LI, P.-F. & LIU, X.-H. 2020c. All-solid-state Z-scheme BiOX(Cl, Br)-Au-CdS heterostructure: Photocatalytic activity and degradation pathway. *Colloids and Surfaces A: Physicochemical and Engineering Aspects,* 602**,** 124778.

ZHANG, T., LIU, Y., ZHONG, S. & ZHANG, L. 2020d. AOPs-based remediation of petroleum hydrocarbons-contaminated soils: Efficiency, influencing factors and environmental impacts. *Chemosphere,* 246.

ZHANG, X., LI, X., ZHANG, D., SU, N. Q., YANG, W., EVERITT, H. O. & LIU, J. 2017. Product selectivity in plasmonic photocatalysis for carbon dioxide hydrogenation. *Nature Communications,* 8.

ZHANG, Y., LIU, J., KANG, Y. S. & ZHANG, X. L. 2022. Silver based photocatalysts in emerging applications. *Nanoscale,* 14**,** 11909-11922.

ZHANG, Y., ZHOU, J., CHEN, X., WANG, L. & CAI, W. 2019. Coupling of heterogeneous advanced oxidation processes and photocatalysis in efficient degradation of tetracycline hydrochloride by Fe-based MOFs: Synergistic effect and degradation pathway. *Chemical Engineering Journal,* 369**,** 745-757.

ZHANG, Z., QIAN, Q., LI, B. & CHEN, K. J. 2018. Interface Engineering of Monolayer MoS2/GaN Hybrid Heterostructure: Modified Band Alignment for Photocatalytic Water Splitting Application by Nitridation Treatment. *ACS Applied Materials & Interfaces,* 10**,** 17419-17426.

ZHAO, C., ZHOU, J., YAN, Y., YANG, L., XING, G., LI, H., WU, P., WANG, M. & ZHENG, H. 2021. Application of coagulation/flocculation in oily wastewater treatment: A review. *Science of The Total Environment,* 765**,** 142795.

ZHAO, H., LI, G., TIAN, F., JIA, Q., LIU, Y. & CHEN, R. 2019a. g-C3N4 surface-decorated Bi2O2CO3 for improved photocatalytic performance: Theoretical calculation and photodegradation of antibiotics in actual water matrix. *Chemical Engineering Journal,* 366**,** 468-479.

ZHAO, W., FENG, Y., HUANG, H., ZHOU, P., LI, J., ZHANG, L., DAI, B., XU, J., ZHU, F., SHENG, N. & LEUNG, D. Y. C. 2019b. A novel Z-scheme Ag3VO4/BiVO4 heterojunction photocatalyst: Study on the

excellent photocatalytic performance and photocatalytic mechanism. *Applied Catalysis B: Environmental*, 245**,** 448-458.

ZHAO, X., DU, P., CAI, Z., WANG, T., FU, J. & LIU, W. 2018. Photocatalysis of bisphenol A by an easy-settling titania/titanate composite: Effects of water chemistry factors, degradation pathway and theoretical calculation. *Environ Pollut*, 232**,** 580-590.

ZHONG, S., LI, C., SHEN, M., LV, C. & ZHANG, S. 2019. Synthesis of modified bismuth tungstate and the photocatalytic properties on tetracycline degradation and pathways. *Journal of Materials Research and Technology*, 8**,** 1849-1858.

ZHOU, Y., LIU, X., XIANG, Y., WANG, P., ZHANG, J., ZHANG, F., WEI, J., LUO, L., LEI, M. & TANG, L. 2017. Modification of biochar derived from sawdust and its application in removal of tetracycline and copper from aqueous solution: Adsorption mechanism and modelling. *Bioresource Technology*, 245**,** 266-273.

ZHU, B., SONG, D., JIA, T., SUN, W., WANG, D., WANG, L., GUO, J., JIN, L., ZHANG, L. & TAO, H. 2021. Effective Visible Light-Driven Photocatalytic Degradation of Ciprofloxacin over Flower-like Fe(3)O(4)/Bi(2)WO(6) Composites. *ACS Omega*, 6**,** 1647-1656.

ZHU, D. & ZHOU, Q. 2020. Novel Bi2WO6 modified by N-doped graphitic carbon nitride photocatalyst for efficient photocatalytic degradation of phenol under visible light. *Applied Catalysis B: Environmental*, 268**,** 118426.

ZYOUD, A., JONDI, W., ALDAQQAH, N., ASAAD, S., QAMHIEH, N., HAJAMOHIDEEN, A., HELAL, M. H., KWON, H. & HILAL, H. S. 2017. Self-sensitization of tetracycline degradation with simulated solar light catalyzed by ZnO@ montmorillonite. *Solid State Sciences*, 74**,** 131-143.

ZYOUD, A. H., ZUBI, A., ZYOUD, S. H., HILAL, M. H., ZYOUD, S., QAMHIEH, N., HAJAMOHIDEEN, A. & HILAL, H. S. 2019. Kaolin-supported ZnO nanoparticle catalysts in self-sensitized tetracycline photodegradation: zero-point charge and pH effects. *Applied Clay Science*, 182**,** 105294.

APPENDIX A – CALIBRATION CURVES

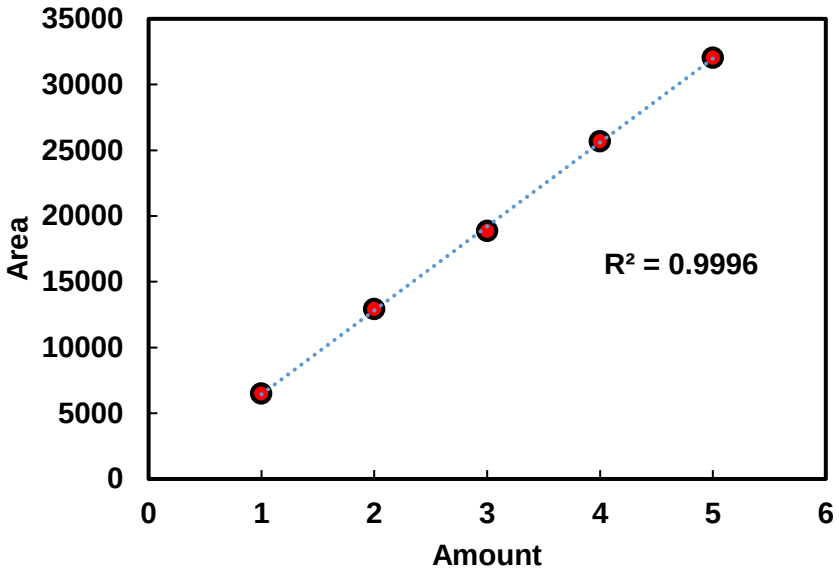

Figure A 1: Phenol HPLC calibration curve

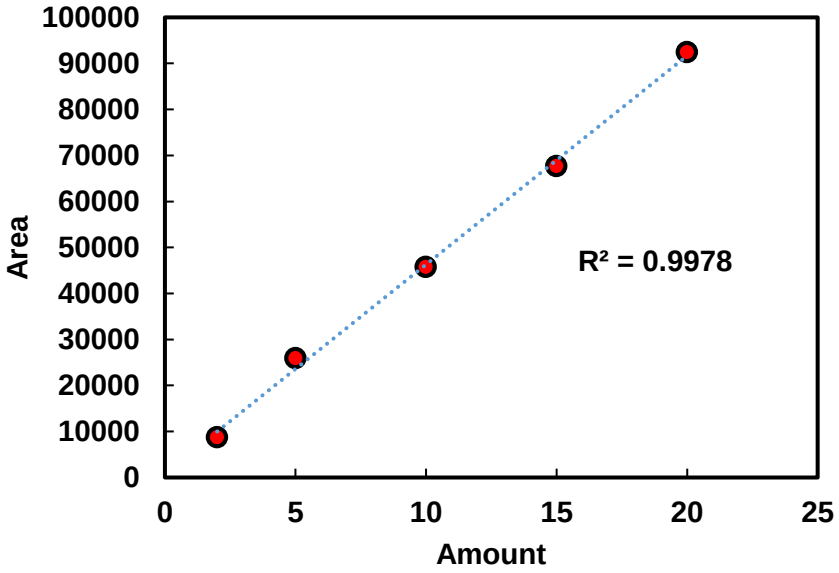

Figure A 2: 2,4-D HPLC calibration curve

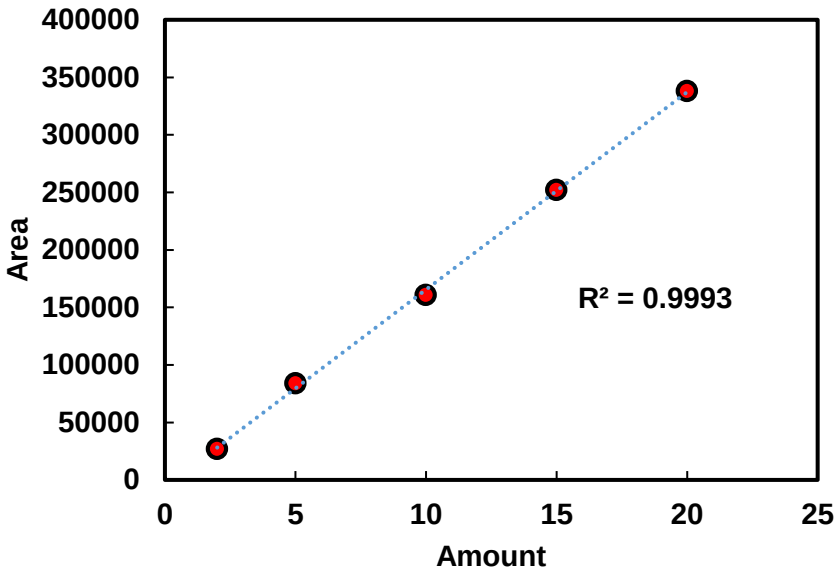

Figure A 3: Tetracycline HPLC calibration curve

APPENDIX B - KINETICS

The TC and 2,4-D photocatalytic experiments were modelled using the zero-order, pseudo-first-order and pseudo-second-order kinetics represented in Equation B1 to Equation B3 for quantitative evaluation using the obtained results. The rate constants and regression coefficients are presented in Table B1 and Table B2.

$$-\frac{dC}{dt}=k_{app} \rightarrow C = C_0 - kt \quad \text{(B1)}$$

$$-\frac{dC}{dt}=k_{app}C \rightarrow \ln\left(\frac{C_0}{C}\right) = kt + 1 \quad \text{(B2)}$$

$$-\frac{dC}{dt}=k_{app}C^2 \rightarrow \left(\frac{1}{C}\right) = kt + \frac{1}{C_0} \quad \text{(B3)}$$

where C_0 and C_t are the initial concentration and final concentration at time t while k is the rate constant in $mg.L^{-1}.min^{-1}$, min^{-1} and $L.mg^{-1}.min^{-1}$ in the zero, pseudo-first and pseudo-second-order respectively.

The pseudo-first-order reaction kinetics is based on the Langmuir-Hinshelwood (L-H) kinetic model which describes single-component kinetics while the pseudo-second-order kinetics describes two or more component reaction rates (Hou et al., 2021). L-H is based on the assumptions that the reaction system is in dynamic equilibrium, reaction with intermediate products and reactive species for active sites are not limiting and the reaction is surface mediated (Ateia et al., 2020). The results confirm that the zero-order kinetics is not a good fit to describe this experimental data and the pseudo-second-order model better fits at optimum conditions. This is consistent with the theory that intermediates will be formed during the photodegradation experiments as well as the reaction rate being proportional to the concentration of the reactant (Gao et al., 2016). The maximum

rate constants for 2,4-D and TC were at 0.5 g/L and 1 g/L respectively with 0.0045 $L.mg^{-1}.min^{-1}$ and 0.0238 $L.mg^{-1}.min^{-1}$ with a coefficient of determination of 0.9937 and 0.9631. In the degradation of 2,4-D and TC, at optimum values of photocatalyst loading, initial concentration and pH, the R^2 values were significantly higher when compared to other conditions. The reaction coefficient also confirms the experimental trends that were noticed which include, higher reaction constants at low initial pollutant concentration, photocatalyst loading effects and the impact of pH on the reaction rate.

Table B1: Kinetic parameters for 2,4-D

Variable parameter	Value	k			R^2		
		Zero-order	First-order	Second-order	Zero-order	First- order	Second- order
Catalyst[a]	BOC	-8E-05	8E-05	9E-05	0.0419	0.043	0.0442
	10%AgCl/BOC	-18E-04	0.0025	0.0035	0.9757	0.9919	0.9925
	20%AgCl/BOC	-0.002	0.0029	0.0045	0.9282	0.9692	0.9937
	50%AgCl/BOC	-18E-04	0.0031	0.0048	0.9235	0.9649	0.9902
Photocatalyst loading[b]	0.25 g/L	-12E-04	0.0014	0.0018	0.8062	0.8244	0.8418
	0.5 g/L	-0.0020	0.0029	0.0045	0.9282	0.9692	0.9937
	1 g/L	-13E-04	0.0017	0.0023	0.6912	0.7195	0.7373
Initial concentration[c]	10 mg/L	-0.0021	0.003	0.0044	0.8712	0.8819	0.8776
	20 mg/L	-0.002	0.0029	0.0045	0.9282	0.9692	0.9937
	50 mg/L	-9E-04	0.001	0.0012	0.5771	0.562	0.5454
Solution pH[d]	3	-0.002	0.0029	0.0046	0.8811	0.9264	0.9582
	4	-0.002	0.0029	0.0045	0.9282	0.9692	0.9937
	7	-9E-04	0.0011	0.0013	0.941	0.9511	0.9556
	11	0.0002	-2E-04	-2E-04	0.1313	0.1195	0.1080

[a] photocatalyst loading = 0.5 g/L, concentration = 20 mg/L, pH= 4
[b] catalyst = 20%AgCl/BOC, concentration = 20 mg/L, pH = 4
[c] catalyst = 20%AgCl/BOC, photocatalyst loading = 0.5 g/L, pH = 4
[d] catalyst = 20%AgCl/BOC, photocatalyst loading = 0.5g/L, concentration = 20 mg/L

Table B2: Kinetic parameters for tetracycline

Variable parameter	Value	k			R^2		
		Zero-order	First-order	Second-order	Zero-order	First-order	Second- order
Catalyst[e]	BOC	-8E-04	0.0009	0.0011	0.6759	0.6798	0.6821
	10%AgCl/BOC	-0.0016	0.0024	0.0037	0.6190	0.6715	0.7155
	20%AgCl/BOC	-0.0021	0.0034	0.0060	0.6870	0.7238	0.7546
	50%AgCl/BOC	-0.0028	0.0062	0.0165	0.8052	0.9196	0.9882
Photocatalyst loading[f]	0.25 g/L	-0.0023	0.0038	0.0070	0.8530	0.9152	0.9340
	0.5 g/L	-0.0028	0.0062	0.0165	0.8052	0.9196	0.9882
	1 g/L	-0.0029	0.0073	0.0238	0.7812	0.9098	0.9631
Initial concentration[g]	20 mg/L	-0.0029	0.0073	0.0238	0.7812	0.9098	0.9631
	30 mg/L	-0.0028	0.0058	0.0141	0.9011	0.9733	0.9769
	50 mg/L	-0.0021	0.0320	0.0051	0.9136	0.9416	0.9400
Solution pH[h]	3	-0.0030	0.0069	0.0202	0.8708	0.9671	0.9523
	5.3	-0.0029	0.0073	0.0238	0.7812	0.9098	0.9631
	7	-0.0031	0.0080	0.0027	0.8028	0.9183	0.9780
	11	-0.0032	0.0081	0.0282	0.7052	0.7596	0.8204

[e] photocatalyst loading = 0.5 g/L, concentration = 20 mg/L, pH= 5.3
[f] Catalyst = 50%AgCl/BOC, concentration = 20 mg/L, pH = 5.3
[g] Catalyst = 50%AgCl/BOC, photocatalyst loading = 1 g/L, pH = 5.3
[h] Catalyst = 50%AgCl/BOC, photocatalyst loading = 1 g/L, concentration = 20 mg/L